Modeling cross-tidal flat mass transport

A study on its magnitude and its effect on tidal constituents in channels using two simplified models

Jan-Willem Meijerink
IMAU / University of Utrecht
supervised by:
Niels Alebregtse
Huib de Swart

12th November 2013

Abstract: Tidal systems are found in many locations in the world. Many of these systems contain tidal flats, i.e. features that fall dry during part of a tidal cycle. The hydrodynamical equations describing tidal systems are nonlinear and, as a consequence, higher harmonics of the primary tidal frequency are produced. Several processes have been identified to produce higher harmonics, such as advection of momentum and depth-dependent bottom friction. The incorporation of tidal flats in the hydrodynamical equations has identified two more processes, mass storage and momentum loss over the tidal flat, as sources of higher harmonics. On some occasions water traverses the tidal flat and flows into a channel on the other side of the tidal flat. This process, called cross-tidal flat mass transport, may be a source of higher harmonics as well. A numerical model, the Network Model with Parameterisation of tidal flat hydrodynamics (NM-P), has been developed to simulate cross-tidal flat mass transport. In a simplified geometry, the NM-P is used to quantify cross-tidal flat mass transport and the effect of cross-tidal flat mass transport on the production of higher harmonics in the channels. A different numerical model, the Network Model with explicit Flat dynamics (NM-F), has been developed to simulate of flow over tidal flats more accurately.
Results obtained with the NM-P model indicate that cross-tidal flat mass transport can be a significant flux in the mass budget of a channel, up to 25% of the total mass flux. A much smaller net cross-tidal flat mass transport exists as well, always directed from the lagging to the leading channel. The effect of cross-tidal flat mass transport in the channels is predominantly present in the seaward part of the tidal channel. Higher (lower) velocities are found in the leading (lagging) channel, while lower (higher) sea level is found in the leading (lagging) channel. The M_4 tidal constituent increases in amplitude with increasing cross-tidal flat mass transport. Results obtained with the NM-F model indicate that mass flow over tidal flat is slow, with the wave front moving at 17cms^{-1} over a dry tidal flat.

Contents

Chapter 1

Introduction

Shallow, tidally dominated estuarine and inlet systems are found on many locations all over the world. Many of these systems contain tidal flats: Area's of land that are flooded during part of a tidal cycle. In general, when tidal systems contain tidal flats, complex network configurations with deeper channels separated by tidal flats exist (e.g. Wadden Sea or Columbia River Estuary (Figure **??**), see e.g. **?**). Tidal motion in the tidal system propagates through the system via the channels, flooding and draining adjacent tidal flats in the process.

Figure 1.1: A helicopter view of the Columbia River Estuary, located at the west coast of the United States. Picture taken from http://www.whsrn.org/.

Tidal flats have been studied for centuries in various research fields. Marine biologistist and zoologists study tidal flats for their importance to wildlife. Tidal flats provide a land-based, predator-free habitat for sea-going mammals, for example seals (**?**). They also host large microphytobenthic communities (e.g. **?**). Coastal hydrologists consider tidal flats for their importance in the hydrodynamics and morphodynamic stability of tidal systems (e.g. **?**, **?**, **?**). Knowledge of the hydrodynamics of the system is required to determine the velocity and sea level at any given moment in time, including predicting maximal ebb and flood currents and high and lower water. This data is also used by ships navigating through tidal systems.

The hydrodynamics in tidal systems is strongly nonlinear by nature. Due to nonlinear interactions, an incoming tidal wave with frequency ω will produce overtides: harmonic constituents with frequency $n\omega$, with $n = [2, 3, 4, ...]$. Overtides are also called higher harmonics, where ω is called the first or primary harmonic. In almost all tidal systems the dominant frequency is the M_2 frequency, a frequency generated by gravitational interaction between water masses on earth and the moon.

Hydrodynamic variables contain both constituents with the original tidal frequency ω and constituents with the frequencies of the overtides. The resulting signal in, for example, the sea level will deviate from a perfect sinusoidal function: It is asymmetric in time. In Figure **??** the sea level is plotted over two tidal cycles at the city of Harlingen, located at the boundary of the Wadden Sea, a tidally dominated inlet system in the north of The Netherlands. The sea level amplitude is larger during high water than during low water. Also, the time between high water and low water is longer than between low water and high water. The asymmetry is caused by the overtides interacting with the original signal with frequency ω.

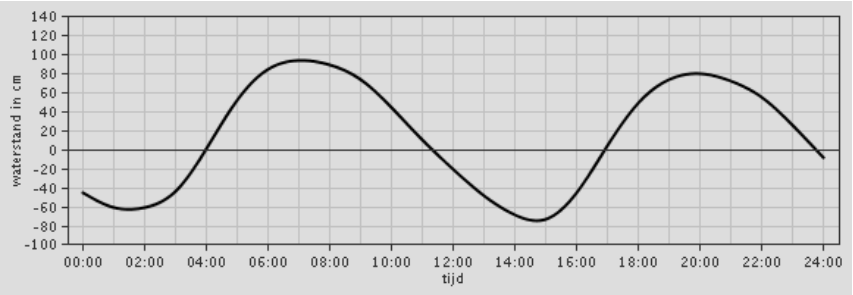

Figure 1.2: The sea level over two tidal cycles in the city of Harlingen, located at the boundary of the Wadden Sea, a tidally dominated inlet system in The Netherlands on October 1st, 2013. On the x-axis time is plotted in hours, on the y-axis sea level is plotted in centimeters.

When tidal currents move over an erodible bottom, sediment is whirled up and transported with the currents. During the flood phase of a tidal cycle, sediment is transported into the tidal system, during the ebb phase of a tidal cycle sediment is transported out of the tidal system. A perfect sinusoidal tidal wave, in which only a M_2 tidal frequency is present, will transport the same amount of sediment into the system as out of the system. In that case there is no net sediment transport. When the tidal wave contains overtides as well, the tidal signal is asymmetrical in time and there will be net sediment transport averaged over a tidal cycle (e.g. **?** and **?**). The asymmetry in the tidal signal depends on the amplitudes and relative phases of the harmonics (see Figure **??**).

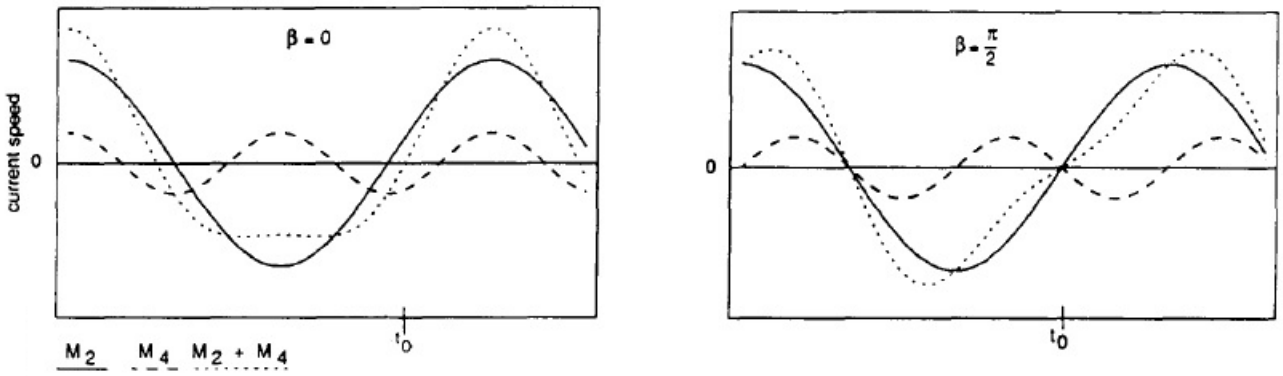

Figure 1.3: The current speed plotted against time. The solid line represents the M_2 constituent, the dashed line represents the first higher harmonic, the M_4 constituent. When the two components are added, an asymmetrical signal is constructed (dotted line). In the left image a phase difference $\beta = 0$ is applied, in the right image the phase difference is $\beta = \frac{\pi}{2}$. Figure is taken from **?**.

Net sediment transport affects the morphodynamic stability of the tidal system, which in turn affects the production of overtides (e.g. **?**). When net sediment export is present over a longer period of time, the tidal system will eventually drown. When there is net sediment import, tidal systems will silt and may become unnavigable for ships. In both cases actions are required to maintain an equilibrium. To predict the evolution of tidal systems over time, an accurate prediction of the direction and magnitude of the net sediment transport is

required. As argued above, knowledge of the production of overtides is essential for this prediction.

Knowledge of the production of overtides is relevant for both short term and long term predictions and applications. A number of processes show up as nonlinear terms in the equations describing the estuarine hydrodynamics and are thus identified as processes that produce overtides. Among these processes are quadratic bottom friction, advection of momentum and divergence of mass transport. For a discussion on these and other nonlinear terms, see **?**. **?** and **?** demonstrated that the inclusion of tidal flats as reservoir for mass storage led to additional generation of overtides. **?** found momentum loss over tidal flats to be a source overtides as well.

A limitation of these models is the assumption that the flooding and drying of tidal flats takes place instantly. The first objective of this thesis is to investigate the effect of non-instant tidal wave progression over the tidal flat. Measurements (e.g. **?**) indicate spatial variation in sea level and velocity over the tidal flat. Model simulations of tidal flat hydrodynamics by **?** also show spatial variation in sea level and cross-shore velocity. In this thesis a numerical model has been developed that applies the shallow water equation to calculate the hydrodynamics over the tidal flat (similar to **?**). This model, the NM-F (Network Model with Flat dynamics) model, has been constructed to answer one of the research questions of this thesis,

- What is the spatial distribution of sea level and velocity over a tidal flat during a tidal cycle?

When the spatial distribution of the hydrodynamic variables over a tidal flat is known, the quality of the assumption that tidal waves progress instantly over tidal flats is assessed. Simulations of the tidal flat hydrodynamics by the NM-F models are compared to two simulations by other numerical models to evaluate the quality of the NM-F model.

In a complex network system, in which channels are separated by tidal flats, mass may be transported from one channel into another channel by flowing over a tidal flat. **?** included this effect in a numerical estuarine hydrodynamic model in his simulations of the Columbia River estuary. When the parametrisation of the cross-tidal flat mass transport by **?** is incorporated in the equations describing the hydrodynamics in the channels, it shows up as a nonlinear term and will lead to the production of higher harmonics. This observation motivates the second objective of this thesis.

? did not quantify this cross-tidal mass transport or considered the effect of cross-tidal flat mass transport on the production of overtides in the adjacent channels. The magnitude of the production of overtides and the magnitude of the cross-tidal flat mass transport cannot be analytically derived from the equations; Model simulations are required to quantify these effects. The NM-F model had difficulties producing accurate results for the cross-tidal flat mass transport. Therefor, a different numerical model has been developed to simulate cross-tidal flat mass transport, the NM-P (Network Model with Parameterisation) model. In the NM-P model, the tidal flat hydrodynamics are parameterised instead of explicitly calculated, as was done in the NM-F model. A simplified geometry is used to minimise the contributions of other overtide producing effects. With the NM-P model, the other research questions of this thesis are assessed:

- How large is the cross-tidal flat mass transport?
- How does the magnitude of the cross-tidal flat mass transport depend on the system parameters?
- What is the effect of cross-tidal flat mass transport on the harmonics of the hydrodynamic variables?

This thesis will describe the process of model development and model application. In section 2 the governing equations for the channel hydrodynamics and tidal flat hydrodynamics are presented for both the NM-P and the NM-F model. Section 3 contains the implementation of the theory in the two numerical models. In section 4 the results of model simulations are shown. First, the results from the NM-P model are presented. After that, the results of the NM-F model are presented, including a comparison to two other numerical models. In section 5 the results of the NM-P model are discussed and the applicability of the NM-F model is evaluated. Finally, in section 6, the conclusions of this thesis are presented.

Chapter 2

Theory

In this section, a theoretical framework for describing tidal wave propagation in tidal networks is presented. A tidal network is defined as a system of interlinked tidal channels with adjacent tidal flats. Such networks occur in many inland seas (e.g. the Wadden Sea) and estuaries (e.g. the Western Scheldt and the Columbia River estuary (see Figure **??**)). In channels, the dominant velocities are in the along-channel direction and fluid motion will be described by the 1D, cross-sectionally averaged, shallow water equations (c.f. **?**). The tidal flat hydrodynamics are simulated differently in the two different models. In the NM-P model a parameterisation is applied to simulate cross-tidal flat mass transport. This parameterisation is based the parameterisation used by **?**. With the NM-P model the cross-tidal flat mass transport is calculated. In the NM-F model the shallow water equations are used to explicitly simulate sea level and velocity over the tidal flat. With the NM-F model a spatial distribution of the hydrodynamic variables is obtained.

Two types of geometries will be used in this thesis. They are depicted in Figure **??**. The geometry with one channel and an adjacent tidal flat will be referred to as the 'T-geometry'. The geometry with two channel connected by a tidal flat will be referred to as an 'H-geometry'. The NM-P model will be applied to the H-geometry, the NM-F model will be applied to the T-geometry and the H-geometry.

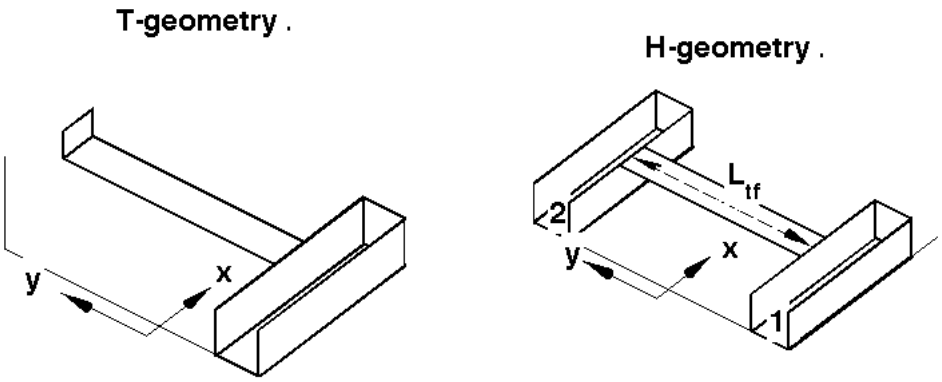

Figure 2.1: The two geometries used in this thesis. On the left is the 'T-geometry' with one channel and an adjacent tidal flat. On the right is the 'H-geometry' with two channels connected by a tidal flat.

First, the general theory is derived for describing the hydrodynamics in the channels, including boundary conditions at the open and closed boundary. The theory is the same in the NM-P and NM-F model. After that, theory is presented for describing the tidal flat hydrodynamics and the internal boundary conditions. This is done

separately for the NM-P and the NM-F model.

2.1 Channel Hydrodynamics

Straight tidal channels are characterised by 1D fluid motion. Without the incorporation of tidal flats the shallow water equations describing 1D fluid motion in tidal channels are given by

$$\frac{\partial A}{\partial t} + \frac{\partial (Au)}{\partial x} = 0, \tag{2.1}$$

$$\frac{\partial (Au)}{\partial t} + \frac{\partial (Auu)}{\partial x} = -Ag\frac{\partial \eta}{\partial x} - wC_d|u|u, \tag{2.2}$$

where the former represents the mass balance and the latter the momentum balance, with rectangular cross-section A ($A(x,t) = w(x)(h(x) + \eta(x,t))$ of the channel. Further, $\eta(x,t)$ is the sea surface elevation with respect to the undisturbed water depth $h(x)$, $u(x,t)$ is the cross-sectionally-averaged along channel velocity, g is the gravitational acceleration and C_d is a bottom friction coefficient. Tidal flats are incorporated in the equations of motion later in this chapter.

One of the goals of this research is to study the effect of cross-tidal flat mass transport on the tidal constituents in the channels. Density differences and wind stresses also have an effect on tidal constituents. To single out the effects of cross-tidal flat mass transport, density differences are neglected (constant salinity and temperature is assumed) and the wind stress is omitted from the equations. Also, tidal channels are generally narrow, with width w small compared to the Rossby radius of deformation $\frac{\sqrt{gh}}{f}$, where g is the gravitational acceleration and f is the Coriolis parameter. This allows neglecting the Coriolis force.

A varying width w or undisturbed water depth h will alter the amplitude of tidal constituents. To limit their contribution to the generation of overtides, only rectangular channels are considered, with constant width W and constant depth H. Under these conditions equation **??** and equation **??** reduce to

$$\frac{\partial \eta}{\partial t} + H\frac{\partial u}{\partial x} + \frac{\partial (u\eta)}{\partial x} = 0, \tag{2.3}$$

$$\frac{\partial u}{\partial t} + u\frac{\partial u}{\partial x} = -g\frac{\partial \eta}{\partial x} - C_d\frac{|u|u}{H+\eta}. \tag{2.4}$$

Equations **??**-**??** form a so-called hyperbolic system of nonlinear partial differential equations. Solutions of hyperbolic systems can be obtained with the method of characteristics. Following **?**, a theoretical framework is derived for constructing characteristics. Within this framework, equations for tidal channels and tidal flats are derived, described in the system's new variables, so called Riemann variables.

Equations in characteristic form have several advantages over equations **??**-**??**. Firstly, characteristics transform a system of partial differential equations (PDE's) into a system of ordinary differential equations (ODE's). ODE's are generally easier to solve. Secondly, at the open boundary an incoming wave can be prescribed (in contrast to prescribing sea level). The advantages of prescribing an incoming wave are that the boundary condition at the open boundary does not depend on the current state of the system and that there is no reflection of outgoing waves at the open boundary. A discussion on these advantages is found in Appendix D. Finally, using characteristics, the propagation of shocks can be calculated. A breaking wave is considered to be a shock.

The theory of characteristics is first generally derived. After that, it is applied to the shallow water equations (equations **??**-**??**).

2.1.1 Characteristics: Theory

Consider a system of differential equations

$$A_{ij}\frac{\partial \phi_j}{\partial t} + a_{ij}\frac{\partial \phi_j}{\partial x} + b_i = 0 \qquad i = 1,...,n, \qquad j = 1,...,n, \tag{2.5}$$

where $\phi = \phi(x,t)$. A repeated subscript i or j is short for a summation over i or j (Einstein notation). Equation **??** can be multiplied by A^{-1}, resulting in

$$\frac{\partial \phi_i}{\partial t} + a'_{ij}\frac{\partial \phi_j}{\partial x} + b'_i = 0 \qquad\qquad i = 1, ..., n, \tag{2.6}$$

where $a' = A^{-1}a$ and $b' = A^{-1}b$. Equation **??** is now multiplied by a $1 \times n$-vector l with components l_i:

$$l_i\Big(\frac{\partial \phi_i}{\partial t} + a'_{ij}\frac{\partial \phi_j}{\partial x}\Big) = l_i b'_i. \tag{2.7}$$

The goal is to write the system in its so called characteristic form

$$l_i\frac{d\phi_i}{dt} = l_i b'_i, \tag{2.8}$$

where $\frac{d}{dt}$ denotes a total time derivative. Equation **??** and **??** are equal when

$$l_i a'_{ij} = l_j c, \tag{2.9}$$

with $c = \frac{\mathrm{d}x}{\mathrm{d}t}$ as characteristic velocity. Note that equation **??** is an eigenvalue problem, with c the eigenvalues and l the left eigenvector. Equation **??** has nontrivial solutions when

$$\det|a' - c\delta| = 0, \tag{2.10}$$

with δ the unity tensor. By solving equations **??**, n values for c are obtained. When solutions for c are plugged back into equation **??**, the left eigenvectors are obtained. Note that any multiple of an eigenvector l, say γl is also a solution of the system, with γ a constant. The system can be rewritten into the form

$$l_i\frac{d\phi_i}{dt} = \frac{dr}{dt} = l_i b'_i, \tag{2.11}$$

where r is a Riemann variable. Equation **??** is now a system of ordinary differential equations (ODE's). When $b'_i = 0$, a Riemann variable is constant on characteristic curves (lines with constant c) and it is also called a Riemann invariant. r is a function of ϕ_i an can be written as

$$\frac{dr}{dt} = \frac{\partial r}{\partial \phi_i}\frac{d\phi_i}{dt}.$$

When

$$\frac{\partial r}{\partial \phi_i} = l_i, \tag{2.12}$$

equation **??** is obtained. The Riemann variables are found when equation **??** is integrated. In a hyperbolic system of n equations, the system has n eigenvectors and n Riemann variables.

2.1.2 Characteristic form of Shallow Water Equations

The general approach on characteristics presented in the previous section can be applied to the shallow water equations described by equations Equations **??**-**??**. With $n = 2$, $\phi_1 = \eta$ and $\phi_2 = u$, equation **??** is written in matrix notation as

$$\begin{bmatrix}(H+\eta)_t \\ u_t\end{bmatrix} + \begin{bmatrix}u & (H+\eta) \\ g & u\end{bmatrix}\begin{bmatrix}\eta_x \\ u_x\end{bmatrix} + \begin{bmatrix}0 \\ C_d\frac{|u|u}{H+\eta}\end{bmatrix} = 0. \tag{2.13}$$

Its eigenvalues c are found via $(u-c)^2 - g(H+\eta) = 0$, which results in

$$c = u \pm \sqrt{g(H+\eta)}. \tag{2.14}$$

The corresponding left eigenvectors $l = \begin{bmatrix} l_1 & l_2 \end{bmatrix}$ are found via

$$\begin{bmatrix} l_1 & l_2 \end{bmatrix} \begin{bmatrix} u-c & H+\eta \\ g & u-c \end{bmatrix} = \begin{bmatrix} l_1 & l_2 \end{bmatrix} \begin{bmatrix} \pm\sqrt{g(H+\eta)} & (H+\eta) \\ g & \pm\sqrt{g(H+\eta)} \end{bmatrix} = 0.$$

Any multiple of an eigenvector is also an eigenvector. It is thus allowed to conveniently pick a value for l_2 and scale l_1 accordingly. A convenient choice for l_2 is $l_2 = 1$, resulting in $l_1 = \pm\sqrt{\frac{g}{H+\eta}}$. The characteristic equation is given by equation **??** and reads $l_i \frac{d\phi_i}{dt} = l_i b_i'$, or

$$\pm\sqrt{\frac{g}{H+\eta}}\frac{d\eta}{dt} + \frac{du}{dt} = -C_d \frac{|u|u}{H+\eta}. \tag{2.15}$$

The Riemann variables are determined by equation **??** via

$$r = \int l_i \mathrm{d}\phi_i = \int l_1 \mathrm{d}\eta + \int l_2 \mathrm{d}u = \int \pm\sqrt{\frac{g}{(H+\eta)}}\mathrm{d}\eta + u,$$

which results in

$$r^{\pm} = u \pm 2\sqrt{g(H+\eta)}. \tag{2.16}$$

Riemann variable r^+ corresponds to the characteristic curve with slope c^+. In general, $c^+ > 0$, and r^+ evolves on a characteristic curve traveling to the right. Likewise, r^- corresponds to the characteristic curve with slope c^-, which is usually (but not always) smaller than zero. Variable r^- thus corresponds to a characteristic curve that travels to the left.

The ODE's describing the evolution of $r^{\pm}$ in time are:

$$\frac{dr^{\pm}}{dt} = -C_d \frac{|u|u}{H+\eta}. \tag{2.17}$$

Note that the derivative is taken on characteristic curves $c^{\pm}$.

In a channel the original variables η and u are reconstructed from $r^{\pm}$ via

$$\eta = \frac{1}{16g}(r^+ - r^-)^2 - H, \tag{2.18}$$

$$u = \frac{1}{2}(r^+ + r^-). \tag{2.19}$$

The hydrodynamics in the channels, in the absence of tidal flats, in both the NM-P model and the NM-F model are described by equation **??**. The hydrodynamics at locations in the channel where tidal flats are connected to the channel are treated as boundary conditions and are found in sections 2.2.2 and section 2.3.3.

2.1.3 Boundary Conditions

Three types of boundaries exist in both the H-geometry and the T-geometry (see Figure **??**): Open boundaries, internal boundaries and closed boundaries. Open and closed boundaries are not model dependent in this thesis and are described in this section. Internal node dynamics (locations where a tidal flat is connected to a channel) are solved differently for the NM-P and the NM-F model and are described in the following sections. Before the conditions at open and closed boundaries are described, first a general remark on boundaries conditions in systems with Riemann variables should be made.

Boundary conditions in channels are assigned at the boundaries of the space-time domain, i.e. at

$\Big(t = 0, x \epsilon [0 \quad L]\Big)$ (initial conditions), at $\Big(t \epsilon [0 \quad T_{end}], x = 0\Big)$ and at $\Big(t \epsilon [0 \quad T_{\text{end}}], x = L\Big)$ (boundary conditions). The x-domain ranges from $x = 0$ to $x = L$ and the time period under consideration is from $t = 0$ to $t = T_{\text{end}}$. The combination of initial conditions and boundary conditions is called mixed boundary conditions. At a certain point in time ($t > 0$), some characteristics will have entered the domain at the $t = 0$ boundary and other at the $x = 0$ and $x = L$ boundaries. In general the positive characteristic (r^+ on c^+) has a positive characteristic velocity and will enter the domain at the $x = 0$ boundary and will leave the domain at the $x = L$ boundary. No condition for r^+ is then required for r^+ at $x = L$. Likewise, for r^- no condition is required at $x = 0$.

Open Boundary

At the open boundary, a channel is prescribed with an external forcing mimicking a tidal wave. The H-geometry has two open boundaries, the T-geometry has one open boundary. In terms of Riemann variables, two approaches are possible: Prescribing sea level and prescribing the incoming wave.

The first approach is prescribing sea level at the open boundary. In this approach, it assumed that r^- is known at the open boundary. In tidal channels this is generally the case, since $c^- < 0$. With a known value for r^-, η is translated into r^+ via $\eta = \frac{1}{16g}(r^+ - r^-)^2 - H$.

The second approach is prescribing the incoming wave. Sea level is a combination of both the incoming wave (r^+ on c^+) and the outgoing wave (r^- on c^-). By prescribing sea level rather than an incoming wave, a condition is posed on r^+ based on the systems current state, although the incoming wave will have the same properties regardless of the systems current state. No information from the system should be available for the incoming tidal wave. Therefore, the dynamic variables (velocity u and sea level η) as perceived by the incoming wave are set to a constant (zero) value. In reality they have nonzero values, but the incoming wave has no knowledge of these nonzero values and acts as if they are zero.

Outside the domain, the r^- is given by

$$r^- = -2\sqrt{gH}.$$

Inside the domain, the dynamic variables are nonzero and the negative Riemann variable r^- is given by

$$r^- = u - 2\sqrt{g(H + \eta)}.$$

At the open boundary both expressions for r^- are valid and the two expressions are equal,

$$-2\sqrt{gH} = u - 2\sqrt{g(H + \eta)}.$$

From this information, a velocity u is constructed that is subsequently plugged into the positive Riemann variable $r^+ = u + 2\sqrt{g(H + \eta)}$, which results in

$$r^+ = 4\sqrt{g(H + \eta)} - 2\sqrt{gH}. \tag{2.20}$$

Closed boundary

At the closed boundary, velocity u is set to zero. Since $u = \frac{1}{2}(r^+ + r^-)$, $r^- = -r^+$ at the closed boundary.

Initial Conditions

The system is initialised with all dynamic variables set to zero, so $u = 0$ and $\eta = 0$ at each location in every channel of the system. Under these conditions, variables $r^\pm$ are given by

$$r^\pm = \pm\sqrt{gH}.$$

Undisturbed water depth H is different for each channel, so initial values for $r^\pm$ differ from channel to channel.

2.2 NM-P model

With the NM-P model the hydrodynamics in the H-geometry (see Figure **??**) are described. The hydrodynamics in the channels are described by the shallow water equations (see Section 2.1.2). The hydrodynamics on the tidal flat are described by a parameterisation based on **?**. First, the hydrodynamics on the tidal flat are described in this section. After that, the dynamics at the boundary between tidal flat and tidal channel are presented.

2.2.1 Tidal Flat

Tidal flats are characterised by the fact that they are partially below sea level and partially above sea level during a tidal cycle. Some tidal flats, when submerged, span from one tidal channel into another. In that case, mass is exchanged over the tidal flat. In the H-geometry (see Figure **??**), channel 1 has undisturbed water depth H_1 and sea level elevation η_1, channel 2 has undisturbed water depth H_2 and sea level elevation η_2. The tidal flat has length L_{tf}, sea level η_{tf}, velocity u_{tf} and depth H_{tf}. When H_{tf} is smaller than η_1 or η_2 during part of a tidal cycle, cross-tidal flat mass transport will take place. For simplicity a tidal flat depth of $H_{tf} = 0$ is chosen. With this choice it is guaranteed that during part of a tidal cycle cross-tidal flat transport will be established, while on the other hand the tidal flat is only submerged for part of the time.

The parameterisation of the hydrodynamics used for the tidal flat is based on **?**. However, some adjustments are made to the original parameterisation by **?**. The original parameterisation is found in Appendix E. Here, there parameterisation that is used in the NM-P model is presented.

The sea level is defined the same as in the original parameterisation by **?**,

$$\eta_{tf} = \frac{\max(\eta_1, 0) + \max(\eta_2, 0)}{2}. \tag{2.21}$$

This corresponds to a linear interpolation of η_1 and η_2 over the tidal flat and taking its value at $x = \frac{L_{tf}}{2}$, at half the length of the tidal flat. When the sea level in a channel adjacent to the tidal flat drops below $H_{tf} = 0$, the sea level on the tidal flat is set to zero instead.

The velocity over the tidal flat, u_{tf}, is based on a balance between the pressure gradient and bottom friction,

$$\frac{\partial u_{tf}}{\partial t} = -g\frac{\max(\eta_2, 0) - \max(\eta_1, 0)}{L_{tf}} - C_{d,tf}\frac{u_{tf}|u_{tf}|}{\eta_{tf}}, \tag{2.22}$$

with $C_{d,tf}$ a bottom friction coefficient, g the gravitational acceleration and L_{tf} the length of the tidal flat. In equation **??** the first term on the r.h.s. is a pressure gradient and the second term on the r.h.s. is bottom friction. The pressure gradient is based on the sea level difference between the two channels on either side of the tidal flat. When the sea level sinks below the tidal flat height ($H_{tf} = 0$), sea level is set to zero. Bottom friction is, in general, stronger over a tidal flat than in a channel, so $C_{d,tf}$ has a higher value than C_d used in the channel.

When both η_1 and η_2 are smaller than zero, velocity u_{tf} is zero.

Momentum Transfer

In the parameterisation by **?** it is implicitly assumed that there is no momentum loss over the tidal flat (see Appendix E). When tidal flats are hundreds of meters long, at least some momentum loss is to be expected. Here, an approach is presented to take the momentum loss over the tidal flat into account.

The time that a water parcel spends on the tidal flat is given by $\tau_v = \frac{L_{tf}}{u_{tf}}$, which is the length of the tidal flat over the velocity of the tidal flat. A typical friction timescale, τ_{fr}, is derived from equation **??** via $\tau_{\text{fr}} = \frac{\eta_{tf}}{C_{d,tf}u_{tf}}$. Momentum transport over the tidal flat then drops off with a factor $\exp[-\frac{\tau_v}{\tau_{\text{fr}}}] = \exp[-\frac{L_{tf}C_{d,tf}}{\eta_{tf}}]$. A stronger friction and a longer tidal flat will lead to more dissipation of momentum. A higher sea level over the tidal flat will decrease the amount of time spent on the tidal flat and will lead to less dissipation.

Example
When sea level in channel 1, η_1 is 1m and sea level in channel 2, η_2 is 0m, a mass transport from channel 1 to channel 2 will exist. The mass originates from channel 1 and has initial velocity u_1, the along-channel velocity in channel 1. While the mass is transported, it loses momentum due to friction. Consider a tidal flat of length $L_{tf} = 100$m and bottom friction $C_d = 0.01$. The sea level on the tidal flat is 0.5m (via equation **??**) and the momentum that reaches channel 2 will have dropped by a factor $\exp[-\frac{L_{tf}C_{d,tf}}{\eta_{tf}}] = \exp[-2] \simeq 0.135$. The momentum that reaches channel 2 is $\tilde{u}_1 = \exp[-2]u_1$.

2.2.2 Boundary Conditions

Boundary conditions are used to close a system of differential equations. The boundary conditions for the open and closed boundary are found in Section 2.1.3. The internal nodes are described in this section.

Internal Boundaries

Internal boundaries are locations where a tidal flat flows into a channel. At locations where a tidal flat flows into a channel, the sea level and velocity on the tidal flat, η_{tf} and u_{tf} (defined positive flowing out of the channel), are known and are incorporated in the shallow water equations in the channel (equations **??**-**??**) via

$$\frac{\partial A}{\partial t} + \frac{\partial (Au)}{\partial x} + \eta_{tf} u_{tf} = 0, \qquad x_{f-} < x < x_{f+}, \tag{2.23}$$

$$\frac{\partial (Au)}{\partial t} + \frac{\partial (Auu)}{\partial x} - \Delta u \eta_{tf} u_{tf} \mathcal{H}(-u_{tf}) = -Ag\frac{\partial \eta}{\partial x} - wC_d|u|u, \qquad x_{f-} < x < x_{f+}. \tag{2.24}$$

In equation **??**, the continuity equation ensures mass conservation along the boundary via the $\eta_{tf}u_{tf}$ term. In equation **??**, the momentum balance contains an extra term compared to equation **??**, $\Delta u \eta_{tf} u_{tf} \mathcal{H}(-u_{tf})$, where $\mathcal{H}$ is the Heaviside function, denoted by

$$\mathcal{H}(x) = \begin{cases} 0 & x < 0, \\ 1 & x \geq 0, \end{cases} \tag{2.25}$$

and Δu is the velocity difference between the velocity in the channel under consideration and the velocity in the channel with which mass is exchanged, corrected for momentum loss over the tidal flat.

Equations **??**-**??** are only valid along the boundary between the tidal flat and the channel. This region is denoted by $x_{f-} < x < x_{f+}$, where x is the along-channel coordinate. The region is also depicted in Figure **??**. Outside this region, equations **??**-**??** are used.

Under the assumption of a rectangular geometry, equations **??**- **??** are transformed into a differential equations for Riemann variables via

$$\frac{dr^{\pm}}{dt} = -\frac{C_d|u|u}{H+\eta} \mp \sqrt{\frac{g}{H+\eta}}\frac{u_{tf}\eta_{tf}}{W} + \mathcal{H}(-u_{tf})\frac{\Delta u}{H+\eta}\frac{u_{tf}\eta_{tf}}{W} \qquad x_{f-} < x < x_{f+}. \tag{2.26}$$

In equation **??**, W is the width of the channel and H is the undisturbed water depth of the channel. Again, equation **??** is only valid along the boundary, between $x = x_{f-}$ and $x = x_{f+}$. Outside this region equation **??** is used.

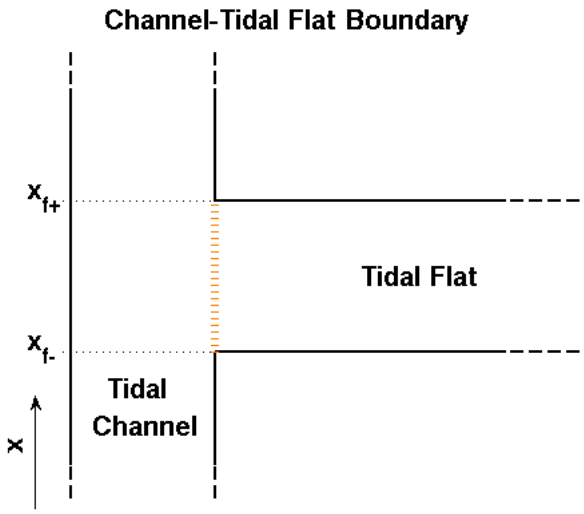

Figure 2.2: Boundary where channel and tidal flat are connected. Mass is exchanged between the channel and tidal flat along the boundary, depicted by the thick, dashed, orange line. The boundary ranges from $x = x_{f-}$ to $x = x_{f+}$

2.3 NM-F model

In this section a description is provided for the hydrodynamics on the tidal flat in the NM-F model. This description includes a method on resolving breaking waves. After that the boundary conditions are discussed. The theory of how channels are described has already been presented in Section 2.1.2. The geometry for which the hydrodynamics are derived is the T-geometry (Figure **??**), although it is also possible to apply the same hydrodynamics to the H-geometry.

2.3.1 Tidal Flat

In the NM-F model the tidal flat is described by the same equations that are used to describe the tidal channel **??**. The only difference is that the depth H is set to zero. Thus, the differential equations describing the tidal flat are

$$\frac{dr^{\pm}}{dt} = -C_d \frac{|u_{tf}|u_{tf}}{\eta_{tf}}, \tag{2.27}$$

where $r^{\pm} = u_{tf} \pm 2\sqrt{g\eta_{tf}}$ on characteristic curves $c^{\pm} = u_{tf} \pm \sqrt{g\eta_{tf}}$.

2.3.2 Breaking Waves

When tidal channels and tidal flats are sufficiently shallow, breaking waves are expected to occur. Waves break when one wave overtakes another. This is best illustrated by considering characteristics, as is shown in Example 1.

Example 1: Breaking Wave over Frictionless Tidal Flat

Consider a tidal flat in which bottom friction is ignored. According to Equation **??**, Riemann variables r^+ and r^- are constants over the tidal flat. Realize that characteristic velocities c^+ and c^- can be written in terms of $r^{\pm}$,

$$c^+ = \frac{3}{4}r^+ + \frac{1}{4}r^-, \qquad c^- = \frac{1}{4}r^+ + \frac{3}{4}r^-.$$

Since $r^{\pm}$ are constant, the characteristic velocities $c^{\pm}$ are also constant. In a space-time diagram of the tidal flat, a characteristic curve shows up as a straight line (Figure **??**). At time $t = t_0$ and location $x = 0$, a wave enters the domain with characteristic velocity c_0^+. The curve in space-time is named $\mathcal{C}_0$ and its slope is c_0.

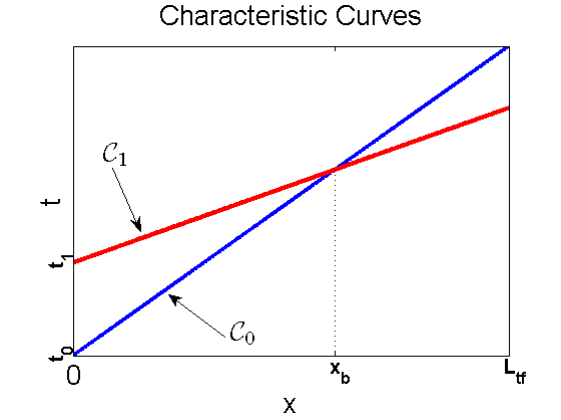

Figure 2.3: Two characteristic curves in the same domain. The wave entering at time t_1 (red) overtakes the wave entering at time t_0 (blue), causing wave breaking at $x = x_b$.

Positive characteristic velocity c^+ is defined as $c^+ = u + \sqrt{g\eta}$ (Equation **??**, with $H = 0$). When water level is rising, c^+ is increases. Consider such a situation. At time $t = t_1 > t_0$ a new wave enters the domain, with $c_1^+ > c_0^+$. The curve it produces is called $\mathcal{C}_1$ and is plotted in Figure **??**, alongside curve $\mathcal{C}_0$. At a specific location, x_b, the two curves intersect each other. The second wave (the wave that entered the domain at $t = t_1$) overtakes the first wave at x_b.

Curves $\mathcal{C}_0$ and $\mathcal{C}_1$ carry information of r^+, in this example a constant value for r^+. At x_b, two values of r^+ are known at the same x-location. The waves will start to break and a shock wave forms.

To avoid multivalued functions for $r^{\pm}$, and thus for sea level η and velocity u, wave breaking should be resolved. When waves of η break, a typical constraint is conservation of mass. When waves of $r^{\pm}$ break, the constraint is less straightforward. In this study it is assumed that Riemann variables $r^{\pm}$ are conserved during wave breaking. The reasoning behind this assumption is that Riemann variables carry all the system's information and the system would lose information if Riemann variables wouldn't be conserved.

During wave breaking, the variables $r^{\pm} = u \pm 2\sqrt{g\eta}$ are conserved. No specific demand is posed on η. As a result, wave breaking may not be mass conserving.

Following **?**, breaking of waves is resolved by placing a vertical line in the breaking area, such that it cuts off exactly the same amount of overhanging wave as is required to fill the space below the remainder of the overhanging wave. This process is demonstrated in Figure **??**. The process is the same for r^+ and r^-.

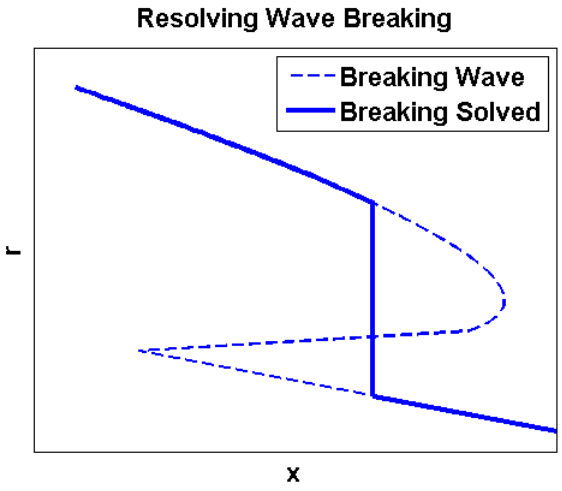

Figure 2.4: The dashed line shows a wave that is breaking. The solid line shows the same wave after the breaking has been resolved. The vertical line in the resolved wave cuts off the same amount of overhanging wave as is required to fill the space below the remainder of the overhanging wave.

2.3.3 Boundary Conditions

The boundary conditions at the open boundary and closed boundary have been described in Section 2.1.3. The boundary condition at the internal boundary is discussed in this section. At locations where a tidal flat is connected to a channel, the channel is split up in two parts: A part seaward of the tidal flat and a part landward of the tidal flat. This allows for a division of the flow between the seaward part of the channel and the landward part of the channel. In the NM-F model, the internal boundary is treated as a single point, a nodal point, to which two channels and one tidal flat are connected.

Internal Nodes

At locations where two or more channels and/or tidal flats join, matching conditions are applied: Conservation of mass and continuity of dynamic pressure. Conservation of mass at the nodal point means that the mass flux going into the node is equal to the mass flux coming out:

$$\sum_{i=1}^{ch_{in}} w_i(h_i+\eta_i)u_i = \sum_{j=1}^{ch_{out}} w_j(h_j+\eta_j)u_j, \tag{2.28}$$

where ch_{in} is the number of channels flowing into the nodal point (u_i is defined positive in the direction of the nodal point) and ch_{out} the number of channels flowing out of the nodal point (u_j positive flowing away from nodal point).

The continuity of dynamic pressure is given by

$$g\eta_i + \frac{1}{2}{u_i}^2 = g\eta_j + \frac{1}{2}{u_j}^2, \qquad \forall \quad i,j, \tag{2.29}$$

and is valid for all channels connected to the nodal point. It provides $N_{ch}-1$ boundary conditions, where N_{ch} is the total number of channels connected to the nodal point. A derivation of the continuity of dynamic pressure is provided in Appendix B.

In other studies (e.g. **?**) continuity of sea level ($\eta_i = \eta_j$ for all i,j) is frequently applied at nodal points instead of continuity of dynamic pressure. In Appendix B it is shown that continuity of dynamic pressure follows from applying the momentum balance at the nodal point and is thus an inherent property of the system, whereas continuity of sea level is not. For linear systems the results happens to be the same, but in nonlinear systems,

such as the system used in this study, the result will not be the same. In reality the boundary condition is more complex, because other physical processes, such as viscous effects, also play a role.

The conditions are currently expressed in terms of u and η. They should be translated to conditions for r^+ and r^-. For incoming channels it is assumed that $c^+ \geq 0$, such that r^+ from incoming channels is known at the nodal point. Likewise, for outgoing channels it is assumed that $c^- \leq 0$, such that r^- is known for outgoing channels at the nodal point.

In terms of Riemann variables, continuity of dynamical pressure is expressed as

$$\frac{1}{8}({r_i}^+ + {r_i}^-)^2 + \frac{1}{16}({r_i}^+ - {r_i}^-)^2 - gH_i = \frac{1}{8}({r_j}^+ + {r_j}^-)^2 + \frac{1}{16}({r_j}^+ - {r_j}^-)^2 - gH_j \qquad \forall\, i,j \quad (2.30)$$

and conservation of mass is expressed as

$$\sum_{i=1}^{ch_{in}} \frac{W_i}{32g}({r_i}^+ + {r_i}^-)({r_i}^+ - {r_i}^-)^2 = \sum_{j=1}^{ch_{out}} \frac{W_j}{32g}({r_j}^+ + {r_j}^-)({r_j}^+ - {r_j}^-)^2. \quad (2.31)$$

In this study only situations with three channels connected to an internal node are considered. The seaward part of the channel is always defined as flowing into the nodal point (with known r^+), the landward part of the channel is always defined flowing out of the nodal point (with known r^-). In the T-geometry, the tidal flat is defined as flowing out of the nodal point. When the NM-F model is applied to an H-geometry, there will be two nodal points. In that case, the tidal flat is defined as flowing out of one nodal point and into the other.

Equations **??-??** provide three matching conditions at the nodal point for six variables, of which three are unknown. By definition, r^+ is known for incoming channels and r^- for outgoing channels. How the system is analytically solved is shown in Appendix A.1 and A.2.

Chapter 3

Methods

In this section the methods are presented that are used to simulate cross-tidal flat mass transport. In section 2, two models (the NM-P model and the NM-F model) are described to simulate flow over dial flats. These numerical models require discretisation of the governing equations. Temporal derivatives are discretised via the Runge-Kutta(4) scheme. No spatial derivatives are present in the equations due to a transformation of variables. In the NM-F model, wave breaking takes place. The methods of solving wave breaking are presented in this chapter. At the end of the chapter a discretisation of boundary conditions is presented.

3.1 Discretisation Channel

A channel is divided in nx equidistant points in the along-channel direction, distance Δx apart. These points are named x_i. When the system is transformed into Riemann variables, there are no spatial derivatives.

A higher order time discretization scheme called the Runge-Kutta(4) (RK4) scheme is used for time integration. It is $\mathcal{O}(\Delta t^4)$ accurate and is, in general, more stable than forward Euler time integration ($\mathcal{O}(\Delta t)$ accurate). Consider a general vector function $\vec{y}(t)$, of which the value at time t_n is known and the value of $t_n + \Delta t$ is to be calculated. The forward Euler method takes one time step to calculate the value at its new position. The RK4 scheme takes three intermediate time steps to find a more accurate solution for $\vec{y}(t + \Delta t)$. For a system of ordinary differential equations, given by $\frac{\mathrm{d}\vec{y}}{\mathrm{d}t} = \vec{f}(\vec{y}, t_n)$, the scheme is as follows:

$$\begin{aligned}
\vec{\kappa_1} &= \Delta t \vec{f}(\vec{y}, t), \\
\vec{\kappa_2} &= \Delta t \vec{f}(\vec{y} + \frac{1}{2}\vec{\kappa_1}, t + \frac{1}{2}\Delta t), \\
\vec{\kappa_3} &= \Delta t \vec{f}(\vec{y} + \frac{1}{2}\vec{\kappa_2}, t + \frac{1}{2}\Delta t), \\
\vec{\kappa_4} &= \Delta t \vec{f}(\vec{y} + \vec{\kappa_3}, t + \Delta t). \\
\vec{y}(t + \Delta t) &= \vec{y}(t) + \frac{1}{6}\vec{\kappa}_1 + \frac{1}{3}\vec{\kappa}_2 + \frac{1}{3}\vec{\kappa}_3 + \frac{1}{6}\vec{\kappa}_4.
\end{aligned}$$

The four stages are shown in Figure **??**. The coefficients $\vec{\kappa}_i$ are added in such a way that error terms of order $\mathcal{O}(\Delta t^2)$, $\mathcal{O}(\Delta t^3)$ and $\mathcal{O}(\Delta t^4)$ exactly cancel each other. When the RK4 scheme is applied to the shallow water equations (equation **??**), vector $\vec{y}$ has length 2, with $y_1 = r^+$ and $y_2 = r^-$.

Each time step Δt, new values of r_i^+ and r_i^- are calculated via equation **??**. With the new values of $r^\pm$, the new characteristic velocities are found, via

$$c_i^+ = \frac{3}{4}r_i^+ + \frac{1}{4}r_i^-, \qquad\qquad c_i^+ = \frac{1}{4}r_i^+ + \frac{3}{4}r_i^-.$$

For both the positive (r^+) and negative (r^-) Riemann variables, the new position is calculated. At each grid point x_i, the new position of the positive Riemann variable is denoted by x_i^+, and the new position for the negative

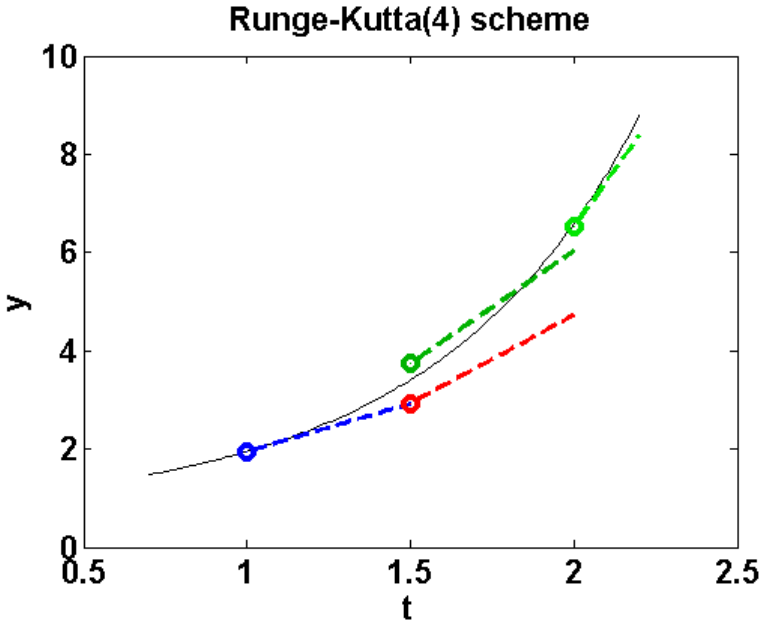

Figure 3.1: Example of Runge-Kutta(4) scheme for function $y(t) = \exp(\frac{2}{3}t^{\frac{3}{2}})$. The blue line indicates the first RK4-step, the red line the second, the green line the third and the yellow line the fourth.

Riemann variable is denoted by x_i^-. The new positions are found via

$$x_i^+ = x_i + c_i^+ \Delta t, \qquad x_i^- = x_i + c_i^- \Delta t.$$

Finally, the values of r^+ and r^- are linearly interpolated back to the original grid points x_i. At x_1, r^+ is prescribed by boundary conditions, at x_{nx}, r^- is prescribed by boundary conditions. To avoid that no value is appointed to an internal grid point ($2 < i < nx - 1$), the Riemann variable should not be allowed to move over a distance larger than the grid size, so $|c_i^+ \Delta t| \leq \Delta x$ and $|c_i^- \Delta t| \leq \Delta x \quad \forall\ i$.

In an earlier version of the NM-P model the shallow water equations were solved without being transformed into Riemann variables. These equations still contained spatial derivatives. A method for nondimensionalising and discretising equations **??-??** is provided in Appendix C.

3.2 Discretisation Tidal Flat

3.2.1 NM-P model

In the NM-P model the sea level and velocity are calculated at a single point on the tidal flat. The variables are assumed to be uniform over the width of the tidal flat. The tidal flat is connected to one grid point on each side of the tidal flat. At these grid points, a single value for sea level exists (η_1 in channel 1 and η_2 in channel 2). After each time step Δt, values for η_{tf} and u_{tf} are calculated based on η_1 and η_2. When $\eta_1 > 0$ and $\eta_2 > 0$, u_{tf} is calculated by discretising equation **??** via the Forward Euler method:

$$u_{tf}^{t+\Delta t} = u_{tf}^t - g\frac{\eta_2^t - \eta_1^t}{L_{tf}} - C_{d,tf}\frac{u_{tf}^t |u_{tf}^t|}{\eta_{tf}^t}. \tag{3.1}$$

Superscript t indicates the value of a variable at time t, superscript $t + \Delta t$ at time $t + \Delta t$. No spatial discretisation is required.

3.2.2 NM-F model

The tidal flat is treated as a channel in the NM-F model. As such, it is also discretised as a tidal channel. See section 3.1.

3.3 Breaking Waves

The breaking is resolved as described in Section 2.3.2. The goal is to find a vertical line that cuts off exactly the same amount of overhanging wave as is required to fill the empty space below the remainder of the overhanging wave. Numerically, for each breaking wave, a number of steps are taken (illustrated in Figure **??**):

1.	The breaking domain is established (x_{min} to x_{max}), $X \equiv x_{max} - x_{min}$
2.	The breaking range is established (r_{min} to r_{max} within domain), $R \equiv r_{max} - r_{min}$
3.	A tolerance error is defined: $\epsilon \equiv \alpha X R$, with α typically $\alpha = 10^{-5}$
4.	A first estimate for x-location of the horizontal line is made: $x_b = \frac{x_{max}-x_{min}}{2}$.
5a.	The area of overhanging part A is calculated via numerical integration
5b.	The area of the remainder of the breaking wave B is calculcated via numerical integration.
6.	If area A and area B are equal within tolerance ϵ, the solution is accepted.
7.	If solution is not accepted, x_b is moved slightly to the left and right with distance δx
8.	At $x = x_b + \delta x$ and $x = x_b - \delta x$, the area's of A and B are calculated.
9.	$\delta x = \delta x/2$,
10.	Via Newton-Raphson a new position x_b is obtained.
11.	Go to point 5a. with new x_b

The wave breaking procedure is applied to breaking waves in both r^+ and r^-.

In step 10 the Newton-Raphson (NR) method is used to find a new position for x_b. NR is a method that finds the zero's of a function. Here, the function $\Delta(x_b)$ that should be zero is $\Delta(x_b) = A(x_b) - B(x_b)$. The derivative of $\Delta(x_b)$ is obtained via

$$\frac{\partial \Delta(x_b)}{\partial x_b} = \frac{\Delta(x_b + \delta x) - \Delta(x_b - \delta x)}{2}.$$

The NR formula is provided in equation **??**.

3.4 Boundary Conditions

3.4.1 Open Boundary

At the open boundary, either the sea level or an incoming wave is prescribed. In case the sea level is prescribed, $\eta_{i=1} = A * \sin(\omega t + \phi)$, which translates to $r^+_{i=1} = r^-_{i=1} + 4\sqrt{g(A\sin(\omega t + \phi) + H)}$. In case the incoming wave is prescribed, the positive Riemann variable is prescribed as $r^+_{i=1} = 4\sqrt{g(H + (A\sin(\omega t + \phi) + H)} - 2\sqrt{gH}$.

3.4.2 Internal Nodes

NM-P model

In the NM-P model, the boundary between the tidal flat and the channel (as shown in Figure **??**) is compressed into a single grid point in the channel. Mass and momentum exchange via the tidal flat only takes place at this single grid point, denoted by x_f. The equation describing the nodal point, **??**, is spatially discretised via

$$\frac{dr^{\pm}_i}{dt} = -\frac{C_d|u_i|u_i}{H+\eta_i} \mp \sqrt{\frac{g}{H+\eta_i}}\frac{u_{tf}\eta_{tf}}{W} + \mathcal{H}(-u_{tf})\frac{\Delta u}{H+\eta_i}\frac{u_{tf}\eta_{tf}}{W} \qquad x_i = x_f, \tag{3.2}$$

and temporally discretised with the RK4 scheme.

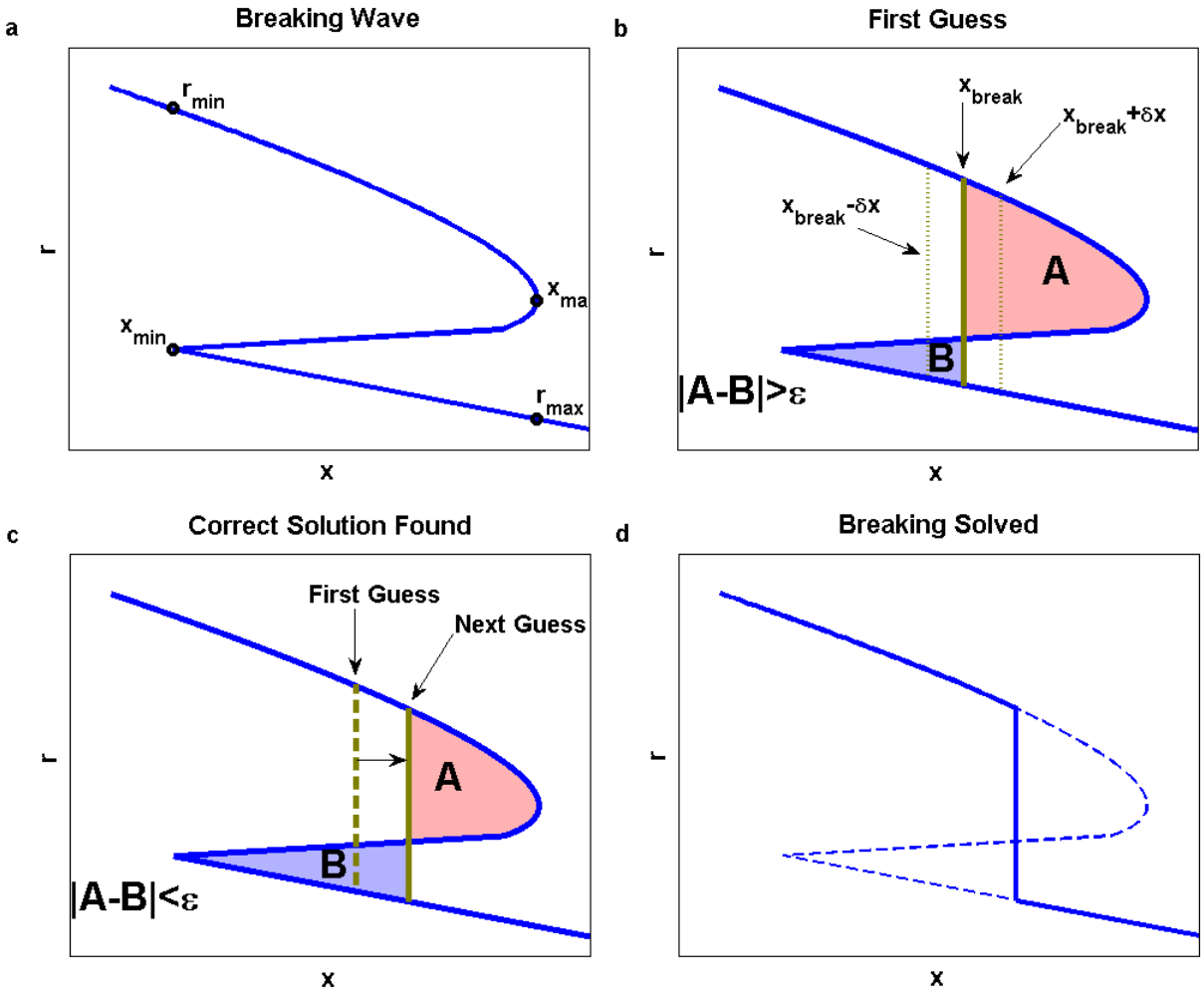

Figure 3.2: Resolving of a breaking wave. In subfigure a, a breaking wave is presented. The extremes x_{min}, x_{max}, r_{min}, r_{max} are calculated. In subfigure b, a first guess for x_{break} is made. Based on this guess, area's A and B are calculated. The same is done for $x_{break} + \delta x$ and $x_{break} - \delta x$. For x_{break}, $|A - B|$ is still larger than the tolerance. In subfigure c, a new position of x_{break} is calculated based on the area's A and B calculated in subfigure b. Now, $|A - B|$ is smaller than the tolerance and the solution is accepted, as is visible in subfigure d.

NM-F model
In the NM-F, the matching conditions from equations **??**-**??** are applied at internal nodes. From the matching conditions, analytical expressions for the unknown values are obtained. The analytical expressions are polynomials of degree three. To obtain a unique numerical value for the unknown variables, the polynomials are solved using a numerical method. This method is presented in Appendix A.3.

3.4.3 Closed Boundary

At closed boundaries, $r^- = -r^+$. After interpolation to the original x_i-grid, $r^-_{nx} = -r^+_{nx}$ is applied at the closed boundaries of the channels. When the NM-F model is applied to the T-geometry, the tidal flat has a closed boundary as well. The tidal flat in the NM-F model is also described in terms of Riemann variables and $r^-_{nx} = -r^+_{nx}$ is applied at the closed boundary of the tidal flat.

Chapter 4

Results

In this chapter the results of experiments done with the NM-P model and the NM-F model are presented. The NM-P model is used to quantify the cross-tidal flat mass transport and the dependence of cross-tidal flat mass transport on various system parameters. The NM-P model is also used to investigate the effect of cross-tidal flat mass transport on tidal dynamics. The NM-F model explicitly calculates the dynamics over a tidal flat, providing a spatial distribution of sea level and velocity over the tidal flat. Simulations by the NM-F model are compared to simulations by other numerical models.

The experiments done with the NM-P model are run in an H-geometry, in which two tidal channels are connected through a tidal flat in their interior (see Figure **??**). The NM-F model is run in a T-geometry (Figure **??**). At the end of the chapter, a simulation with the NM-F model run in the H-geometry is presented as well. First, the results of the NM-P model are shown.

4.1 Results NM-P Model

The NM-P model is run for the H-geometry (Figure **??**). The system is defined by a large number of parameters that can all be varied. Each parameter may affect the cross-tidal flat mass transport and the overtides generated in the tidal channels. The parameters are varied one at a time, while other parameters are kept constant. A control run will serve as reference for runs with varied parameters. Analysis of the results will be based on the amount of (net) cross-tidal flat mass transport, the amplitudes of the harmonics and the phases of the harmonics.

The parameters of the control run are found in Table **??**. In reality, the geometries of tidal systems in which cross-tidal flat mass transport occurs vary greatly. Channel depth may vary from several hundreds of meters up to almost zero meters, the width may vary from very narrow (several tens of meters) up to kilometres wide. The geometry of the channels is chosen such that channel length, width and depth have typical values for tidal systems, much smaller than their maximal values in reality and much larger than their minimal values in reality. The geometry of the tidal flat is chosen based on the same arguments as the geometry of the channel. From a physical point of view, the width of the tidal flat is limited to the grid size in the adjacent channels, Δx, in this model $\Delta x = 2$km. At the open boundary the sea level oscillation has an amplitude of approximately 1m, typical for tidal systems.

Parameters that will be varied in this section are phase difference at the open boundary ϕ, the boundary condition at the open boundary, the location of the tidal flat in the channels, tidal flat width, depth and bottom friction, and channel width and depth. Also, a simulation by the NM-P model is compared to a simulation run with the original tidal flat parameterisation by **?** (see Appendix ??).

Two tidal cycles are used spin-up the system to an equilibrium state. The analysis of the results is based on three more cycles after the spin-up.

Run	L_1 (km)	L_2 (km)	H_1 (m)	H_2 (m)	W_1 (m)	W_2 (m)	L_{tf} (m)	H_{tf} (m)
Control	40	40	10	10	200	200	2000	0
	W_{tf} (m)	$C_{d,tf}$	$\phi(^\circ)$	B.C.O.B.	A_1(m)	A_2(m)	C_1(km)	C_2(km)
Control	2000	0.01	30	inc.wave	0.6	0.6	20	20

Table 4.1: The parameters used in the control run. Subscript 1 indicates channel 1, subscript 2 indicates channel 2, subscript tf indicates tidal flat. L represents channel length, H channel depth, W channel width, C_d is bottom friction coefficient, ϕ is the phase difference, B.C.O.B. stands for boundary condition at the open boundary (either incoming wave or sea level), A is the amplitude of the prescribed boundary conditions at the open boundary and C is the location in the channel at which the tidal flat is connected to the tidal channel, measured in distance from open boundary

4.1.1 Control Run

The control run is executed with the parameter values as shown in Table **??**. Here, its main features are discussed. In Figure **??** the instantaneous mass transport and the cumulative mass transport are shown.

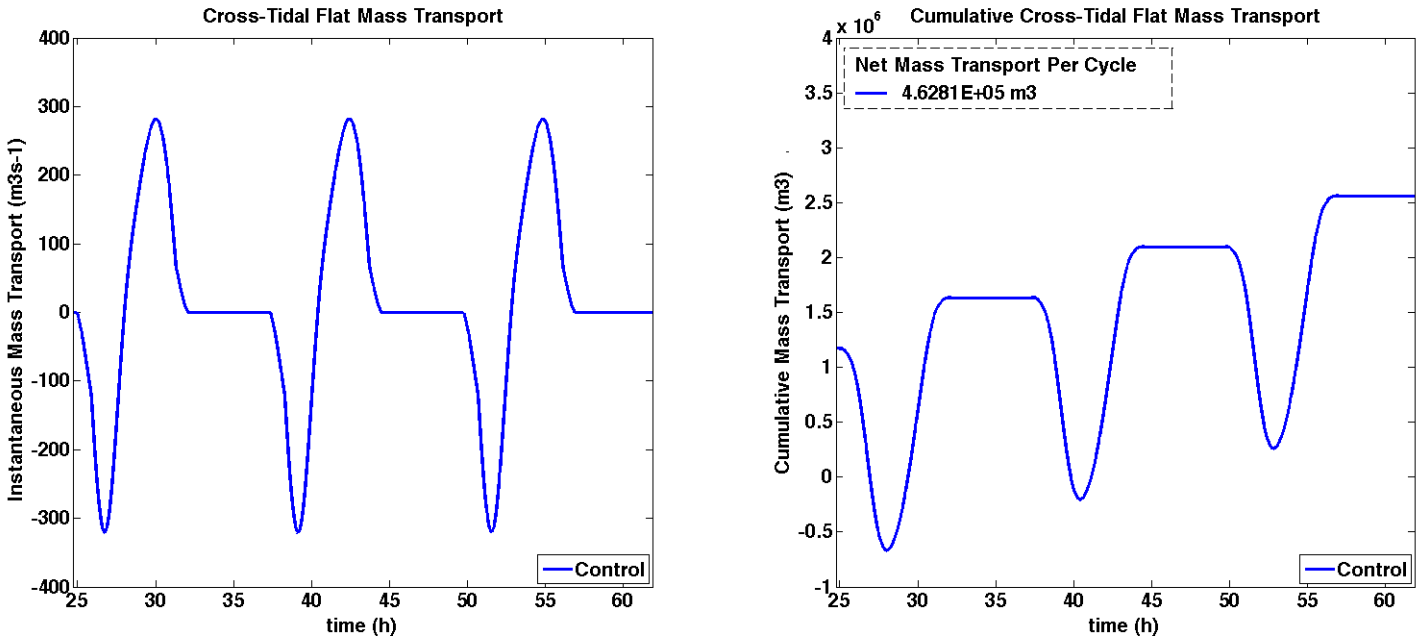

Figure 4.1: On the left the instantaneous mass transport (in $m^3\ s^{-1}$)is shown for three consecutive tidal cycles for the control run. On the right the sum of all mass transported over the tidal flat is plotted against time for the control run. The net transport per cycle(in m^3) is shown in the top left corner.

In the control run, the tidal wave enters channel 2 before it enters channel 1. While water level is rising in both channels, water level in channel 2 will be higher than in channel 1, leading to a mass transport from channel 2 into channel 1. Mass transport is defined positive from channel 1 into channel 2. When water levels are falling again, water level in channel 1 is higher than in channel 2 and mass will be transported from channel 1 to channel 2. In one tidal cycle $1.84 * 10^6 m^3$ of mass flows from channel 2 to channel 1, after which $2.30 * 10^6 m^3$ of mass flows from channel 1 to channel 2, resulting in a net mass transport of $4.63 * 10^5 m^3$ from channel 1 into channel 2. This is approximately 3% of the total mass that enters channel 1 via the open boundary during a tidal cycle. These mass transports are shown in Table **??**

A harmonic analysis decomposes the signal in sea level and velocity into sinusoidal waves with a frequency of (higher) harmonics. This technique is applied to the sea level and velocity in channel 1 and channel 2 of

Run	Leading channel	$T_{2\to1}$ (m^3)	$T_{1\to2}$ (m^3)	T_{net} (m^3)	$T_{inc,ch1}$ (m^3)
Control	2	$1.84 * 10^6$	$2.30 * 10^6$	$4.63 * 10^5$	$1.60 * 10^7$

Table 4.2: Transports per cycle in the control run. The leading channel indicates in which channel high water first arrives at the tidal flat. $T_{2\to1}$ and $T_{1\to2}$ indicate cross-tidal flat mass transport from channel 2 to channel 1 and from channel 1 to channel 2. The net cross-tidal flat mass transport is denoted by T_{net} (transport from channel 1 to channel 2 is defined positive). As a reference value, the amount of mass entering channel 1 at the open boundary, $T_{inc,ch1}$ is shown.

the control run. The results are shown in Figure **??**. The signal in sea level in both channel 1 and channel 2 is dominated by the M_2 tidal constituent, with an amplitude of 1m and larger. In channel 1 the M_4 tidal constituent has an amplitude of 5cm at the open boundary, rising to 8cm at the closed boundary. In channel 1, the M_0 and M_6 constituents have amplitudes of 2cm and less. The largest amplitude of the higher harmonics is found at the location of the tidal flat, where mass leaves and enters the channel, both in channel 1 and channel 2. In channel 2 the amplitude of the higher harmonics is smaller than in channel 1.

The amplitude of the velocity harmonics is also dominated by the M_2 constituent. At the location of the tidal flat, the velocity signal perturbed by the cross-tidal flat mass transport. In both channel 1 and channel 2, a shift in trend is visible; In channel 1 the velocity shift is downwards (relatively smaller velocities), in channel 2 the shift is upwards. At the open boundary, the M_2 velocity amplitude in channel 1 is 0.54ms^{-1}, in channel 2 it is 0.68ms^{-1}. The other harmonic components show a similar shift at the location of the tidal flat, albeit smaller in amplitude.

The phases of the different harmonic components are plotted in Figure **??**. The M_2-signal in sea level has a constant phase in channel 1 and channel 2. Combined with the fact that the M_2 velocity phases are constant and are lagging the sea level signal by 90°, the M_2 signal is a standing wave. In channel 1, the M_4 sea level signal has a decreasing phase from the open boundary to the tidal flat, indicating that a wave is moving out of the domain. Landward of the tidal flat, a standing M_4 wave is present. A possible explanation is that a M_4 sea level signal is generated at the location of the tidal flat by cross-tidal flat mass transport. This M_4 sea level signal is reflected at the closed boundary, leading to a standing wave landward of the tidal flat. Seaward of the tidal flat, the wave leaves the domain at the open boundary. In channel 1, the M_6 sea level signal shows a continuous decreasing trend in the phase, with a disturbance at the tidal flat. The M_4 sea level signal in channel 2 shows the same qualitative behaviour as the M_4 sea level in channel 1. The velocity signals in channel 1 and 2 show the same qualitative behaviour. The M_2 signal is constant. The M_4 and M_6 signal have a decreasing phase from the open boundary to the tidal flat. At the tidal flat, a phase jump is observed, after which the phases are constant.

The results shown in this section will be used as a reference for the proceeding experiments, in which parameters are varied. The new results are compared to the control run by looking at the difference between the two runs.

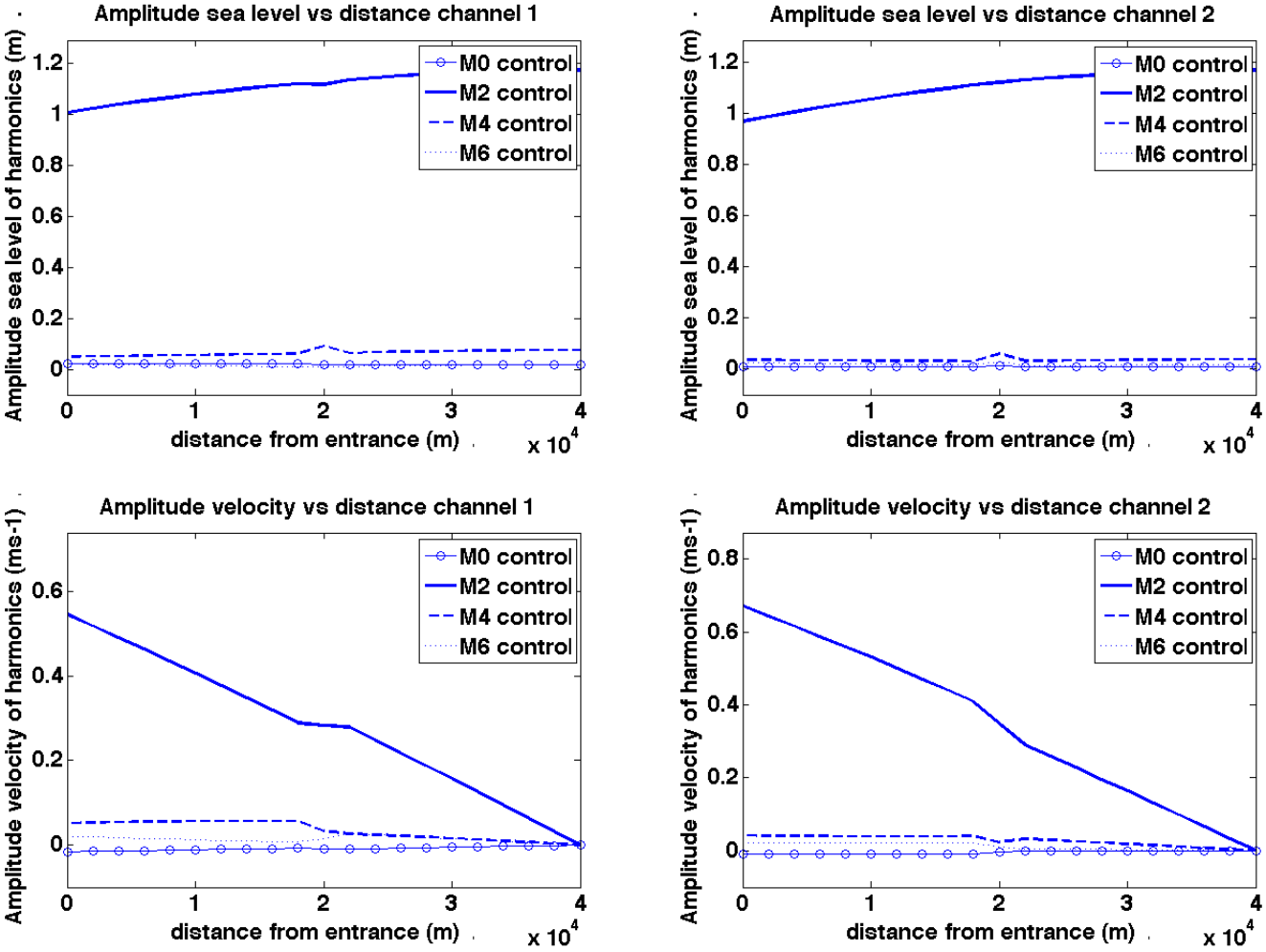

Figure 4.2: Top: Harmonic analysis of the sea level in channel 1 (left) and channel 2 (right) for the control run . Bottom: Harmonic analysis of the along-channel velocity in channel 1 (left) and channel 2 (right) for the control run.

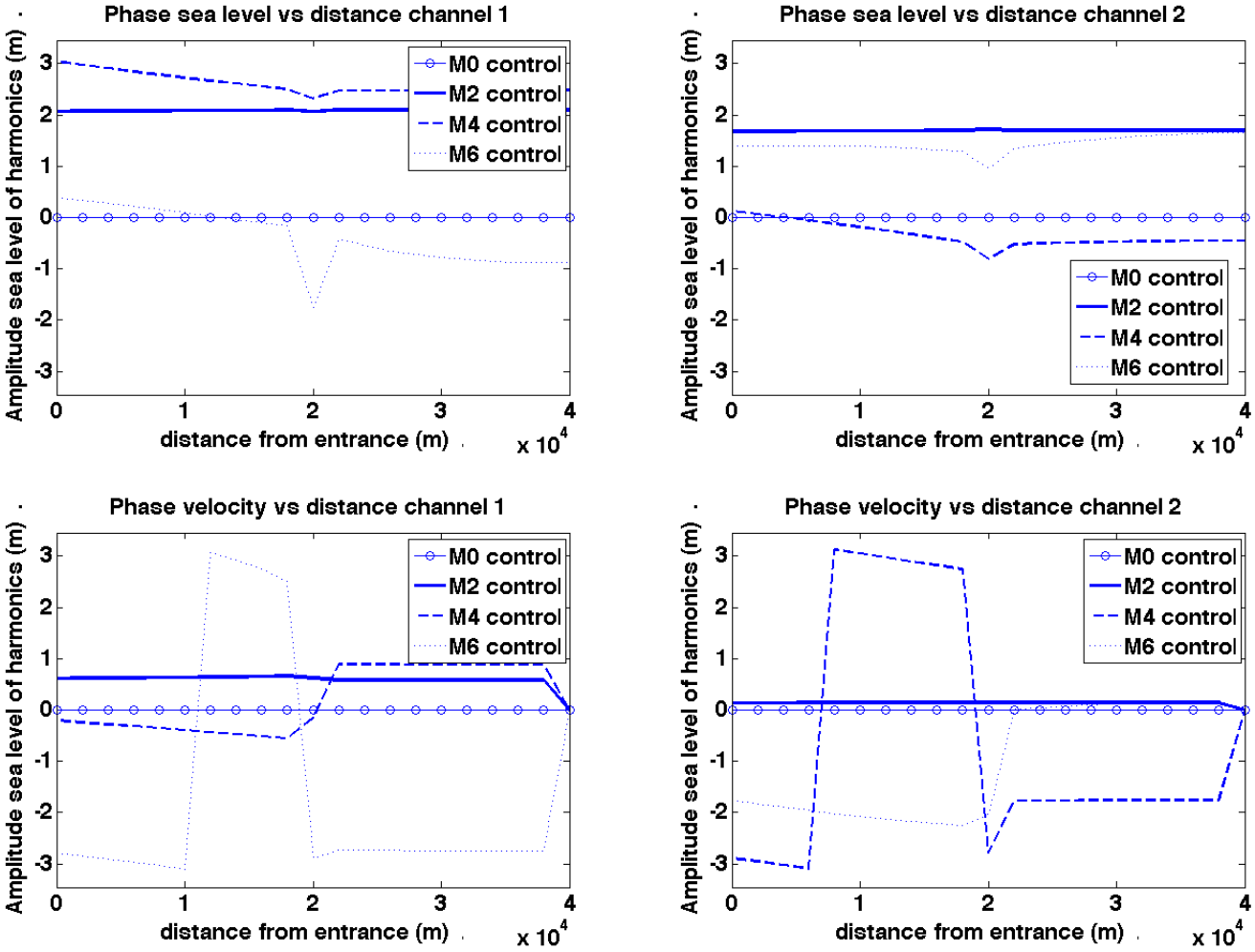

Figure 4.3: Top: Phases of the different sea level constituents in channel 1 (left) and channel 2 (right) for the control run . Bottom: Phases of the along-channel velocity constituents in channel 1 (left) and channel 2 (right) for the control run.

4.1.2 Phase difference

In the control run, a phase difference of $+30^\circ$ is applied to the forcing at the open boundary in channel 2. The phase difference results in cross-tidal flat mass transport. In this subsection the sensitivity of cross-tidal flat mass transport to the phase difference is considered. The cross-tidal flat mass transport is calculated for a wide range of phases. The harmonic analysis for runs with phases differences of 0° and $+90^\circ$ is compared to the harmonics of the control run.

In Table **??**, the cross-tidal flat mass transport is shown for various phase differences. When the phase difference increases, more cross-tidal flat mass transport takes place, both from channel 2 to channel 1 and vice versa. Maximal transport values are found with the largest phase difference of $\phi = 180^\circ$. In that case, the magnitude of the cross-tidal flat mass flux is three times as small as the mass flux entering channel 1 at the open boundary, thus, 25% of the mass that enters channel 1 enters the channel via cross-tidal flat mass transport. The mass flux that enters the channels is strongly affected by the cross-tidal flat mass transport. When $\phi = +90^\circ$ the mass flux at the open boundary in channel 1 is 30% smaller compared to a run in which $\phi = -60^\circ$. The largest net transport is found at $\phi = \pm 60^\circ$, directed from the lagging to the leading channel.

In the harmonic analysis (both amplitude and phase), the runs with $\phi = 0^\circ$ and $\phi = 90^\circ$ are compared to the control run ($\phi = 30^\circ$). To visualise the effects of the cross-tidal flat mass transport, the difference between $\phi = 30^\circ$ and $\phi = 0^\circ$, and between $\phi = 90^\circ$ and $\phi = 0^\circ$ is plotted. In Figure **??** the amplitude difference of the harmonics is plotted, in Figure **??** the phase difference of the harmonics is plotted.

Compared to a run without any phase difference in the prescribed incoming wave at the open boundary (and thus without cross-tidal flat mass transport), differences are observed with runs in which a phase difference is applied at the open boundary. The sea level in channel 1 shows small changes in M_0 and M_6 throughout the channel. A strong increase in M_4 sea level amplitude is present in both channel 1 and channel 2. The increase is stronger when the phase difference at the open boundary is larger. The M_2 sea level in channel 1 has small differences for a 30° phase difference, but a large negative difference for the 90° phase difference. In channel 2 the differences between no phase difference and phase difference are larger than in channel 1. The M_2 sea level is a couple of centimetres smaller throughout the channel for the 30° phase difference run, for the 90° phase difference run M_2 is 15 centimetres smaller throughout the channel. The differences in M_6 sea level remain small in channel 2, differences in M_0 sea level are larger, and more negative with increasing phase difference.

The difference in velocity amplitude is large seaward of the tidal flat. Relatively small differences exists landward of the tidal flat. At the tidal flat, all harmonics experience a jump in their amplitude, most strongly the M_2 tidal constituents. In both channels M_4 increases. Larger increases in M_4 coincide with larger phase differences. A strong jump in the M_2 is observed in both channels at the location of the tidal flat. In channel 1 this jump is negative, in channel 2 the jump is positive. The jumps are larger when phase differences and cross-tidal flat mass transport are larger. In channel 1, differences in M_0 and M_6 are small. In channel 2, differences in M_6 are small as well, but differences in M_0 are larger (up to 1.5cms^{-1} for 30° phase difference, up to 3cms^{-1} for 90° phase difference).

In channel 1 the M_2 the phase of the sea level signal is not affected by cross-tidal flat mass transport. The phase of the M_4 sea level signal in channel 1 has been shifted. Landward of the tidal flat is has a constant phase, seaward of the tidal flat the phase decreases from the open boundary to the tidal flat. This is associated with a wave progressing from the tidal flat to the open boundary. The phase difference between the $\phi = 30^\circ$ run and the $\phi = 90^\circ$ run is constant in the entire domain, and their mutual difference is approximately $\phi = 60^\circ$, with the $\phi = 30^\circ$ run lagging the $\phi = 90^\circ$ run. The same is true for the other M_4 signals in sea level and velocity, although the phase difference is slightly smaller than $\phi = 60^\circ$ in channel 1 and slightly larger in channel 2. The M_4 signal is thus dominantly caused by cross-tidal flat mass transport. In channel 1, the M_2 velocity signal is only weakly affected by cross-tidal flat mass transport. In channel 2 both the M_2 velocity and sea level difference is strongly affected by cross-tidal flat mass transport, with the difference becoming larger with increasing phase difference at the open boundary. The phase shift is constant throughout the channel and has approximately the same magnitude in the sea level and in the velocity signal. The shift in the run with $\phi = 30^\circ$ is approximately -30° (-26° in sea level, -28° in velocity), the shift in the run with $\phi = 30^\circ$ is approximately -90° (-85° in

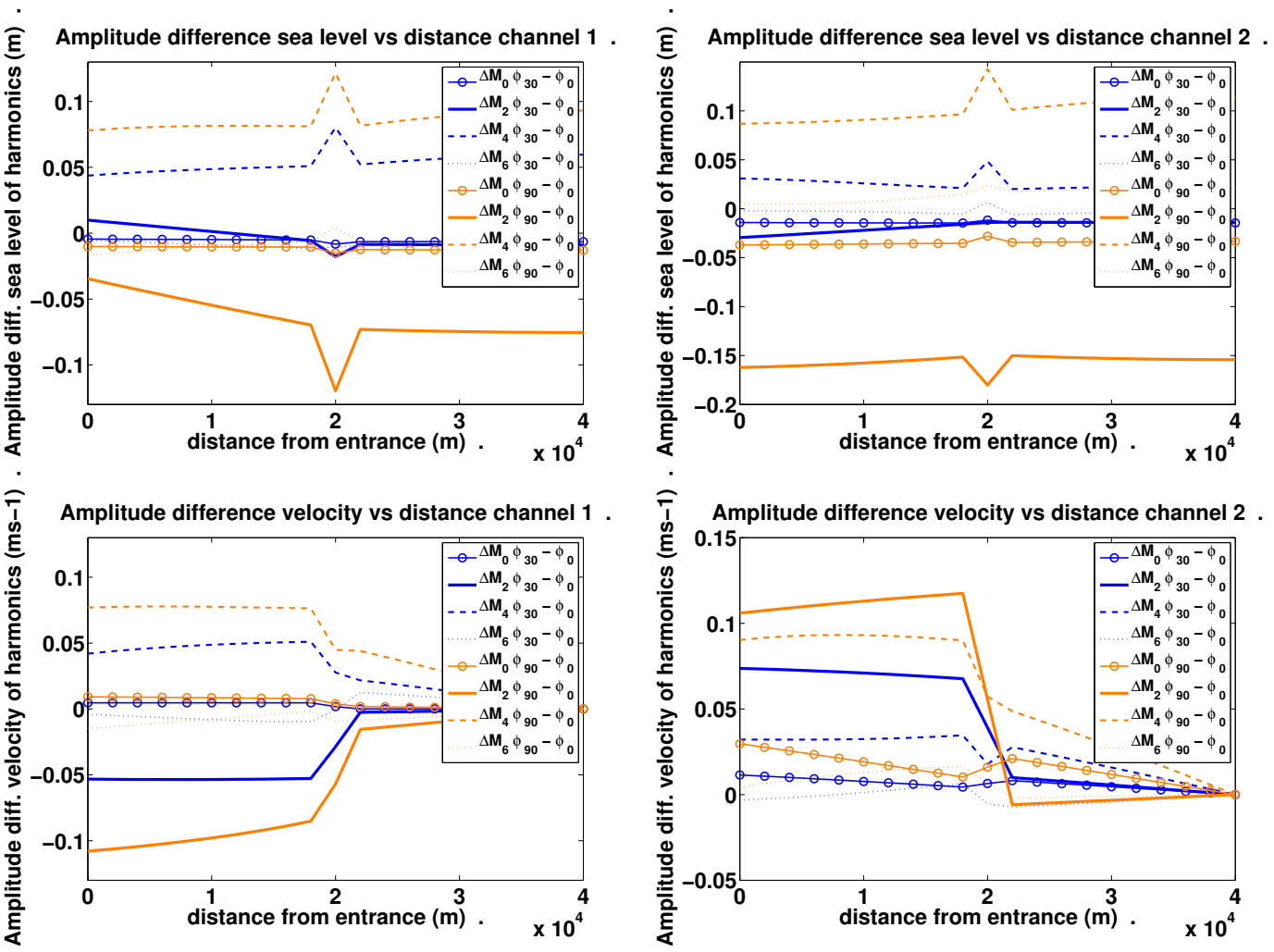

Figure 4.4: Top: Harmonic analysis of the sea level amplitude difference between $\phi = 30°$ phase difference at the open boundary and $\phi = 0°$ (in blue) and between $\phi = 90°$ phase difference at the open boundary and $\phi = 0°$ (in orange) in channel 1 (left) and channel 2 (right). Bottom: Harmonic analysis of the along-channel velocity amplitude difference between $\phi = 30°$ phase difference at the open boundary and $\phi = 0°$ (in blue) and between $\phi = 90°$ phase difference at the open boundary and $\phi = 0°$ (in orange) in channel 1 (left) and channel 2 (right).

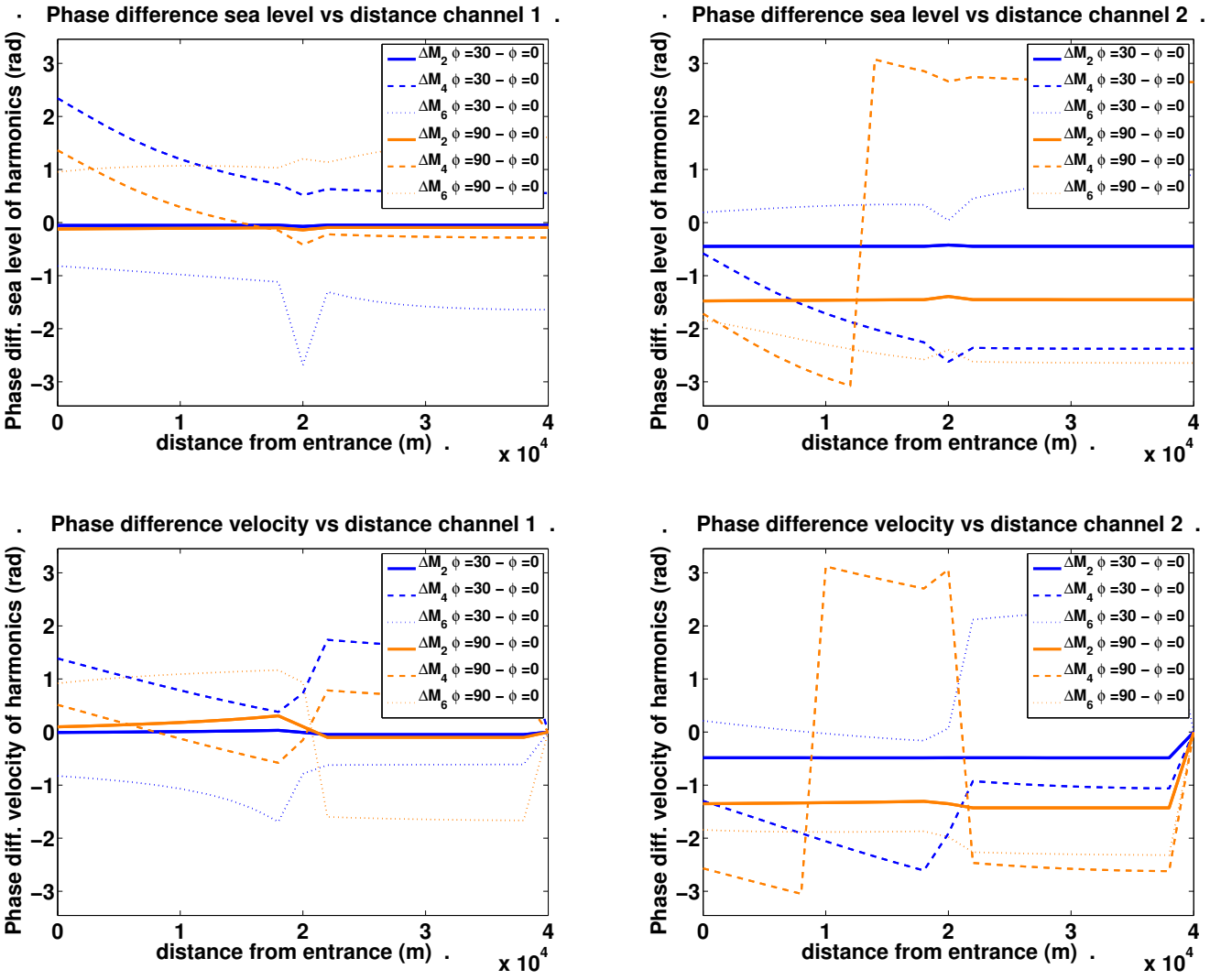

Figure 4.5: Top: Harmonic analysis of the sea level phase difference between $\phi = 30°$ phase difference at the open boundary and $\phi = 0°$ (in blue) and between $\phi = 90°$ phase difference at the open boundary and $\phi = 0°$ (in orange) in channel 1 (left) and channel 2 (right). Bottom: Harmonic analysis of the along-channel velocity phase difference between $\phi = 30°$ phase difference at the open boundary and $\phi = 0°$ (in blue) and between $\phi = 90°$ phase difference at the open boundary and $\phi = 0°$ (in orange) in channel 1 (left) and channel 2 (right).

Run	Leading channel	$T_{2\to1}$ (m^3)	$T_{1\to2}$ (m^3)	T_{net} (m^3)	$T_{inc,ch1}$ (m^3)
$\phi = 0°$	-	0	0	0	$1.80 * 10^7$
$\phi = 30°$ (Control)	2	$1.84 * 10^6$	$2.30 * 10^6$	$4.63 * 10^5$	$1.60 * 10^7$
$\phi = 45°$	2	$2.60 * 10^6$	$3.17 * 10^6$	$5.72 * 10^5$	$1.52 * 10^7$
$\phi = 60°$	2	$3.31 * 10^6$	$3.92 * 10^6$	$6.06 * 10^5$	$1.46 * 10^7$
$\phi = 90°$	2	$4.50 * 10^6$	$4.97 * 10^6$	$4.71 * 10^5$	$1.43 * 10^7$
$\phi = 120°$	2	$5.19 * 10^6$	$5.39 * 10^6$	$2.01 * 10^5$	$1.43 * 10^7$
$\phi = 180°$	-	$5.81 * 10^6$	$5.80 * 10^6$	$-1.19 * 10^4$	$1.59 * 10^7$
$\phi = -30°$	1	$2.99 * 10^6$	$2.53 * 10^6$	$-4.62 * 10^5$	$1.96 * 10^7$
$\phi = -45°$	1	$3.95 * 10^6$	$3.38 * 10^6$	$-5.73 * 10^5$	$2.00 * 10^7$
$\phi = -60°$	1	$4.70 * 10^6$	$4.10 * 10^6$	$-6.04 * 10^5$	$2.01 * 10^7$
$\phi = -90°$	1	$5.53 * 10^6$	$5.07 * 10^6$	$-4.53 * 10^5$	$1.98 * 10^7$
$\phi = -120°$	1	$5.63 * 10^6$	$5.48 * 10^6$	$-1.47 * 10^5$	$1.88 * 10^7$

Table 4.3: Transports per cycle for runs with varying phase differences at open boundary. The leading channel indicates in which channel high water first arrives at the tidal flat. $T_{2\to1}$ and $T_{1\to2}$ indicate cross-tidal flat mass transport from channel 2 to channel 1 and from channel 1 to channel 2. The net cross-tidal flat mass transport is denoted by T_{net} (transport from channel 1 to channel 2 is defined positive). As a reference value, the amount of mass entering channel 1 at the open boundary, $T_{inc,ch1}$ is shown.

sea level, $-77°$ in velocity). The phase difference of the M_6 signal does not show deviations associated with the phase difference applied at the open boundary. Also, the M_6 signal shows no qualitative agreement between the $\phi = 30°$ run and the $\phi = 90°$ run. It should be mentioned that the M_6 signal has a small amplitude throughout the channels in both velocity and sea level and is thus easily affected by small changed. This may explain the lack of consistent phase shifts in M_6. The phase shift in M_0 is 0 and is not shown here, because M_0 has no phase by construction.

4.1.3 Varying Tidal Flat Parameterisation

In section 2.2.1 the parameterisation of sea level and velocity is described for the NM-P model. The parameterisation is based on a parameterisation by **?** (see Appendix E), but is adjusted at two places. Firstly, **?** applies a velocity parameterisation developed for describing weirs during part of the tidal cycle, whereas the velocity parameterisation in the NM-P model is based on a balance between pressure gradient and bottom friction. Secondly, **?** assumes no momentum loss over the tidal flat. The NM-P model does account for momentum loss over the tidal flat. The effect of both adjustments is assessed in this experiment.

The NM-P model can be run in three modes, mode 1, mode 2 and mode 3. Mode 1 corresponds to the original parameterisation by **?**. In mode 2, the velocity over the tidal flat is described by a balance between pressure gradient and bottom friction during the entire cycle, but momentum is assumed to be conserved over the tidal flat. Mode 3 is the mode that is described in section 2.2.1 and is used in the control run. Compared to mode 2, mode 3 also takes momentum loss over the tidal flat into account.

In Figure **??** the instantaneous mass transport is plotted for mode 1 and mode 3 (control run). In mode 1, the instantaneous mass transport two spikes are visible per cycle, associated with the Broad Crested Weir Formula (BCWF) . The BCWF is only used when water level on one side of the tidal flat is below the height of the tidal flat and water level on the other side is above tidal flat level. Due to the phase difference of $\phi = 30°$, the BCWF is only applied for a short time interval each cycle. During these time intervals the BCWF strongly overestimates the cross-tidal flat mass transport. Mode 2 produces almost exactly the same instantaneous cross-tidal flat transport as Mode 3. Based on this it is concluded that adding momentum loss over the tidal flat is only a minor improvement to the NM-P model. Values for cross-tidal flat mass transport are shown in Table **??**.

A harmonic analysis, comparing runs in mode 2 and mode 3, shows maximum amplitude difference in the order of $\mathcal{O}(10^{-3})$ m for sea level and $\mathcal{O}(10^{-3})$ ms^{-1}. Phase shifts are also minimal.

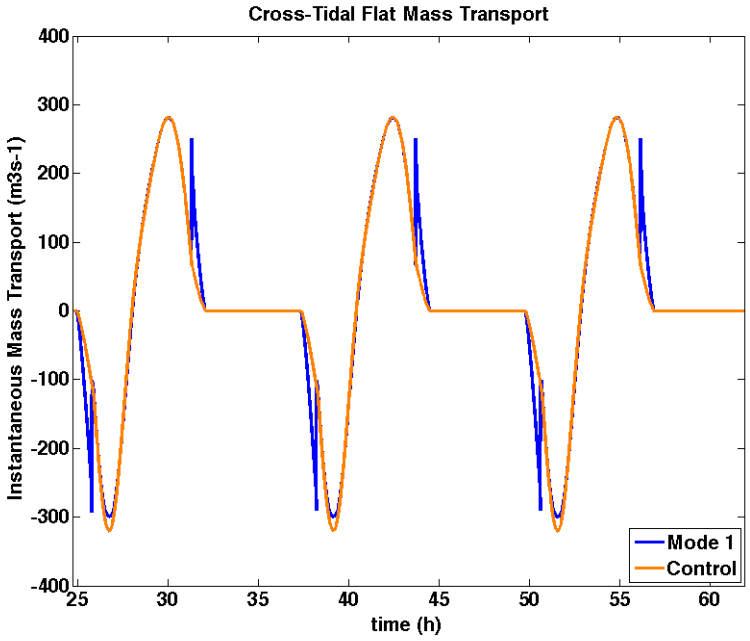

Figure 4.6: The instantaneous mass transport in the control run (Mode 3) compared to the instantaneous mass transport in Mode 1, in which the Hamilton parametrisation is used.

Run	Leading channel	$T_{2\to1}$ (m^3)	$T_{1\to2}$ (m^3)	T_{net} (m^3)	$T_{inc,ch1}$ (m^3)
Mode 1	2	$2.01 * 10^6$	$2.45 * 10^6$	$4.38 * 10^5$	$1.58 * 10^7$
Mode 2	2	$1.84 * 10^6$	$2.30 * 10^6$	$4.68 * 10^5$	$1.60 * 10^7$
Mode 3 (control)	2	$1.84 * 10^6$	$2.30 * 10^6$	$4.63 * 10^5$	$1.60 * 10^7$

Table 4.4: Transports per cycle for runs with different modes. The leading channel indicates in which channel high water first arrives at the tidal flat. $T_{2\to1}$ and $T_{1\to2}$ indicate cross-tidal flat mass transport from channel 2 to channel 1 and from channel 1 to channel 2. The net cross-tidal flat mass transport is denoted by T_{net} (transport from channel 1 to channel 2 is defined positive). As a reference value, the amount of mass entering channel 1 at the open boundary, $T_{inc,ch1}$ is shown.

4.1.4 Boundary Condition at Open Boundary

At the open boundary a boundary condition is prescribed. The model allows for two different boundary conditions to be prescribed, an incoming wave and sea level. A discussion on the difference between the two methods is found in Section 2.1.3. The implication of the different boundary condition is elaborately discussed in Appendix D. The bottom-line is that, when sea level is prescribed, an outgoing wave is reflected at the open boundary whereas an outgoing wave is free to leave the channel when an incoming wave is prescribed. The result is that a reflected outgoing wave also reflects harmonics back into the channel, increasing the amplitude of the some harmonics in the channel when sea level is prescribed at the open boundary. A comparison between runs in which sea level and an incoming wave are prescribed should be carried out with care. To mimic the boundary condition of in the incoming wave as closely as possible, a harmonic analysis of the sea level in the control run has been performed, providing the amplitude and phase of the M_0, M_2, M_4 and M_6 tidal constituent at the open boundary. The sea level prescribed at the open boundary is constructed by combining the tidal constituents.

The magnitude of the cross-tidal flat mass fluxes is shown in Table **??**. When sea level is prescribed at the open boundary less mass is transported over the tidal flat during one tidal cycle, but the net mass transport is larger. The harmonic analysis is shown in Figure **??**. The M_2-components of the velocity and sea level show small differences. As expected from theory (see Appendix D), runs in which sea level is prescribed contain stronger higher harmonics. The sea level and velocity in channel 1 and channel 2 contain stronger M_6 constituents. The sea level in channel 1 has a M_6 component difference increasing to 5cm at the closed boundary. A less strong increase is observed in the sea level in channel 2. The M_2 and M_0 signals remains almost unaffected in sea level and velocity in both channel 1 and channel 2. The difference in M_4 constituents remain small in general, except for the velocity in channel 1. Where the M_4 differences in sea level show a maximal deviation of 1cm and the M_4 difference in velocity in channel 2 has a maximal deviation of 7mms^{-1}, the deviation in the velocity in channel 1 is almost 3cms^{-1} at the open boundary. This deviation is negative: The M_4 signal is stronger when an incoming wave is prescribed at the open boundary.

Phase differences are also observed (see Figure **??**). The M_2 component remains almost unaffected, but the M_4 and M_6 signals are affected. The M_4 signals experience a phase shift of at most 38° (velocity channel 1). The M_6 signal has much stronger phase shifts at some occasions. It should be mentioned that both the M_4 and M_6 components have a small amplitude in the control run and are thus easily affected by changes in forcing.

Run	Leading channel	$T_{2\to1}$ (m^3)	$T_{1\to2}$ (m^3)	T_{net} (m^3)	$T_{inc,ch1}$ (m^3)
Sea Level	2	$1.66 * 10^6$	$2.20 * 10^6$	$5.41 * 10^5$	$1.54 * 10^7$
Incoming Wave	2	$1.84 * 10^6$	$2.30 * 10^6$	$4.63 * 10^5$	$1.60 * 10^7$

Table 4.5: Transports per cycle for a run in which sea level is prescribed at the open boundary and a run in which an incoming wave is prescribed at the open boundary. The leading channel indicates in which channel high water first arrives at the tidal flat. $T_{2\to1}$ and $T_{1\to2}$ indicate cross-tidal flat mass transport from channel 2 to channel 1 and from channel 1 to channel 2. The net cross-tidal flat mass transport is denoted by T_{net} (transport from channel 1 to channel 2 is defined positive). As a reference value, the amount of mass entering channel 1 at the open boundary, $T_{inc,ch1}$ is shown.

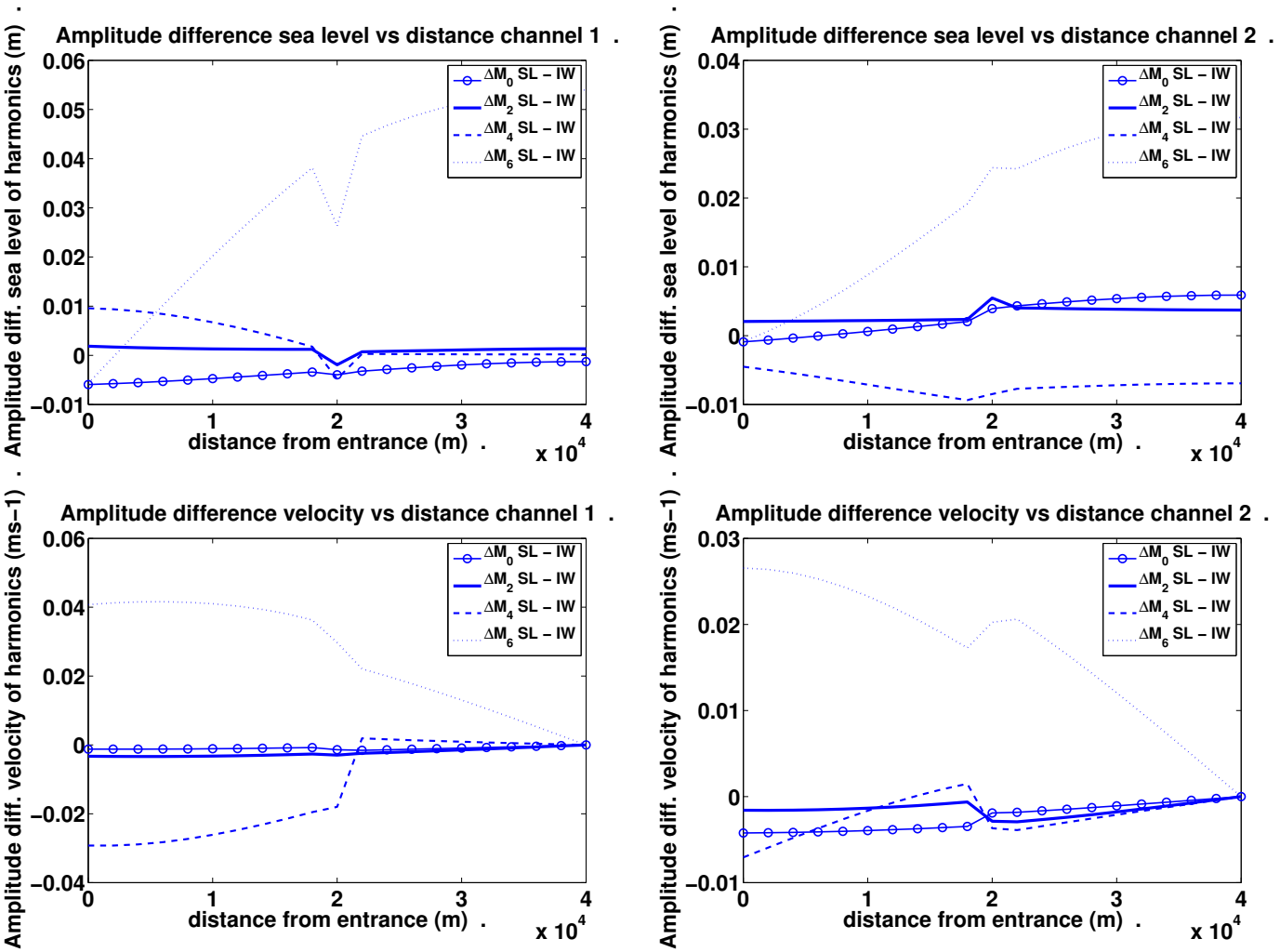

Figure 4.7: Top: Harmonic analysis of the sea level amplitude difference between prescribing an incoming wave (IW) and sea level (SL) at the open boundary in channel 1 (left) and channel 2 (right). Bottom: Harmonic analysis of the along-channel velocity amplitude difference between prescribing an incoming wave (IW) and sea level (SL) at the open boundary in channel 1 (left) and channel 2 (right)

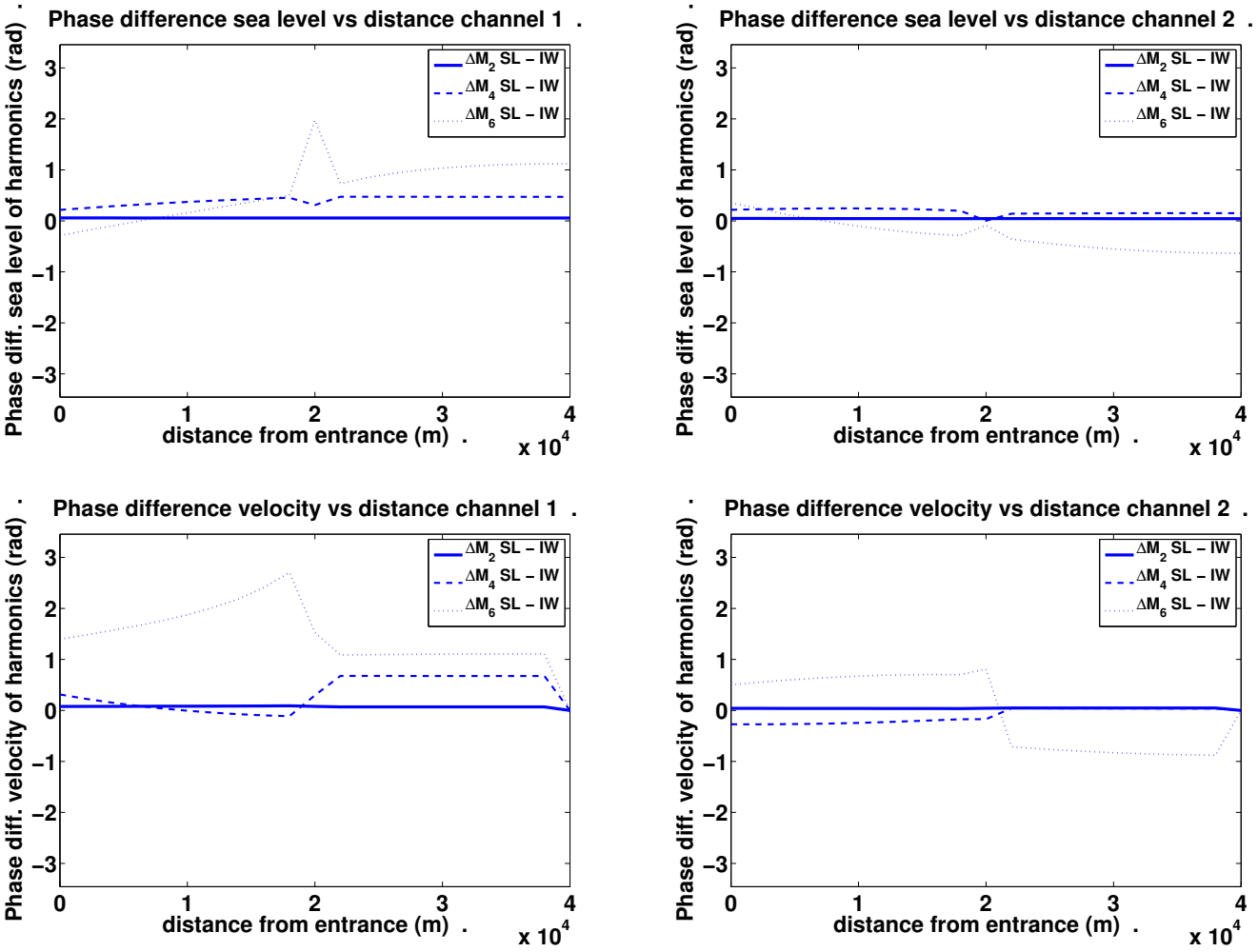

Figure 4.8: Top: Harmonic analysis of the sea level phase difference between prescribing an incoming wave (IW) and sea level (SL) at the open boundary in channel 1 (left) and channel 2 (right). Bottom: Harmonic analysis of the along-channel velocity phase difference between prescribing an incoming wave (IW) and sea level (SL) at the open boundary in channel 1 (left) and channel 2 (right)

4.1.5 Varying Connection Points

In the harmonic analyses shown earlier this section the importance of the location of the tidal flat is apparent. Jumps in both phase and amplitude in the along-channel velocity constituents are present at the location of the tidal flat. In all previous runs the location of the tidal flat was at 20km in a 40km channel. Here, the location of the tidal flat is varied, placing it at 10km and 30km from the open boundary. These runs are indicated by C_{10} and C_{30} (connection point at 10km, 30km).

The cross-tidal flat mass transport is shown in Table **??**. The transports from channel 2 to channel 1 and from channel 1 to channel 2 do not show large deviations with the relocation of the tidal flat. The net mass transport shows a stronger dependence on the location of the tidal flat: The closer the tidal flat is to the open boundary, the larger the net cross-tidal flat mass transport is.

A harmonic analysis of the amplitude (Figure **??**) and of the phase (Figure **??**) have been made. The actual amplitude and phase of the tidal constituents in plotted instead of their deviation from the control run. The harmonic analysis compares the M_2 and M_4 components of the runs with tidal flats at 10km, 20km and 30km from the open boundary. The M_0 and M_6 constituents are now shown. Their amplitudes are small, typically $\mathcal{O}(1\text{cm})$ for sea level and $\mathcal{O}(1\text{cms}^{-1})$ for velocity.

The harmonic analysis of the sea level amplitude does not show large differences with varying the location of the tidal flat. Small positive spikes are visible for M_4 at the location of the tidal flat. The velocity amplitude shows a stronger dependence on the location of the tidal flat. A jump in M_2 amplitude is observed at the location of the tidal flat. In channel 1 the jump is negative, decreasing the amplitude of the velocity seaward of the tidal flat, in channel 2 the jump is positive, increasing the amplitude of the velocity seaward of the tidal flat. The M_4 velocity amplitude is approximately constant seaward of the tidal flat and decreases linearly to zero landward of the tidal flat. The amplitude of the M_4 velocity signal is slightly stronger when the tidal flat is further away from the open boundary.

In Figure **??** the phases of the M_2 constituents are not affected by the location of the tidal flat. The phase of the M_4 sea level decreases from the open boundary to the tidal flat, indicating a wave entering the domain at the location of the tidal flat and progressing to the open boundary. Landward of the tidal flat, the phase of the M_4 sea level is constant. The phase of the M_4 velocity shows qualitative similarities, with a decreasing phase from the open boundary to the tidal flat and a constant phase landward of the tidal flat. Landward of the tidal flat, a standing M_4 wave exists.

Run	Leading channel	$T_{2\to1}$ (m^3)	$T_{1\to2}$ (m^3)	T_{net} (m^3)	$T_{inc,ch1}$ (m^3)
C_{10}	2	$1.90 * 10^6$	$2.51 * 10^6$	$6.03 * 10^5$	$1.60 * 10^7$
C_{20} (control)	2	$1.84 * 10^6$	$2.30 * 10^6$	$4.63 * 10^5$	$1.60 * 10^7$
C_{30}	2	$1.89 * 10^6$	$2.14 * 10^6$	$2.55 * 10^5$	$1.61 * 10^7$

Table 4.6: Transports per cycle for runs in which the location of the tidal flat in the tidal channel is varied from 10km to 30km from the open boundary. The leading channel indicates in which channel high water first arrives at the tidal flat. $T_{2\to1}$ and $T_{1\to2}$ indicate cross-tidal flat mass transport from channel 2 to channel 1 and from channel 1 to channel 2. The net cross-tidal flat mass transport is denoted by T_{net} (transport from channel 1 to channel 2 is defined positive). As a reference value, the amount of mass entering channel 1 at the open boundary, $T_{inc,ch1}$ is shown.

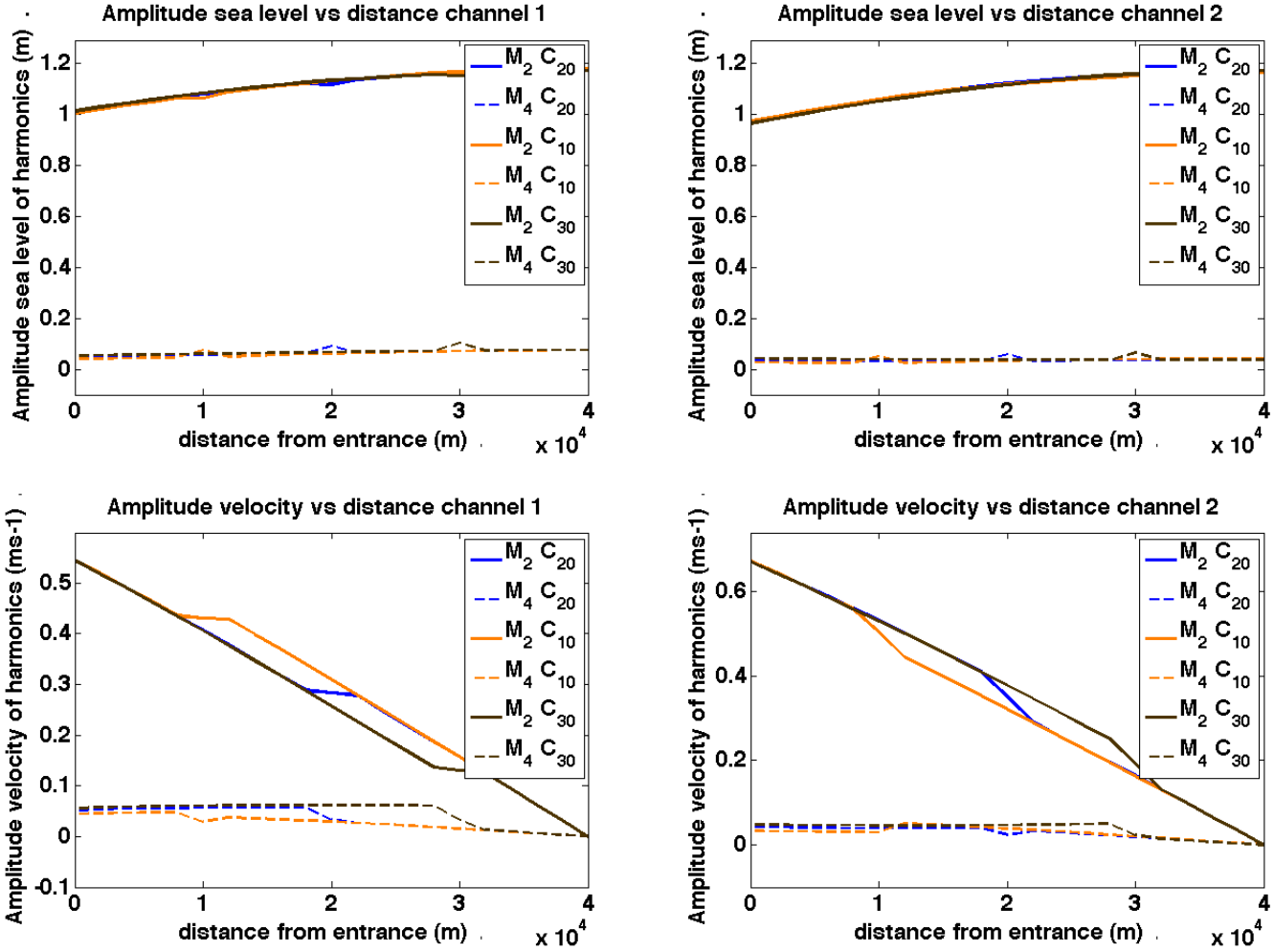

Figure 4.9: Top: Harmonic analysis for runs with tidal flats at three locations, 10km (C_{10}), 20km (C_{20}) and 30km (C_{30}) from the open boundary. Top: Amplitude harmonics sea level in channel 1 (left) and channel 2 (right). Bottom: Amplitude harmonics along-channel velocity in channel 1 (left) and channel 2 (right).

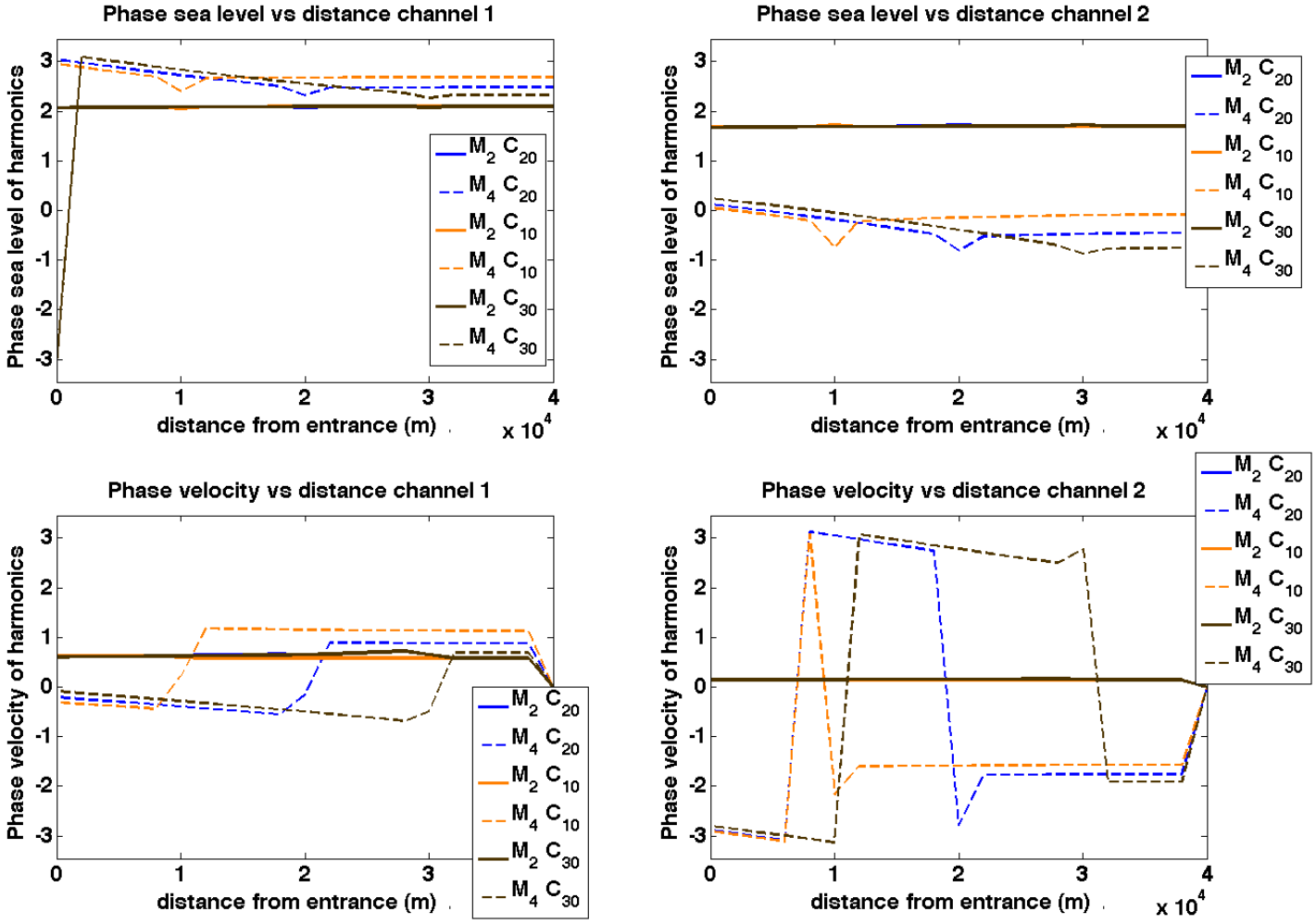

Figure 4.10: Top: Harmonic analysis for runs with tidal flats at three locations, 10km (C_{10}), 20km (C_{20}) and 30km (C_{30}) from the open boundary. Top: Phase of harmonics sea level in channel 1 (left) and channel 2 (right). Bottom: Phase harmonics along-channel velocity in channel 1 (left) and channel 2 (right).

4.1.6 Varying Tidal Flat Height

In the previous runs, the height of the tidal flat has been 0.0m. In this section, two runs are done in which the height of the tidal flat is +0.5m and -0.5. Note that a positive height corresponds to a higher tidal flat. It is expected that an increase of height of the tidal flat will lead to a decrease of cross-tidal flat mass transport, because water levels in the channel will be lower than the tidal flat for a larger part of the tidal cycle. The cross-tidal flat mass transports are shown in Table **??**

More mass is transported when the tidal flat is lower. This is in line with expectations. Also, the net mass transport increases when tidal flats are lower. The net mass transport is approximately 20% of the tidal mass transport from channel 1 to channel 2.

The harmonic analyses of the amplitude and phase of the tidal constituents are plotted in Figures **??**-**??**. The amplitude of the sea level is most strongly affected in the M_4 constituent, that is small when a small amount of cross-tidal flat mass transport is observed. The M_2 sea level component increases in amplitude seaward of the tidal flat in channel 1, and decreases in M_2 sea level amplitude seaward of the tidal flat in channel 2. These changes coincide with a decrease in M_2 velocity in channel 1 and an increase of M_2 velocity in channel 2 seaward of the tidal flat. When the M_2 velocity amplitude is smaller, the M_2 sea level amplitude is larger and vice versa. The M_0 and M_6 sea level differences remain small (smaller than 1cm). The same is true for the M_0 and M_6 velocity differences, with deviations under 2cms^{-1}. The jump in M_2 velocity is stronger when there is more cross-tidal flat mass transport. Phase differences are small, except for the M_6 tidal constituents. The M_6 constituents, both in sea level and velocity, have a small amplitude and are easily affected by small changes in cross-tidal flat transport. The M_4 component shows a larger difference between $H_{tf} = 0.5$m and $H_{tf} = 0.0$m than between $H_{tf} = -0.5$m and $H_{tf} = 0.0$m. In the run with $H_{tf} = 0.5$m the cross-tidal flat mass transport is weak and a relatively small part of the M_4 constituent is generated by cross-tidal flat mass transport. In the runs with $H_{tf} = 0.0$m and $H_{tf} = -0.5$m, cross-tidal flat mass transport generates most of the M_4 component. The generation of M_4 via cross-tidal flat mass transport has the same phase in all three runs. This may explain the stronger difference with the run with $H_{tf} = 0.5$m.

H_{tf} (m)	Leading channel	$T_{2\to1}$ (m^3)	$T_{1\to2}$ (m^3)	T_{net} (m^3)	T_{net} / $T_{1\to2}$	$T_{inc,ch1}$ (m^3)
-0.5	2	$2.94 * 10^6$	$3.57 * 10^6$	$6.31 * 10^5$	0.18	$1.47 * 10^7$
0.0 (control)	2	$1.84 * 10^6$	$2.30 * 10^6$	$4.63 * 10^5$	0.20	$1.60 * 10^7$
+0.5	2	$0.82 * 10^6$	$1.01 * 10^6$	$1.87 * 10^5$	0.19	$1.72 * 10^7$

Table 4.7: Transports per cycle for runs in which the height of the tidal flat is varied from -0.5m to 0.5m. The leading channel indicates in which channel high water first arrives at the tidal flat. $T_{2\to1}$ and $T_{1\to2}$ indicate cross-tidal flat mass transport from channel 2 to channel 1 and from channel 1 to channel 2. The net cross-tidal flat mass transport is denoted by T_{net} (transport from channel 1 to channel 2 is defined positive). As a reference value, the amount of mass entering channel 1 at the open boundary, $T_{inc,ch1}$ is shown.

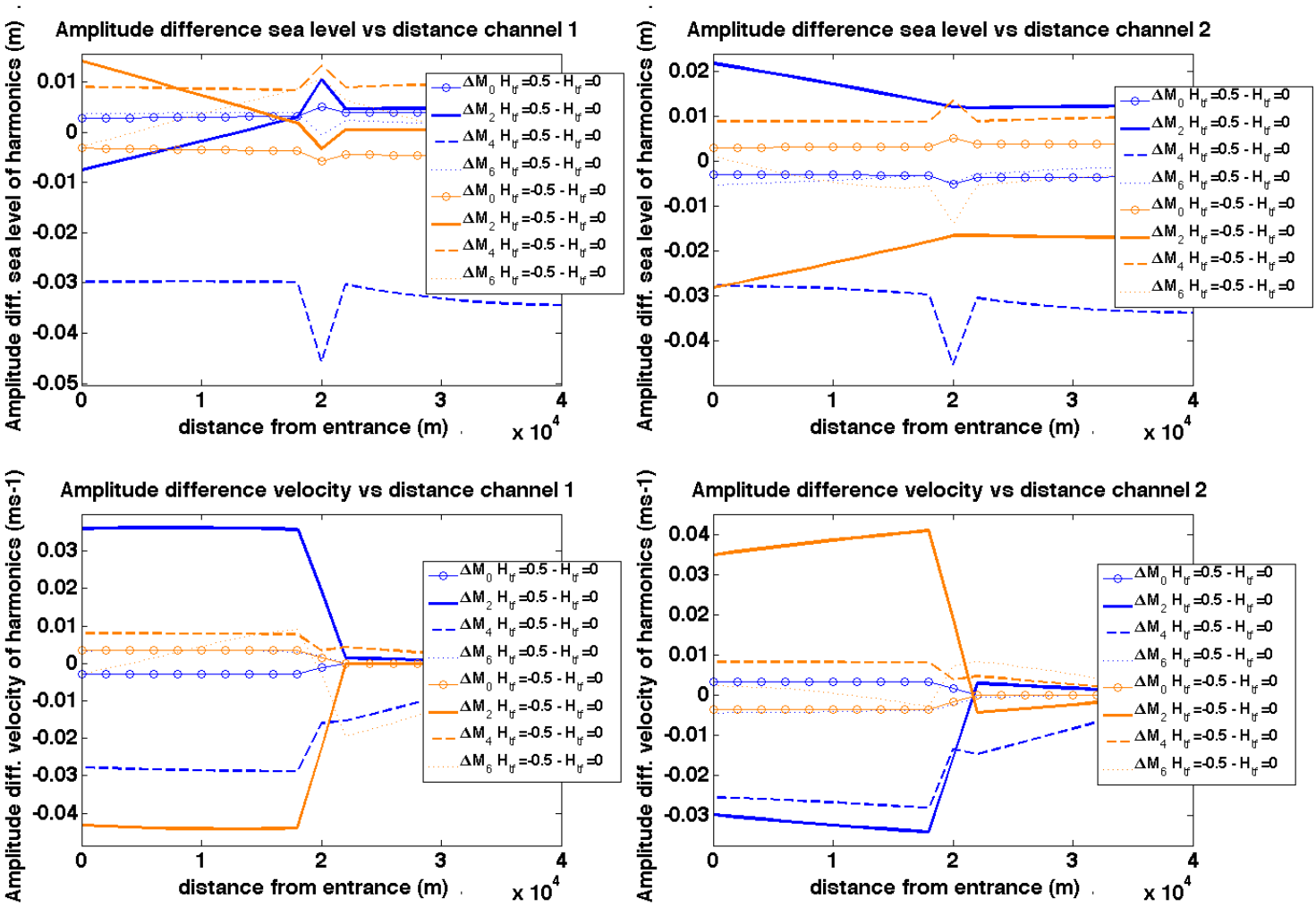

Figure 4.11: Harmonic analysis of amplitude difference. Runs with height of the tidal flat equal to +0.5m and -0.5m are compared to the control run (with tidal flat height at 0m). Top: Sea level amplitude differences for channel 1 (left) and channel 2 (right). Bottom: Along-channel velocity amplitude differences for channel 1 (left) and channel 2 (right).

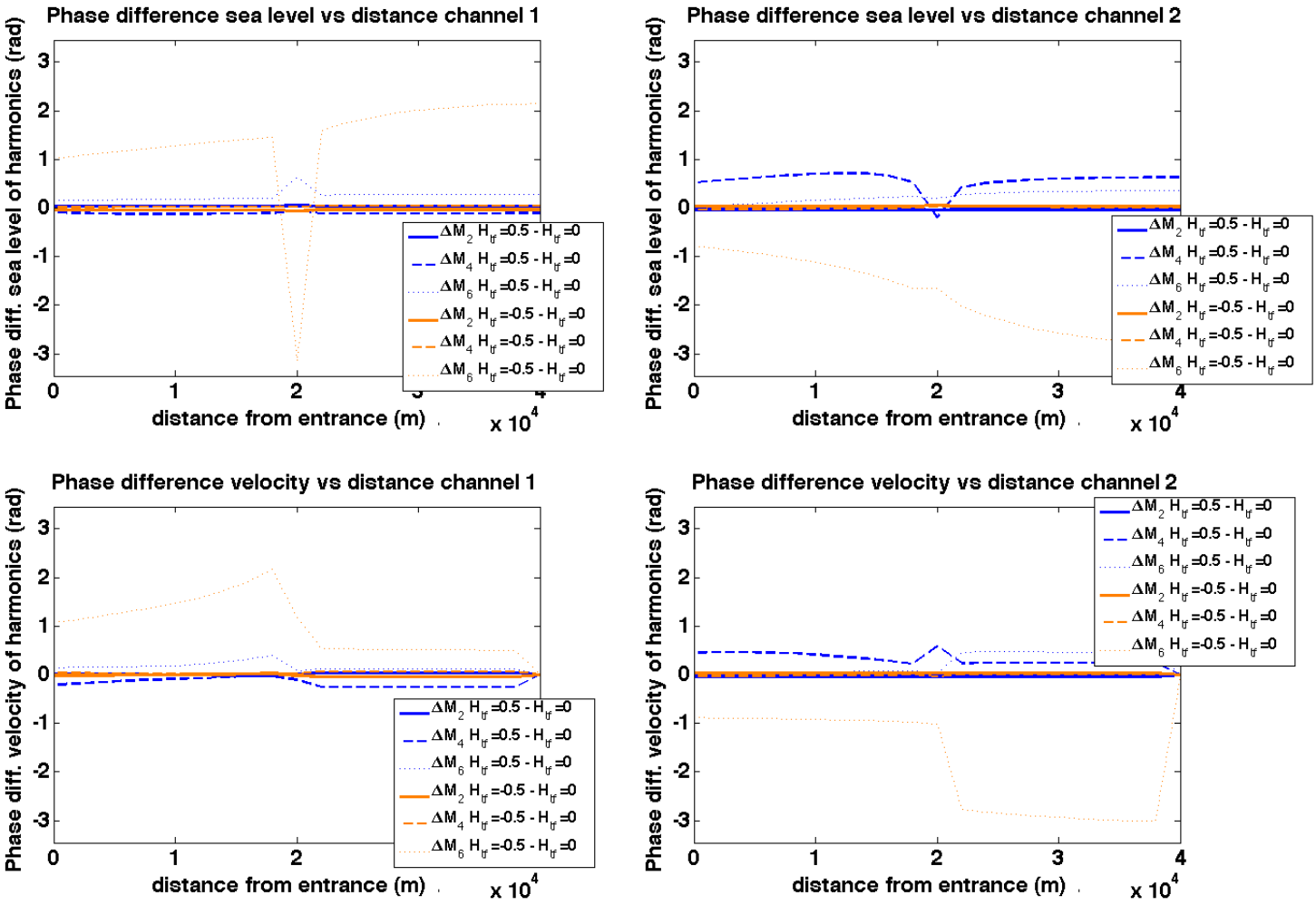

Figure 4.12: Harmonic analysis of phase difference. Runs with height of the tidal flat equal to +0.5m and -0.5m are compared to the control run (with tidal flat height at 0m). Top: Sea level amplitude differences for channel 1 (left) and channel 2 (right). Bottom: Along-channel velocity amplitude differences for channel 1 (left) and channel 2 (right).

4.1.7 Varying Tidal Flat Width

The cross-channel mass transport is calculated via $M = \eta_{tf} u_{tf} W_{tf}$. The mass transport thus varies linearly with the tidal flat width. Increasing the tidal flat width will lead to a larger mass transport and decreasing the width will lead to a smaller mass transport. The width of the tidal flat is limited to the length of an along-channel spatial step Δx from a physical point of view. If W_{tf} is larger than Δx, mass would be distributed over more than 1 grid point. In that case, the physically more realistic solution would be to add another tidal flat. The current version of the NM-P model does not allow for more than one tidal flat. In the control run $W_{tf} = \Delta x$. To look into the effect of varying tidal flat width while keeping the same Δx, width can only become smaller. The control run is compared to runs in which $W_{tf} = 1000$m and $W_{tf} = 250$m. The cross-tidal flat mass transports are shown in Table **??**

The mass transport does not scale linearly with the width. When width is small, a small amount of mass is transported from the channel with higher water to the channel with lower water. The sea level gradient, that defines the cross-tidal flat velocity, is only weakly affected by the mass transport. The pressure gradient remains strong in that case, and the cross-tidal flat velocity will obtain a higher maximum value. This effect partially counteracts the decrease in mass transport due to a smaller width. The net mass transport per cycle increases with increasing tidal flat width. It is remarkable that the increase in tidal flat width from $W_{tf} = 250$m to $W_{tf} = 1000$m leads to a ten times larger net mass transport, but the increase from $W_{tf} = 1000$m to $W_{tf} = 2000$m only leads to a net mass transport that is 1.5 times larger. A possible explanation is the fact that net mass transport requires a deviation from the original sinusoidal signal to cause an asymmetry in the net mass transport. Instantaneous mass transport causes this asymmetry, and the stronger the asymmetry, the stronger the net mass transport is. When $W_{tf} = 250$m, the instantaneous mass transport is small and the corresponding asymmetry in the sea level on either side of the tidal flat is weak, resulting in a small net mass transport. When $W_{tf} = 1000$m, the instantaneous mass transport is stronger, resulting in a stronger asymmetry in sea level and a stronger net mass transport.

A harmonic analysis shows few interesting features. When the width becomes smaller there is less cross-tidal flat mass transport and thus, the effect of cross-tidal flat mass transport on the harmonics becomes smaller. This is shown in Figure **??**, where the results from the control run ($W_{tf} = 2000$m) and the $W_{tf} = 250$m run are compared to a run without cross-tidal flat mass transport. A run without cross-tidal flat mass transport can be interpreted as a run in which $W_{tf} = 0$m, and it is indicated as such in the figure. The amplitude of M_2 and M_4 in both sea level and velocity shows the same qualitative deviations for the runs with $W_{tf} = 2000$m and $W_{tf} = 250$m, but the deviations are much stronger when $W_{tf} = 2000$m. The same is true for M_0 and M_6 in channel 1, but in channel 2 M_0 and M_6 show deviations in amplitude that are sometimes stronger for the $W_{tf} = 250$m run than in the $W_{tf} = 2000$m run. This may be explained by the fact that M_0 and M_6 are small and are easily affected by a change in cross-tidal flat mass transport.

The phase differences (Figure **??**) in channel 1 only show strong deviations in the M_6 constituents. This can, again, be explained by the fact that M_6 has a small amplitude and is thus easily affected by changes in cross-tidal flat mass transport. In channel 2 the M_6 constituents shows large deviations, but the M_4 constituents also shows large deviations, up to 180° in the sea level. The phase of the M_2 constituent in channel 2 is hardly affected by the increase of tidal flat width.

W_{tf} (m)	Leading channel	$T_{2\to1}$ (m^3)	$T_{1\to2}$ (m^3)	T_{net} (m^3)	$T_{inc,ch1}$ (m^3)
2000 (control)	2	$1.84 * 10^6$	$2.30 * 10^6$	$4.63 * 10^5$	$1.60 * 10^7$
1000	2	$1.38 * 10^6$	$1.68 * 10^6$	$3.03 * 10^5$	$1.66 * 10^7$
250	2	$0.55 * 10^6$	$0.58 * 10^6$	$0.27 * 10^5$	$1.76 * 10^7$

Table 4.8: Transports per cycle for runs in which the width of the tidal flat is varied from 2000m to 250m. The leading channel indicates in which channel high water first arrives at the tidal flat. $T_{2\to1}$ and $T_{1\to2}$ indicate cross-tidal flat mass transport from channel 2 to channel 1 and from channel 1 to channel 2. The net cross-tidal flat mass transport is denoted by T_{net} (transport from channel 1 to channel 2 is defined positive). As a reference value, the amount of mass entering channel 1 at the open boundary, $T_{inc,ch1}$ is shown.

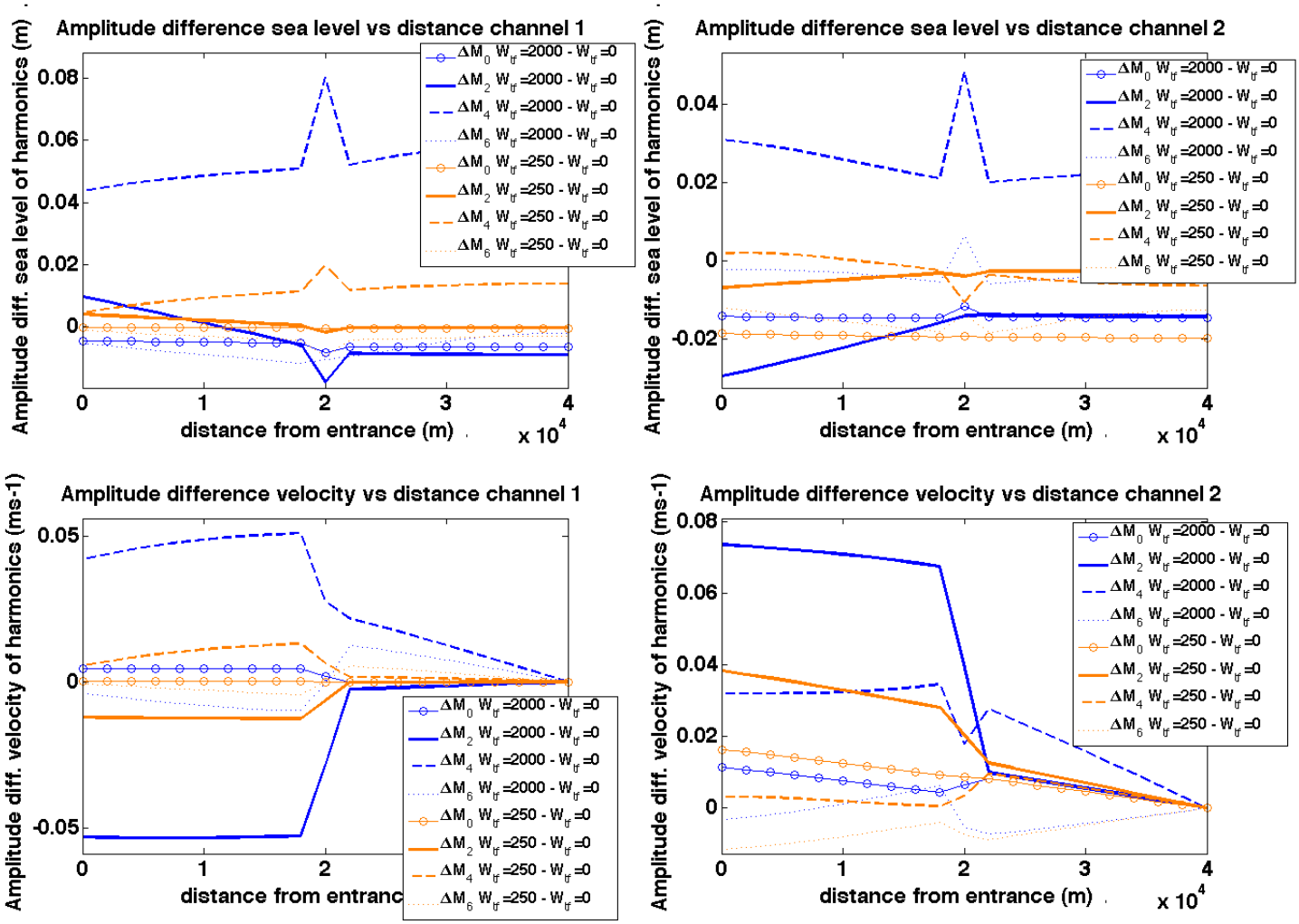

Figure 4.13: Harmonic analysis of amplitude difference. Runs in which the width of the tidal flat is varied are compared to a run in which there is no cross-tidal flat mass transport (or $W_{tf} = 0$m). Top: Sea level amplitude differences for channel 1 (left) and channel 2 (right). Bottom: Along-channel velocity amplitude differences for channel 1 (left) and channel 2 (right).

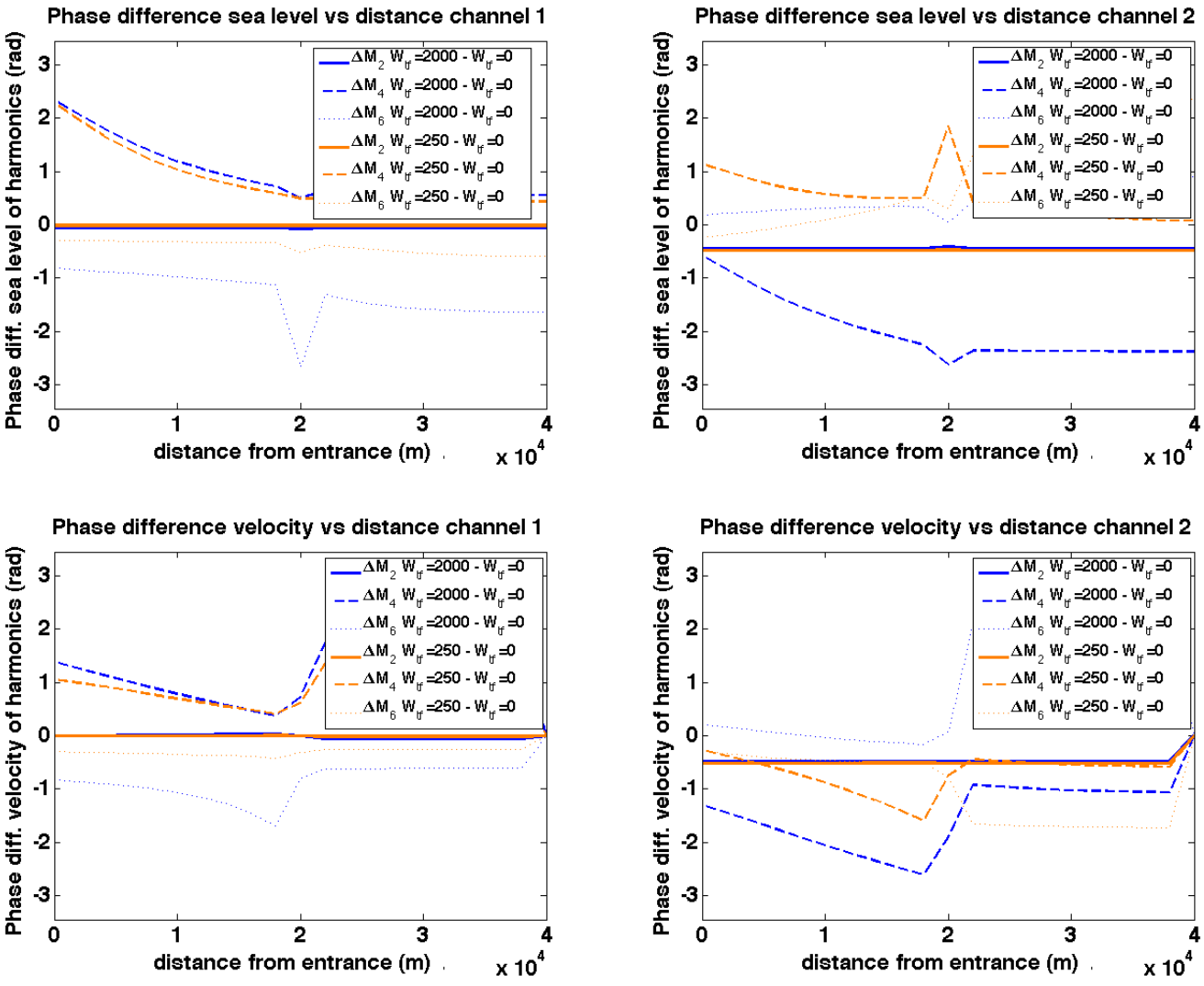

Figure 4.14: Harmonic analysis of phase difference. Runs in which the width of the tidal flat is varied are compared to a run in which there is no cross-tidal flat mass transport (or $W_{tf} = 0$m). Top: Sea level amplitude differences for channel 1 (left) and channel 2 (right). Bottom: Along-channel velocity amplitude differences for channel 1 (left) and channel 2 (right).

4.1.8 Varying Channel Width

The channel width is an important parameter for the impact of the cross-tidal flat mass and momentum transfer. Sea level and along-channel velocity are cross-sectionally averaged quantities. When the channel width goes to infinity, the cross-section goes to infinity and any cross-tidal flat mass transport will have an infinitely small impact on the sea level. When the width of the channel is small, the impact of the cross-tidal flat mass transport will be large. To investigate this effect, two experiments are carried out: One in which the channel width of only 1 channel is varied and one in which the channel width of both channels is varied. The impact of cross-tidal flat mass transport on the channels scales with W_{tf}/W_i, with $i = [1, 2]$. The effect of a wider channel is thus already simulated in the previous experiment (Varying Tidal Flat Width). In this section only channel widths are considered that are narrower than in the control run. In the first experiment the width of channel 1 is decreased to 50m, in the second experiment the width of channel 2 is also decreased to 50m (coming from 200m in the control run). The cross-tidal flat mass transports are shown in Table **??**

The mass transport decreases when one of the two channels is narrower and decreases further when both are narrower. The effect on the net mass transport is even larger. In the run in which $W_1 = 50$m and W_2=100m the net mass transport is 17 times smaller than in the control run. The mass that is transported from channel 1 to channel 2 is also much smaller compared to the control run. A possible explanation is that cross-tidal flat mass transport requires a pressure gradient between channel 1 and channel 2, and pressure gradients are reduced faster when the cross-sectional area is smaller. The same argument can be used to explain the results for the run in which both channel widths are 50m.

In Figures **??**-**??** the results of a harmonic analysis of the run in which W_1=50m is shown, with both amplitude and phase. It is compared to a run without cross-tidal flat mass transport (the zero-run). As a reference, the deviation from the control run compared to the zero-run is also shown. In channel 1 all deviations from the zero-run are larger than the deviations from the control run to the zero-run. The impact of the cross-tidal flat mass transport on the harmonics becomes larger when the channel width is smaller. The opposite is true for channel 2. The strongest harmonics, M_2 and M_4, have smaller deviations from the zero-run, most likely caused by a decrease in cross-tidal flat mass transport. M_0 and M_6 show smaller changes between the run with W_1=50m and the control run. The phases (Figure **??**) of M_2 and M_4 coincide almost perfectly in the control run and the run with $W_1 = 50$m. Only M_6 is strongly affected, but it has a small amplitude and is easily affected by small changes in cross-tidal flat mass transport. The phases of M_2 and M_4 are only weakly changed by the change in cross-tidal flat mass transport.

In Figures **??**-**??** the results of a harmonic analysis of the run in which W_1=50m and W_2=50m is shown, with both amplitude and phase. All harmonic deviations from the zero-run are enhanced when the width of the channel is smaller, both in sea level and velocity. Only the amplitude of M_6 shows qualitatively different behavior, but it is small in amplitude throughout the domain. The impact that the cross-tidal flat mass transport has on the harmonics of the system is stronger when the channels are narrower. The phases of the M_2 and M_4 tidal constituents coincide almost perfectly. The fact that cross-tidal flat mass transport is over 30 times smaller compared to the control run does not affect the phases of M_2 and M_4, in both channels and both in sea level and velocity. The phases of M_6 show a less coherent picture.

W_1 (m)	W_2	Leading channel	$T_{2\rightarrow1}$ (m^3)	$T_{1\rightarrow2}$ (m^3)	T_{net} (m^3)	$T_{inc,ch1}$ (m^3)
200 (control)	200 (m)	2	$1.84 * 10^6$	$2.30 * 10^6$	$4.63 * 10^5$	$1.60 * 10^7$
50	200	2	$1.02 * 10^6$	$1.05 * 10^6$	$0.27 * 10^5$	$0.35 * 10^7$
50	50	2	$0.64 * 10^6$	$0.78 * 10^6$	$0.15 * 10^5$	$1.76 * 10^7$

Table 4.9: Transports per cycle for runs in which the width of the channels is varied. The leading channel indicates in which channel high water first arrives at the tidal flat. $T_{2\rightarrow1}$ and $T_{1\rightarrow2}$ indicate cross-tidal flat mass transport from channel 2 to channel 1 and from channel 1 to channel 2. The net cross-tidal flat mass transport is denoted by T_{net} (transport from channel 1 to channel 2 is defined positive). As a reference value, the amount of mass entering channel 1 at the open boundary, $T_{inc,ch1}$ is shown.

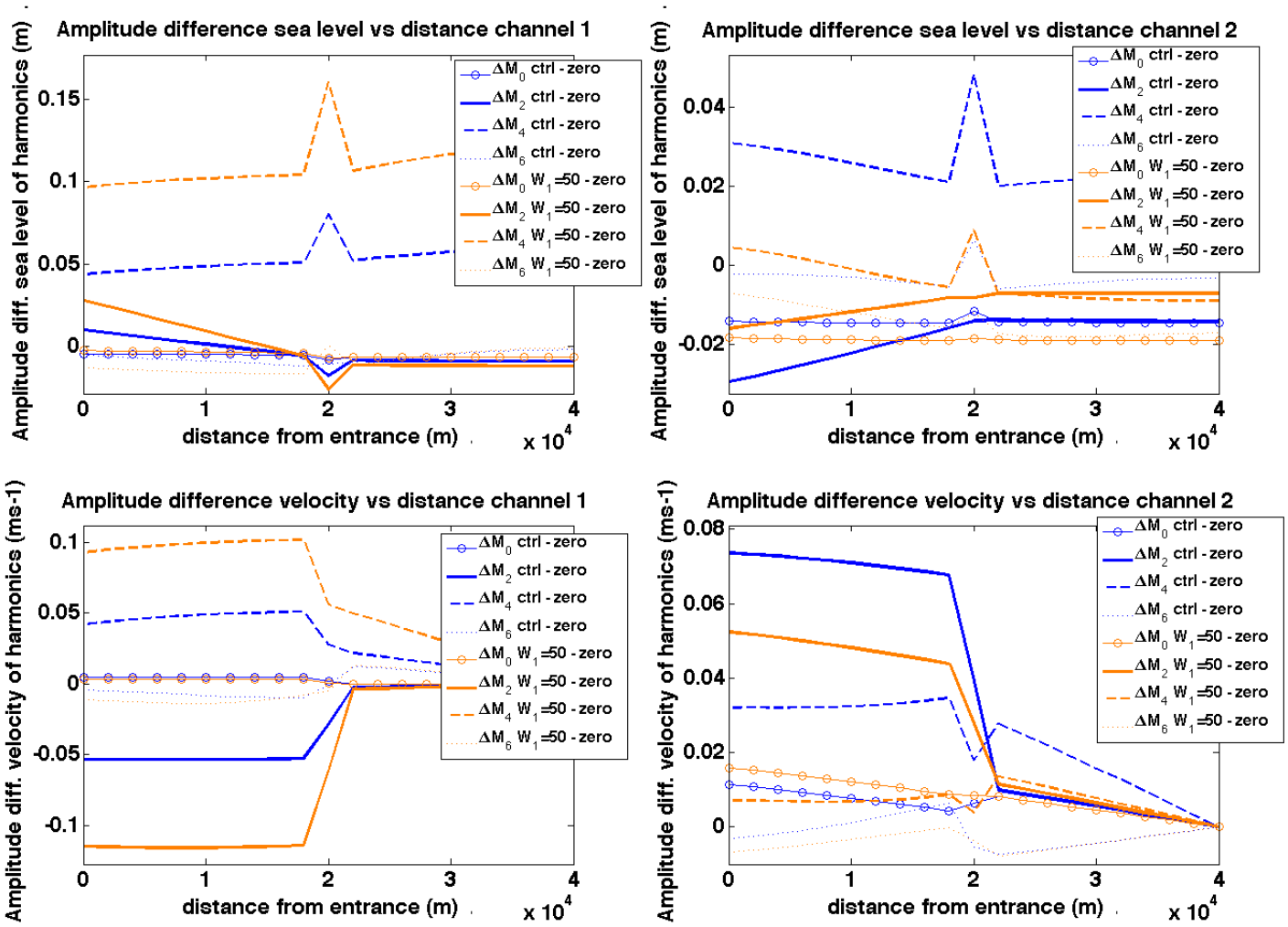

Figure 4.15: Harmonic analysis of amplitude difference. A run in which the channel width of channel 1 is 50m (orange) and the control run (blue) are compared to a run without cross-tidal flat mass transport. Top: Sea level amplitude differences for channel 1 (left) and channel 2 (right). Bottom: Along-channel velocity amplitude differences for channel 1 (left) and channel 2 (right).

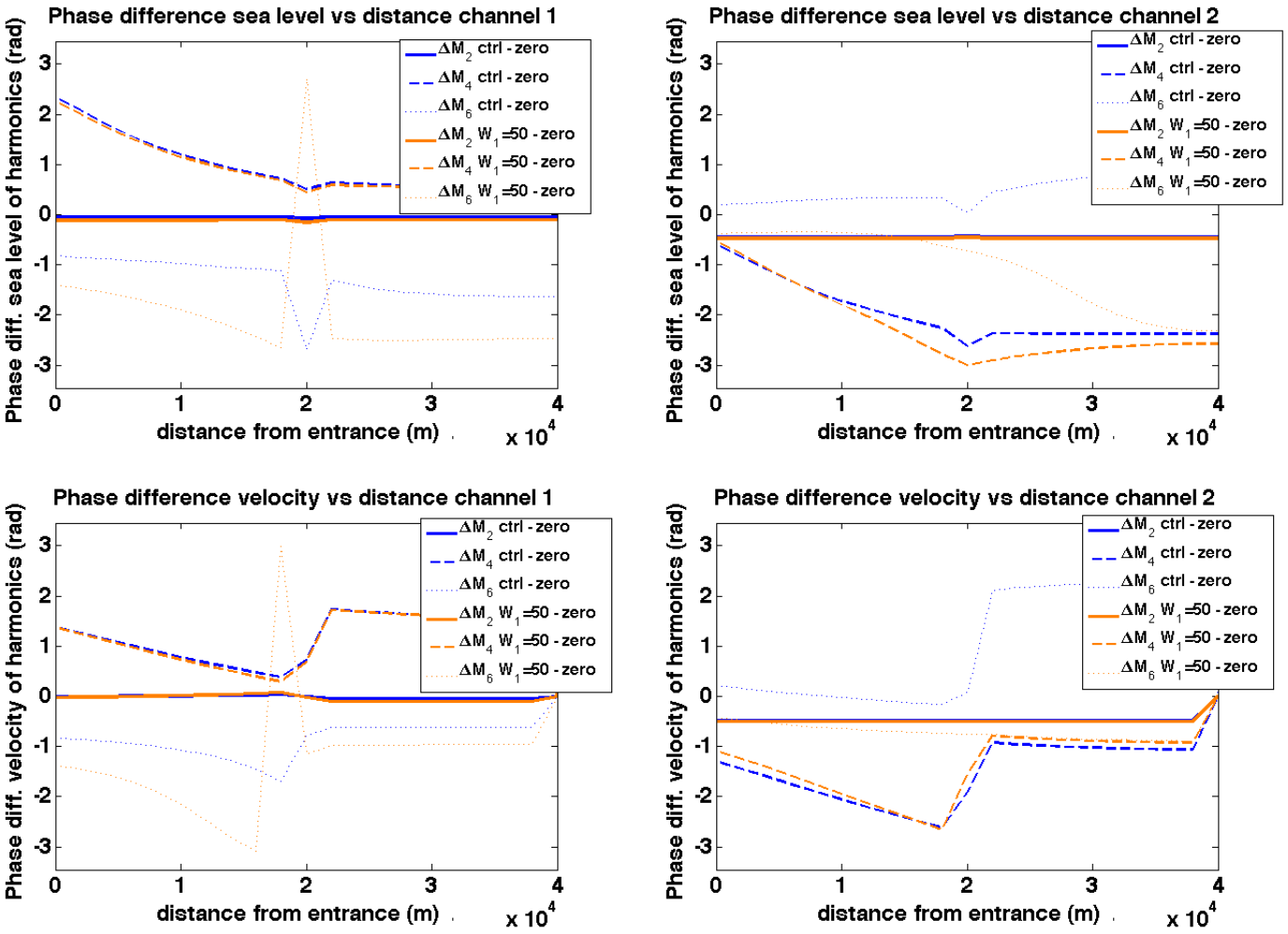

Figure 4.16: Harmonic analysis of phase difference. A run in which the channel width of channel 1 is 50m (orange) and the control run (blue) are compared to a run without cross-tidal flat mass transport. Top: Sea level amplitude differences for channel 1 (left) and channel 2 (right). Bottom: Along-channel velocity amplitude differences for channel 1 (left) and channel 2 (right).

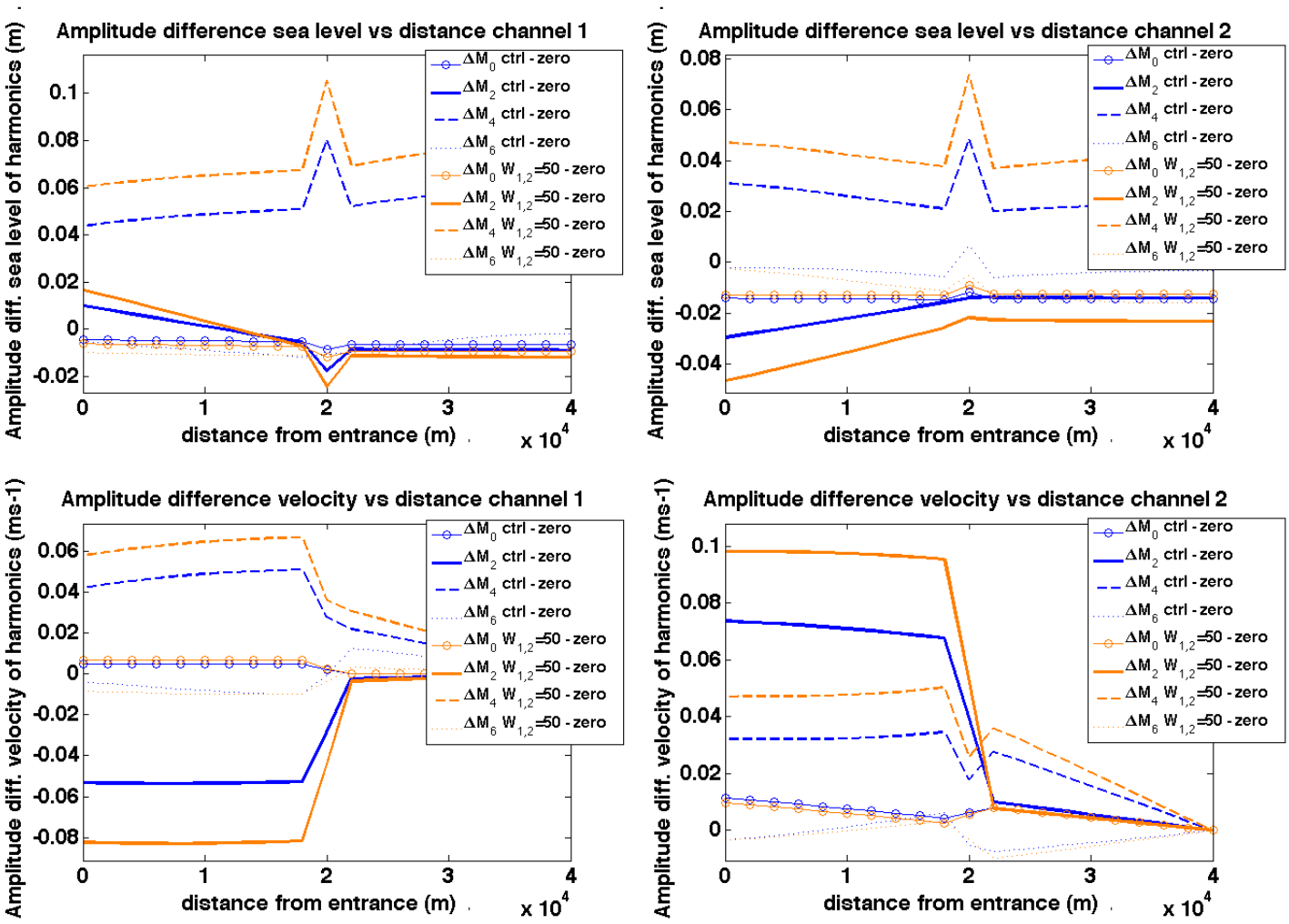

Figure 4.17: Harmonic analysis of amplitude difference. A run in which the channel width of channel 1 and channel 2 is 50m (orange) and the control run (blue) are compared to a run without cross-tidal flat mass transport. Top: Sea level amplitude differences for channel 1 (left) and channel 2 (right). Bottom: Along-channel velocity amplitude differences for channel 1 (left) and channel 2 (right).

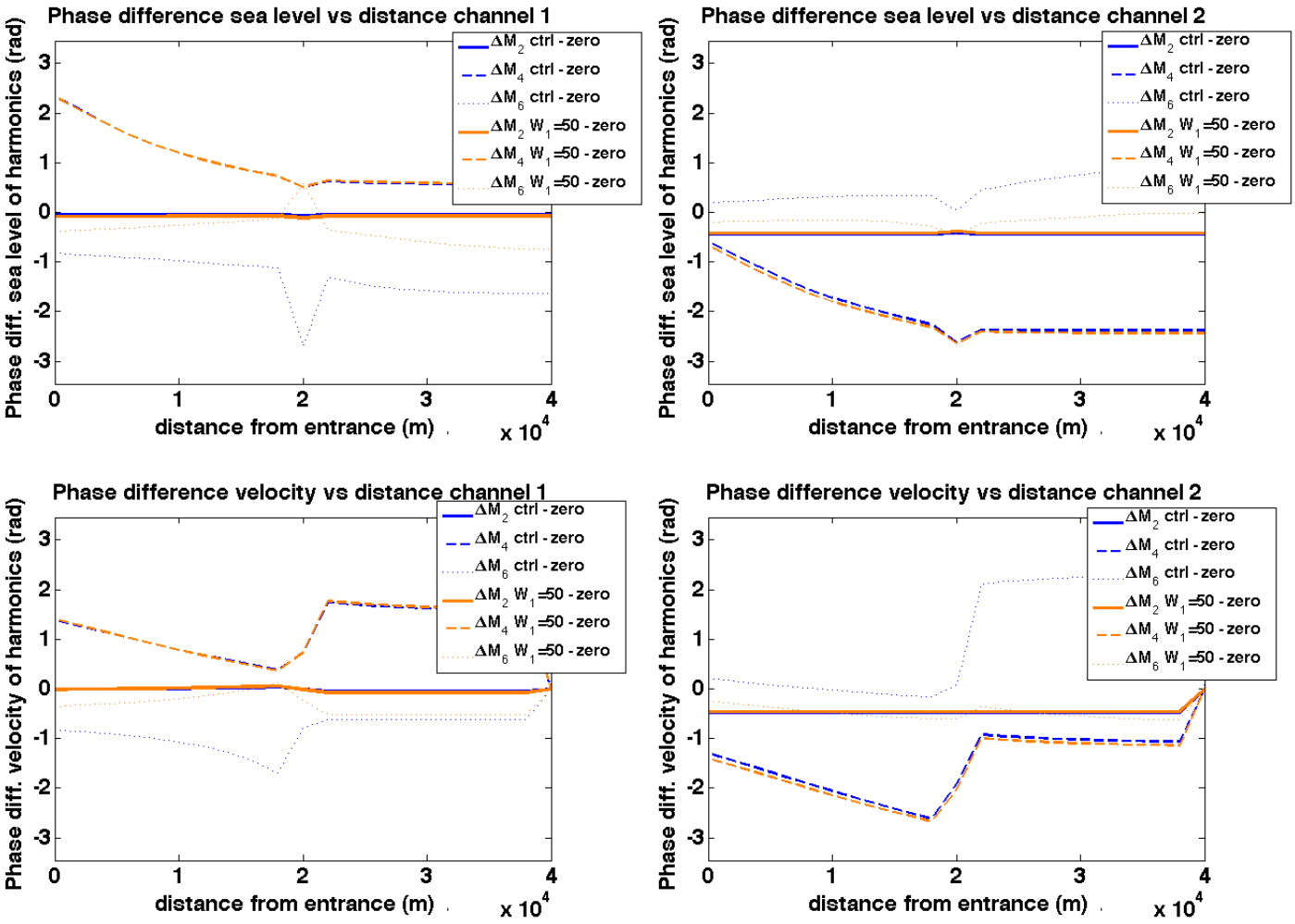

Figure 4.18: Harmonic analysis of phase difference. A run in which the channel width of channel 1 and channel 2 is 50m (orange) and the control run (blue) are compared to a run without cross-tidal flat mass transport. Top: Sea level amplitude differences for channel 1 (left) and channel 2 (right). Bottom: Along-channel velocity amplitude differences for channel 1 (left) and channel 2 (right).

4.1.9 Varying Channel Depth

The runs up till now have had channels with a constant depth of 10m. Varying depth has an impact on three processes: The cross-sectional area, the bottom friction and the wave propagation speed. The consequences of varying the cross-sectional area are the same as when channel width is varied (see previous runs, Varying Channel Width). The second effect of varying the channel depth is a change in bottom friction. The final effect is that wave propagate slower in shallower waters. The result is that, even when there would be no phase difference between the forcings in channel 1 and channel 2, high water at the location of the tidal flat is first reached in the deeper channel and cross-tidal flat mass transport will take place. Also, due to the shallower water, friction will be stronger and the amplitude of the tidal wave will be damped.

To investigate the effect of a shallower channel, one channel is made shallower, while the other channel still has water depth 10m. Both channels are forced with an incoming wave with an amplitude of 0.6m. This time, no phase difference is applied to the incoming wave. Channel width will be changed such that $W_i H_i =$ constant. This counters the effect of varying cross-sectional area. A comparison between the suggested setup and the control run seems otiose, because the sea level difference on either side of the channel is generated by the system internally and not externally forced as in the control run. To investigate the effect of cross-tidal flat mass transport on both channels, several supporting runs have been made as well, in which the same geometry has been forced with the same incoming wave while no cross-tidal flat mass transport was present. The difference between these runs is compared in a harmonic analysis of amplitude and phase.

Runs with several different depths for channel 2 have been made, with H_2 ranging from 8m to 2m. The harmonic analysis is applied on the run with $H_2 = 5$m. First, the cross-tidal flat mass transport is shown in Table **??**.

The cross-tidal flat mass transport is small when the depth differences are small. Both the total mass transported over a tidal flat per tidal cycle and the net cross-tidal flat mass transport increase with decreasing H_2. The increase is strongest when channel 2 becomes reaches very shallow depths.

A harmonic analysis is performed on a run with $H_2 = 5$m. It is compared to the same run without cross-tidal flat mass transport in Figures **??**-**??**. In channel 1 the amplitude of the M_2 sea level has decreased by 1.5cm and the amplitude of the M_4 sea level constituent has increased by 2.5cm at the open boundary. The M_0 and M_6 sea level constituents in channel 1 are less affected by the cross-tidal flat mass transport. The velocity in channel 1 shows the same qualitative velocity jump at the location of the tidal flat as channel 2 in most previous experiment, including the control run. In these runs channel 2 was leading channel 1. Now, channel 1 is leading channel 2 and channel 1 has a positive M_2 velocity jump seaward of the tidal flat. The M_4 tidal constituents is larger as well, while M_0 and M_6 show only small deviations from the run without cross-tidal flat mass transport. In channel 2 deviations of the same order of magnitude as in channel 1 are observed. The M_2 sea level increases

H_2 (m)	Leading channel	$T_{2\to1}$ (m^3)	$T_{1\to2}$ (m^3)	T_{net} (m^3)	$T_{inc,ch1}$ (m^3)
10 (control)	-	0	0	0	$1.80 * 10^7$
8	1	$0.28 * 10^6$	$0.29 * 10^6$	$0.14 * 10^5$	$1.82 * 10^7$
7	1	$0.47 * 10^6$	$0.50 * 10^6$	$0.24 * 10^5$	$1.84 * 10^7$
6	1	$0.65 * 10^6$	$0.68 * 10^6$	$0.32 * 10^5$	$1.85 * 10^7$
5	1	$0.90 * 10^6$	$0.94 * 10^6$	$0.44 * 10^5$	$1.86 * 10^7$
4	1	$1.26 * 10^6$	$1.29 * 10^6$	$0.33 * 10^5$	$1.89 * 10^7$
3	1	$1.65 * 10^6$	$1.75 * 10^6$	$0.98 * 10^5$	$1.90 * 10^7$
2	1	$2.43 * 10^6$	$2.63 * 10^6$	$2.06 * 10^5$	$1.92 * 10^7$

Table 4.10: Transports per cycle for runs in which the depth of channel 2 is varied from 10m to 2m. The leading channel indicates in which channel high water first arrives at the tidal flat. $T_{2\to1}$ and $T_{1\to2}$ indicate cross-tidal flat mass transport from channel 2 to channel 1 and from channel 1 to channel 2. The net cross-tidal flat mass transport is denoted by T_{net} (transport from channel 1 to channel 2 is defined positive). As a reference value, the amount of mass entering channel 1 at the open boundary, $T_{inc,ch1}$ is shown.

towards the open boundary, seaward of the tidal flat. The M_4 signal is strongly affected by the cross-tidal flat mass transport, whereas the M_0 and M_6 tides show small deviations. The M_2 velocity component in channel 2 has a strong negative jump at the location of the tidal flat, just as channel 1 in many runs shown earlier this section, including the control run. An increase in M_4 velocity amplitude is visible, with larger values seaward of the tidal flat. The M_0 and M_6 velocity deviations are small.

The M_2 phase deviations are almost zero for sea level and tidal flat in channel 1 and 2. The M_4 phase deviation for sea level and velocity in channel 1 are constant landward of the tidal flat and have a negative slope seaward of the tidal flat. This indicates that the M_4 that is produces by cross-tidal flat mass transport progresses from the tidal flat to the open boundary. In channel 2 M_4 phase deviations are smaller than in channel 1. This may be caused by the fact that amplitude of the M_4 sea level and velocity in channel 2 is larger than in channel 1 due to stronger nonlinearities. The M_6 phase deviations are small in both channel 1 and channel 2 for sea level and velocity.

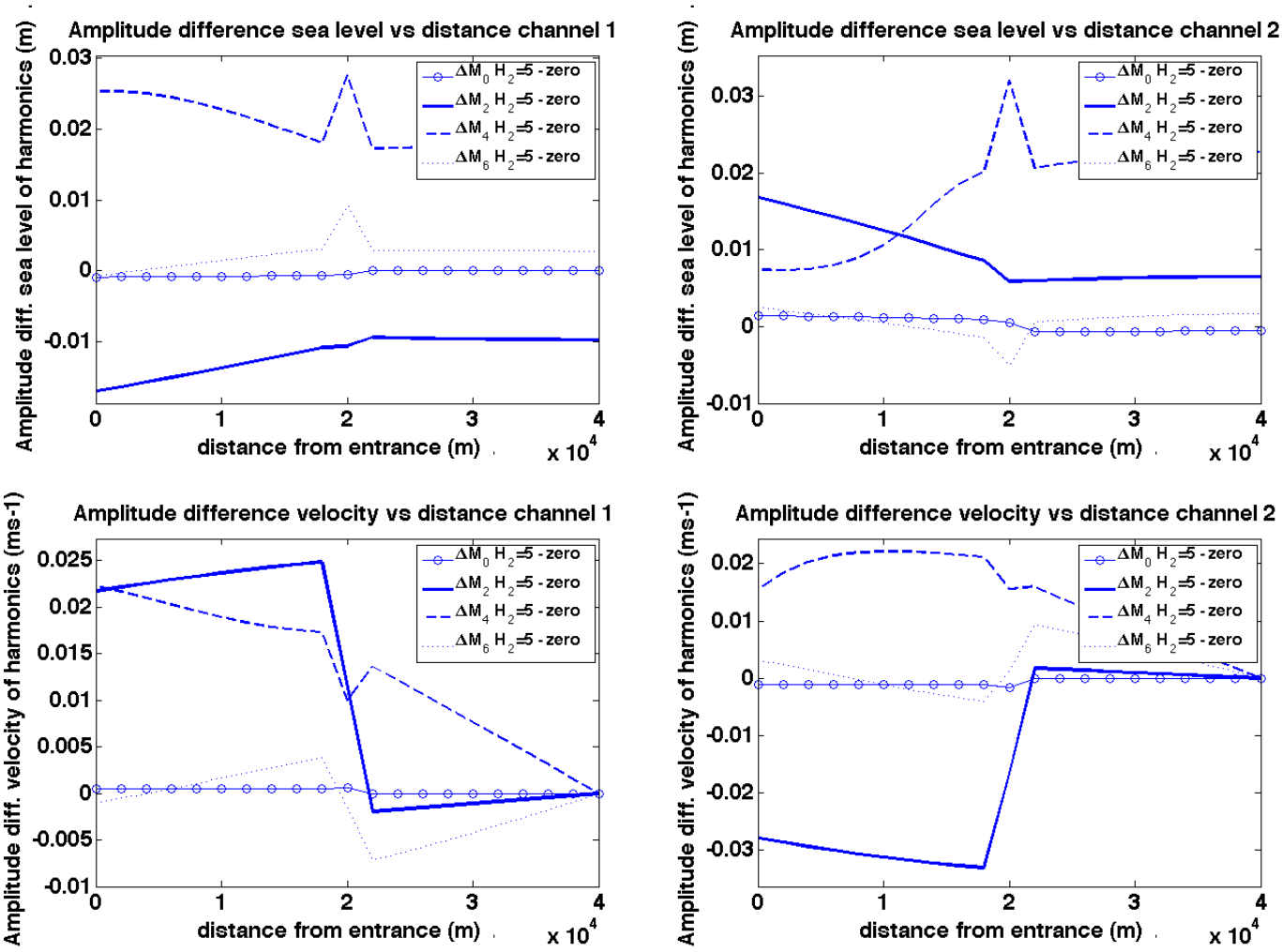

Figure 4.19: Harmonic analysis of amplitude difference. A run in which the water depth of channel 2 is 5m is compared to the same run without cross-tidal flat mass transport.. Top: Sea level amplitude differences for channel 1 (left) and channel 2 (right). Bottom: Along-channel velocity amplitude differences for channel 1 (left) and channel 2 (right).

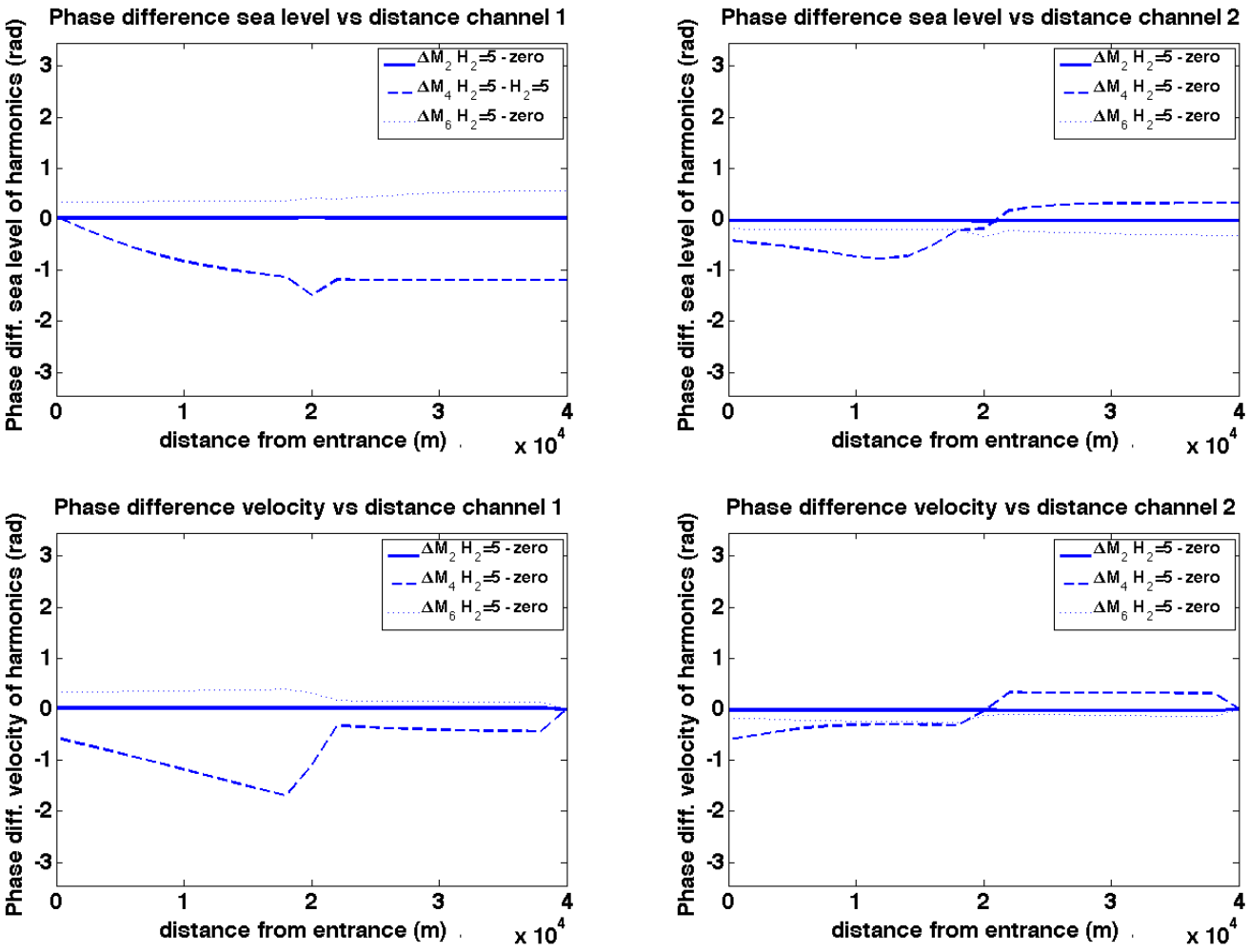

Figure 4.20: Harmonic analysis of phase difference. A run in which the water depth of channel 2 is 5m is compared to the same run without cross-tidal flat mass transport.. Top: Sea level amplitude differences for channel 1 (left) and channel 2 (right). Bottom: Along-channel velocity amplitude differences for channel 1 (left) and channel 2 (right).

4.1.10 Varying Bottom Friction on Tidal Flat

The tidal flat bottom friction is an important parameter in determining the strength of the cross-tidal flat mass transport. When bottom friction is weak, velocities can obtain higher values. Cross-tidal flat mass transport will have stronger maximal and minimal values and pressure gradients between channel 1 and channel 2 will be resolved faster. The theory is backed-up by results in this section. The model is run with four different values for the bottom friction on the tidal flat, $C_{d,tf}$ = 0.1, $C_{d,tf}$ = 0.01 (control run), $C_{d,tf}$ = 0.001 and $C_{d,tf} = 10^{-5}$. The cross-tidal flat mass transport is given in Table **??**.

The cross-tidal flat mass transport increases when friction is lower. The velocity at the tidal flat is calculated via a balance between the pressure gradient and the bottom friction on the tidal flat. When the friction becomes smaller, the flow is accelerated more easily. The net cross-tidal flat mass transport also increases when $C_{d,tf}$ is

$C_{d,tf}$ (m)	Leading channel	$T_{2\to1}$ (m^3)	$T_{1\to2}$ (m^3)	T_{net} (m^3)	$T_{inc,ch1}$ (m^3)
0.1	2	$1.04 * 10^6$	$1.27 * 10^6$	$2.25 * 10^5$	$1.70 * 10^7$
0.01 (control)	2	$1.84 * 10^6$	$2.30 * 10^6$	$4.63 * 10^5$	$1.60 * 10^7$
0.001	2	$2.51 * 10^6$	$3.00 * 10^6$	$4.88 * 10^5$	$1.52 * 10^7$
10^{-5}	2	$3.48 * 10^6$	$3.47 * 10^6$	$0.06 * 10^5$	$1.48 * 10^7$

Table 4.11: Transports per cycle for runs in which the depth of channel 2 is varied from 10m to 2m. The leading channel indicates in which channel high water first arrives at the tidal flat. $T_{2\to1}$ and $T_{1\to2}$ indicate cross-tidal flat mass transport from channel 2 to channel 1 and from channel 1 to channel 2. The net cross-tidal flat mass transport is denoted by T_{net} (transport from channel 1 to channel 2 is defined positive). As a reference value, the amount of mass entering channel 1 at the open boundary, $T_{inc,ch1}$ is shown.

decreased from 0.1 to 0.001. However, when $C_{d,tf} = 10^{-5}$ the net mass transport is almost zero.

Increasing the friction has a similar effect on the harmonics in the channels as decreasing the tidal flat width. Qualitatively the harmonics of a run with $C_{d,tf} = 0.1$ compared to the control run does not differ from the results shown for a tidal flat with width $W_3 = 250m$, shown in Figures **??**-**??**. Likewise, decreasing the friction has a similar effect on the harmonics in the channels as increasing the tidal flat width. To achieve a similar effect on the harmonics in the channel the channel width can also be decreased. The difference between a run with $C_{d,tf} = 0.001$ compared to the control run and a run with $H_{1,2} = 50$m (Figures **??**-**??**) compared to the control run is both qualitatively and quantitatively minimal. The amplitude of the harmonics differ by a maximum of 2mm for sea level and 2mms^{-1}. The phases of the M_2 and M_4 differ by a maximum of 2°.

4.1.11 Velocity Jump

In all runs the M_2 component of the velocity show a strong deviation from a run without cross-tidal flat mass transport seaward of the location of the tidal flat. In the analysis of the results this strong deviation at the location of the tidal flat has been described as a jump. In channel 1 (lagging 30° behind channel 2), the jump is negative and smaller velocities are observed seaward of the tidal flat. In channel 2 higher velocities are observed seaward of the tidal flat. This phenomenon is explained by the theory stated below.

Velocity in the channels is dominantly determined by pressure gradients (sea level gradients) in the channels. When sea level is changed at a specific location (i.e. at the location of the tidal flat), the sea surface gradient will change and hence the velocity will also change. During the flooding phase, when the sea level in channel 2 is above the tidal flat height, mass flows from channel 2 to channel 1. This reduces the sea surface gradient in channel 1 and increases the sea surface gradient in channel 2 seaward of the tidal flat, slowing down the water seaward of the tidal flat in channel 1 and accelerating the water seaward of the tidal flat in channel 2.

During the ebb phase a similar process occurs. Sea level in channel 1 is higher than in channel 2 and mass will flow from channel 1 to channel 2. The sea surface gradient in channel 2 is increased and the sea surface gradient in channel 1 is decreased. The result is that, also during the ebb phase, the flow in channel 2 is accelerated seaward of the tidal flat and the flow in channel 1 is decelerated seaward of the tidal flat.

4.2 Results NM-F model

The NM-F model has a more advanced description of the tidal flat hydrodynamics than the NM-P model. The hydrodynamics on the tidal flat are solved at each location on the tidal flat. The NM-F model can thus be used to obtain a spatial distribution of sea level and velocity over the tidal flat at each moment in time.

First, two simulations by the NM-F model are compared to simulations by two other numerical hydrodynamical models, Delft3D and the Defina model (as used in a simulation by **?**). The simulations are carried out in a T-geometry (see Figure **??**). The comparison is based on both qualitative and quantitative agreement. When the agreement between the simulations is satisfactory, the NM-F model is used to answer one of the research questions of this thesis; How sea level and velocity are distributed over the tidal flat during a tidal cycle.

At the end of the section the NM-F model is applied to the H-geometry. When simulations are successful, cross-tidal flat mass transport is calculated in the NM-F model, as well as its effect on channel hydrodynamics.

4.2.1 Comparison NM-F

The NM-F model calculates the hydrodynamics in the channels and on the tidal flat. In the channel the hydrodynamics are described by the 1D shallow water equations. The hydrodynamics on the tidal flat have been developed specifically for the NM-F model. The quality of the tidal flat hydrodynamics is yet unknown. To address this issue, simulations run in the NM-F model is compared to simulations by two other numerical models, Delft3D and the Defina model. Delft3D and the Defina model are also capable of simulating the hydrodynamics over the tidal flat. A Delft3D simulation is compared to a simulation of the same situation by the NM-F model. After that, a simulation by the Defina model is compared to a simulation by the NM-F model. Both the Delft3D simulation and the Defina model simulation are executed on a T-geometry (see Figure **??**).

The comparisons between Delft3D and the NM-F model and between the Defina model and the NM-F model are used to assess the quality of the NM-F model. If the simulations by the NM-F model show small deviations, both quantitatively and qualitatively, from the more advanced models, there is good reason to believe the produced results from the NM-F model are credible.

Delft3D

Delft3D is a computational model that simulates 2D and 3D hydrological and morphological processes, such as flow, waves and sediment transport. Delft3D has been developed by Deltares, a technological institute in The Netherlands. For more information on the model, see **?**.

With Delft3D, a tidal channel with adjacent tidal flat is simulated in 2D (depth averaged variables). The domain is presented in Figure **??**. The main channel has a depth of 10 meters, is 50 kilometers long and 750 meters wide. It has one open boundary and one closed boundary. The tidal flat is connected to the tidal channel at 25 kilometers from the open boundary. The tidal flat is 2 kilometers long, 2250 meters wide and has an undisturbed water depth of 10 centimeters. Delft3D has a drying routine that requires a small amount of water to remain on the tidal flat. This minimum water level has been chosen as 10 centimeters. When water level in the tidal channel is zero, no water will flow from tidal flat to tidal channel or vice versa, just as in the Network Model. For more information, see Box 1.

Box 1: Delft3D Drying Routine

Delft3D requires a minimum water depth $\eta_{tf,min}$ on the tidal flat to avoid dividing by zero when friction on the tidal flat is considered ($\frac{\partial u}{\partial t} = ... - C_d \frac{|u_{tf}|u_{tf}}{H_{tf}+\eta_{tf}}$). Whenever η_{tf} would drop below $\eta_{tf,min}$, it is replaced by $\eta_{tf,min}$.

At the first grid point of the tidal flat, x_1, the tidal flat is connected to a channel in which sea level is allowed to drop below $\eta_{tf,min}$. When that happens, sea level $\eta_{tf}|_{x_1}$ is replaced by $\eta_{tf,min}$ and no flow is allowed from tidal flat to the channel ($u_{tf,x_1} = 0$, with u_{tf} defined positive from channel to tidal flat).

However, when sea level in the channel is only just below $\eta_{tf,min}$, Delft3D does allow the sea level to adjust. Due to sea level gradients at the first grid point, a flow will develop at the first grid point, flowing from the tidal flat to the tidal channel ($u_{tf}|_{x_1} < 0$). During the ebb phase of the tidal cycle this behavior is expected, during the flood phase it is not. Thus, when the velocity profile is analysed in time, negative velocities will show up over the tidal flat just before the tidal flat is flooded.

The blue squares in figure **??** represent observation points. At these points, quantities such as flow velocities and sea level are stored at each time step. They are not to be confused with grid points.

	Variable	Value
Length Tidal Channel	L	50km
Width Tidal Channel	W	750m
Depth Tidal Channel	H	10m
Length Tidal Flat	L_{tf}	2000m
Width Tidal Flat	W_{tf}	2250m
Depth Tidal Flat	H_{tf}	0m
Bottom Friction Coefficients Tidal Channel	C_d	variable
Bottom Friction Coefficient Tidal Flat	$C_{d,tf}$	10^{-2}

Table 4.12: Values for parameters used for comparison between Delft3D and NM-F model.

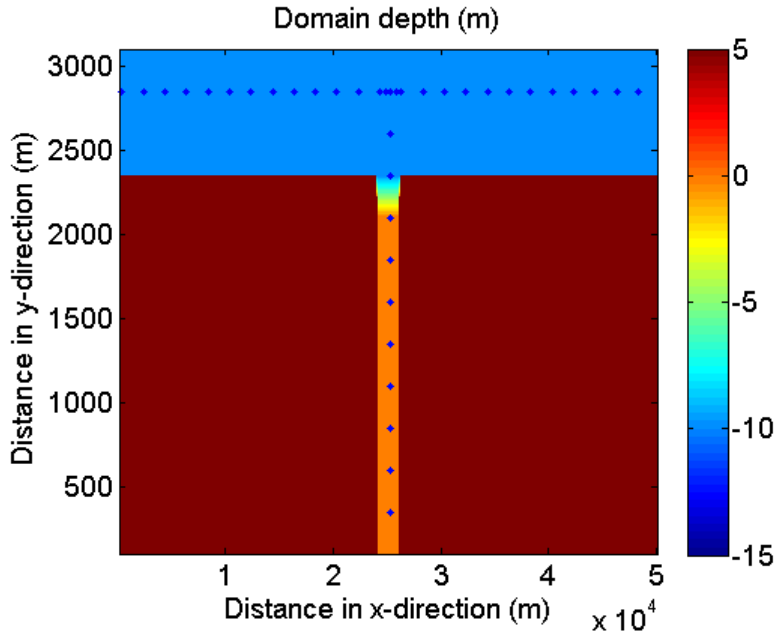

Figure 4.21: The domain of the Delft3D run, contour colors represent undisturbed water depth in meters. The tidal channel has a open boundary at $x = 0m$ and a closed boundary at $x = 50km$. The tidal flat is connected to the tidal channel at $x = 25km$ and has a closed boundary at $y = 0m$.

The NM-F model is set up for the same domain and boundary conditions as Delft3D. In Delft3D, the sea level at prescribed at the open boundary as a sinusoidal wave with amplitude 1m and tidal frequency $1.41 * 10^{-4}\text{s}^{-1}$. An overview of the parameters used in the NM-F model is found in Table **??**. The results from the NM-F model and Delft3D are compared based on sea level and velocity. They are plotted at four locations: at the open boundary, at 16km from the open boundary, at 30km from the open boundary and at the first grid point of the tidal flat. After a spin-up of two tidal cycles, four complete cycles are shown.

In the NM-F model, either sea level or an incoming wave can be prescribed at the open boundary. The two methods are mutually exchangeable; when an incoming wave is prescribed, the sea level can be calculated and vice versa. When a sinusoidal incoming wave is prescribed, the corresponding sea level will most likely not have the shape of an exact sine function, and when sea level is prescribed sinusoidally, the incoming wave will most likely not have a perfect sine profile.

At the open boundary, an incoming wave is superposed on the outgoing wave, adding their amplitudes. When an incoming wave with amplitude 1m is prescribed, the resulting sea level at the open boundary may have a maximum value of 2m (in an idealised, frictionless case and a tidal channel of specific geometry). When the

sea level is prescribed with amplitude 1m, the sea level amplitude at the open boundary will in fact be 1m.

Despite the fact that sea level and incoming waves are exchangeable, prescribing a sinusoidal shape of one might be better at reproducing the results from Delft3D than the other. Therefore, results for both configurations are shown in this section, starting with prescribing sea level at the open boundary.

Prescribing Sea Level at Open Boundary

The results for the NM-F model are shown in Figure **??**, along with the results from Delft3D for the same geometry. At the open boundary, the sea level is prescribed an no difference between the Delft3D and the NM-F model is observed. The along-channel velocity does show a difference at the open boundary. In the NM-F model maximum flood currents are observed later than in Delft3D and have a smaller magnitude. Maximal ebb currents are observed simultaneously and have approximately the same magnitude. A harmonic analysis (Figure **??**) shows that M_0 and M_4 tidal constituents have a larger amplitude in the NM-F model than in Delft3D, causing a different velocity profile at the open boundary.

A similar conclusion is drawn from the other observation points in the tidal channel, at 16km and 30km. The sea level is still well synchronised, although the NM-F model shows an increasing deviation from Delft3D with increasing distance from the open boundary. The maximum sea level in Delft3D is higher during high water and lower during low water, with a larger difference during lower water than during high water. The along-channel velocity at observation points at 16km and 30km has a more asymmetric profile in the NM-F model, with maximal flood currents smaller in amplitude and occurring at a later moment, and maximal ebb currents with a similar amplitude and occurring simultaneously. The harmonic analysis of the sea level (Figure **??**) shows that the M_2 constituent is larger in Delft3D than in the NM-F model, whereas M_0 and M_4 are larger in the NM-F model. Harmonic analysis of the along-channel velocity reveals a similar picture in the first 25km of the channel. The NM-F model has a smaller M_2 component and a larger M_0 and M_6 component. At 25km, where the tidal flat is attached to the channel, a large jump in the tidal constituents is observed in the NM-F model. In Delft3D, this jump is also present, but a lot smaller.

The arrival of the tidal wave at the tidal flat takes place at the same moment in Delft3D and the NM-F model. By construction Delft3D has a minimum sea level of approximately 10cm. Right before the tidal wave arrives, sea level suddenly drops below this minimum sea level in Delft3D. The system shifts from a state in which sea level is prescribed by the minimum sea level to a state in which the sea level is determined by the dynamics of the system. The adjustment causes sea level to drop below the minimum sea level just before the tidal wave comes in (see Box 1). The drop in sea level is accompanied by negative along-channel velocities that only show up in Delft3D. Just as in the tidal channel, the maximum sea level on the tidal flat is slightly higher in Delft3D. In Delft3D, larger maximum flood currents and larger maximum ebb currents are observed. This may be explained by the fact that Delft3D has a water depth that is, by construction, 10cm deeper than the NM-F model due to the Delft3D drying routine. The phase speed of a wave depends on the water depth; in deeper water, a wave travels faster. Thus, a tidal wave entering the tidal flat progresses faster in Delft3D and a tidal wave leaving the tidal flat needs less time to leave.

The NM-F model has also been run with other friction coefficients. To obtain the same M_2 tidal constituent as in Delft3D in the tidal channel, the friction should be chosen unrealistically small ($C_d = \mathcal{O}(10^{-7})$). A consequence was that the M_4 constituents also increased a lot, with amplitudes up to 0.5m s^{-1} for velocity and 0.4m for sea level (results not shown). The setup for Figure **??** ($C_d = 0.001$) appears to mimic the result of Delft3D most accurately, qualitatively and quantitatively.

The purpose of comparing the NM-F model with Delft3D is to find qualitative and quantitative agreement between the two models, most importantly on the tidal flat. On the tidal flat, sea level differs only slightly between Delft3D and the NM-F model, and the difference between the along-channel velocities can be explained and justified. In the tidal channel there is good qualitative agreement between the models. The NM-F model produces a M_2 tidal constituent that is smaller than in Delft3D, and a M_0 and M_4 that are, in general, larger than in Delft3D. Despite these differences, the results of the comparison between the NM-F model and Delft3D are promising.

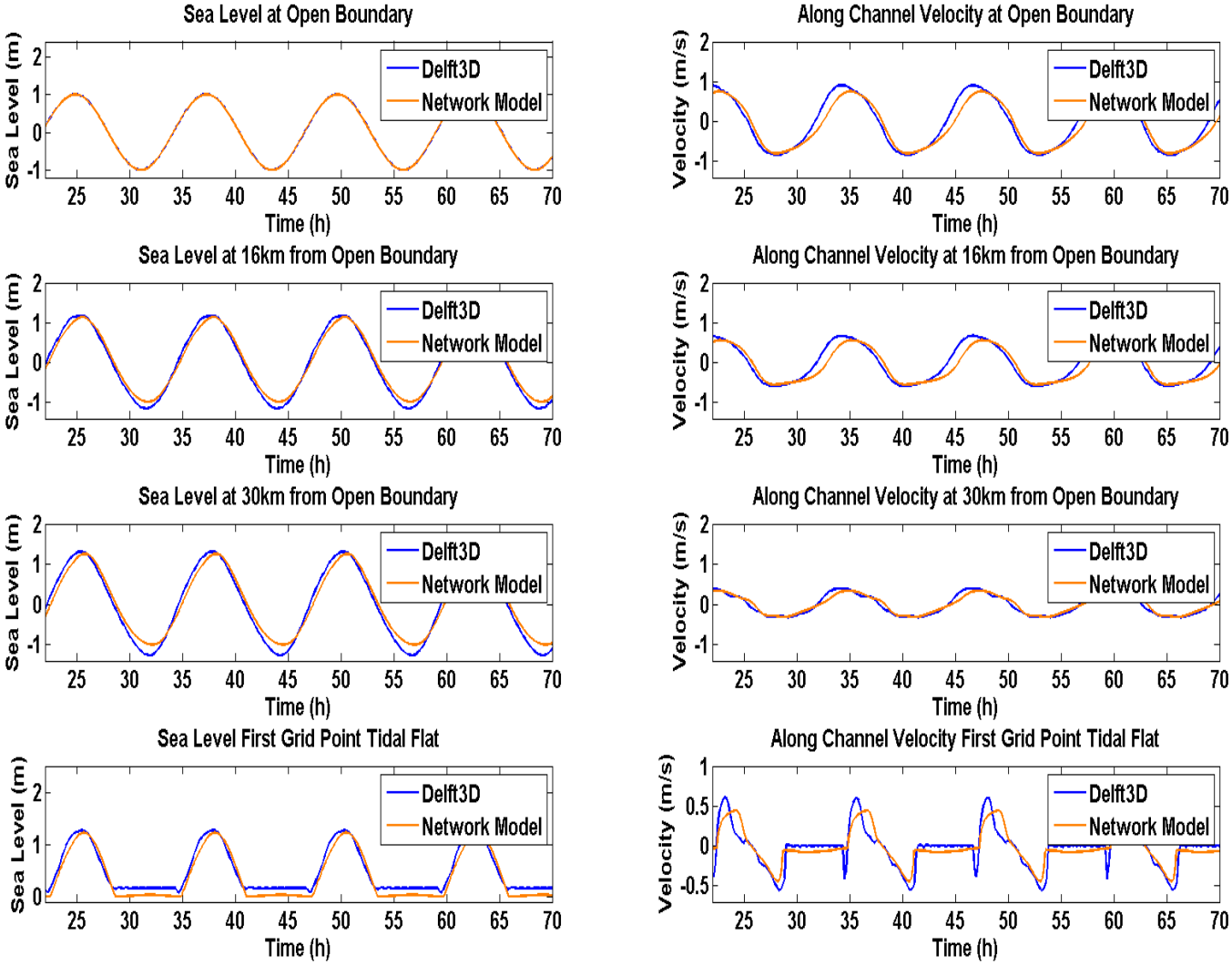

Figure 4.22: The sea level and along channel velocity are plotted for Delft3D and the NM-F model at four different locations in the system. At the open boundary sea level is prescribed.

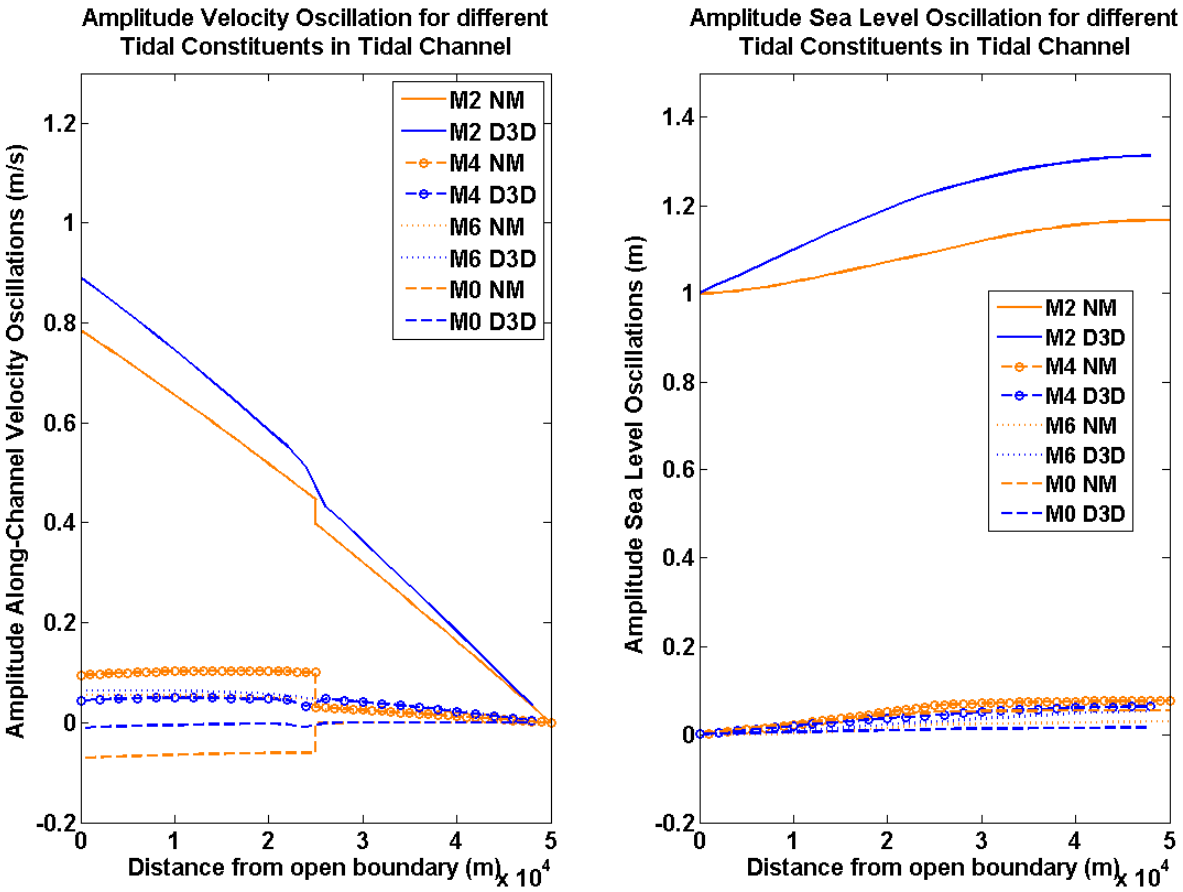

Figure 4.23: A harmonic analysis of sea level and along channel velocity in the tidal channel from both the NM-F model (NM) and Delft3D (D3D) with sea level prescribed at the open boundary. Blue lines indicate Delft3D results, orange lines indicate NM-F model results. Higher harmonics (M_8 and higher) have negligible amplitude.

Prescribing Incoming Wave at Open Boundary

The two models can also be compared when the NM-F model is forced with an incoming wave instead of sea level at the open boundary. These results are shown in Figure **??**. The results from the NM-F model are tuned to mimic the results from Delft3D. The friction coefficient on the tidal flat has a very small value ($C_d = 10^{-4}$). When an incoming wave with an amplitude of 1m is prescribed at the open boundary, the resulting sea level oscillation at the open boundary has an amplitude of approximately 1.3m. To obtain a better match, the amplitude of the incoming wave has been chosen as 0.75m, producing a much better fit.

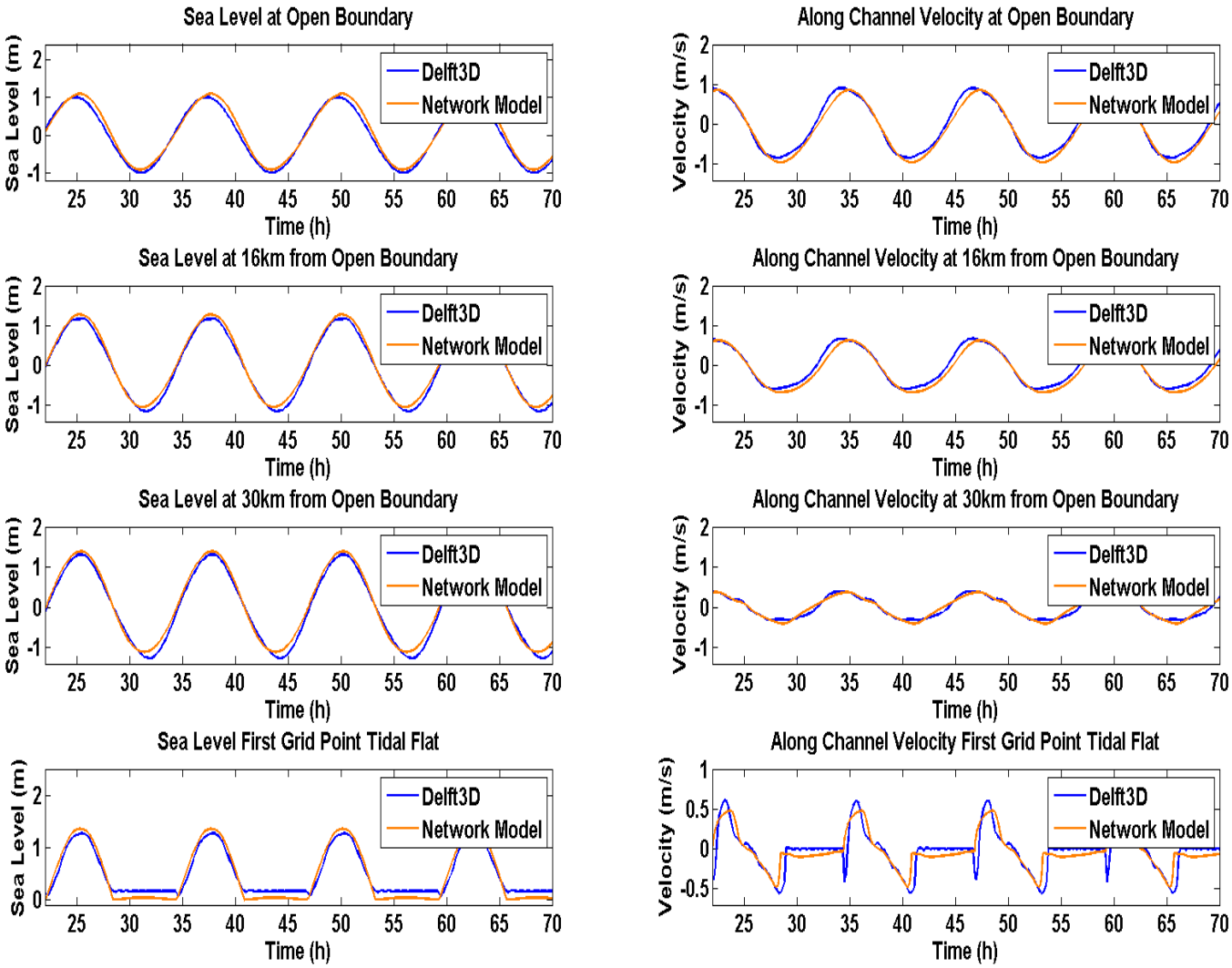

Figure 4.24: The sea level and along channel velocity are plotted for Delft3D and the NM-F model at four different locations in the system. At the open boundary an incoming wave is prescribed.

The sea level in the channel shows a good fit with the results from Delft3D. Both maximum and minimum sea levels are slightly higher in the NM-F model. Harmonic analysis (Figure **??**) shows a permanent sea level setup

of approximately 10cm in the NM-F model (M_0 tidal constituent). In Delft3D, the sea level setup has a much smaller amplitude. The difference between the sea level setups explains higher sea level extremes in the NM-F model.

The velocity in the channel shows slightly lower minimal and maximal values in the NM-F model. The harmonic analysis shows that there is constant negative velocity in the NM-F model seaward of the tidal flat, associated with the M_0 tidal constituent. In Delft3D, the amplitude of the M_0 tidal constituent is approximately 0.01ms^{-1}, in the NM-F model 0.08ms^{-1}. The M_0 tidal constituents vanishes after 25km. At the point, the tidal flat is connected to the channel. The along-channel velocity range produced by the NM-F model appears to be consistent with Delft3D.

At the tidal flat the sea levels of the NM-F model and Delft3D overlap almost perfectly. The sea level in the NM-F model has a slightly higher maximum value, caused by the sea level setup in the channel. When the water level is below zero in the channel, the sea level in the NM-F model can drop to zero, whereas Delft3D requires a constant minimal sea level as part of its drying routine. This explains the difference between the NM-F model and Delft3D when water level is below zero in the channel. The velocity of the NM-F model has smaller maximum and minimum currents. Delft3D requires a minimum sea level to be present, and waves travel faster in deeper water, so when the tidal wave comes in, it can progress faster on the tidal channel. This explains the fact that the maximum current has a higher value and a shorter duration in Delft3D. Compared to the NM-F model with prescribed sea level at the open boundary (previous subsection), a better fit is obtained. When the sea level in the channel is below zero, no sea level change can occur in Delft3D, so all velocities are zero. This is not the case for the NM-F model, where small negative velocities are observed (water flows from the flat into the channel).

Prescribing Sea Level versus Prescribing Incoming Wave

The NM-F model is capable of reproducing the results of Delft3D to a large extent, both with prescribing a sinusoidal sea level and prescribing a sinusoidal incoming wave at the open boundary. When an incoming wave is prescribing, the results are, in general, closer to the results of Delft3D. The harmonic analysis shows that, when prescribing sea level, the M_2 tidal component can be perfectly reproduced, while the other constituents are an order of magnitude smaller. When the NM-F model aims to reproduce the M_2 tidal component with prescribing sea level, it is accompanied by a disturbingly large M_4 tidal component and the resulting sea level and velocity show qualitatively different signals than Delft3D.

In conclusion, prescribing a sinusoidal incoming wave at the open boundary produces results that are, in general, closer to the results of Delft3D.

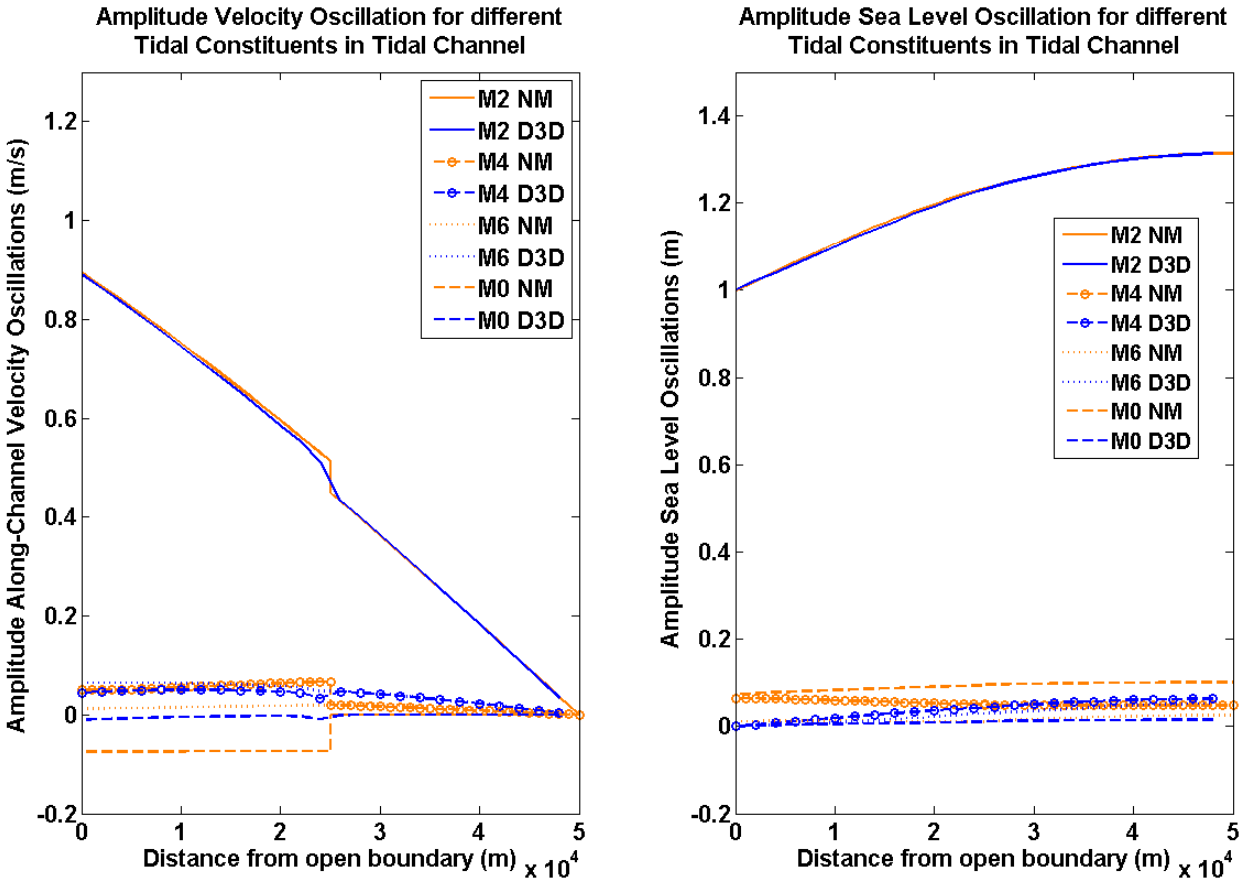

Figure 4.25: A harmonic analysis of sea level and along channel velocity in the tidal channel from both the NM-F model (NM) and Delft3D (D3D) with at the open boundary an incoming wave prescribed. Blue lines indicate Delft3D results, orange lines indicate NM-F model results. Higher harmonics (M_8 and higher) have negligible amplitude.

4.2.2 Van Oyen (2012)

? developed an analytical model to describe flow over frictionally dominated tidal flats. They compared the results of their model to the results obtained with a full-fledged finite element model (**?**, **?**, from here on called 'Defina Model'). The domain they modelled is shown in Figure **??**. The domain contains one tidal channel (length, width and depth are unspecified in **?**) and two tidal flats (both depth 1m, width 500m and length 1km). The tidal flats have the same geometry and are located at the same location in the tidal channel. In the NM-F simulation of this geometry, the two tidal flats are combined into a tidal flat of width 1000m, that is located at the same location as the tidal flats in the setup by **?**. With this adjustment, a T-geometry is obtained. At the open boundary of the channel, a tidal wave with amplitude 1m is prescribed. At the end of the channel, the tidal flats are connected to the channel. The NM-F model has been set up to simulate the same domain.

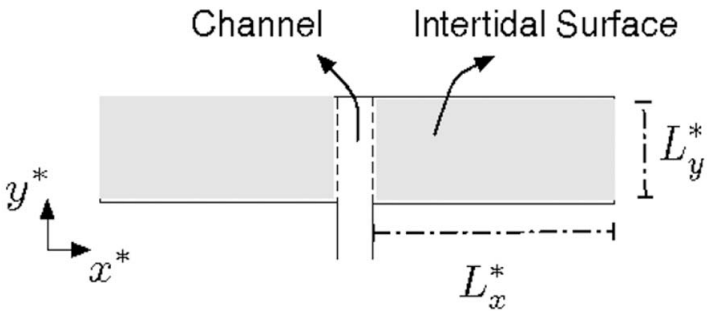

Figure 4.26: Domain in study by **?**. The channel is 10 meters deep, has a width of 300 meters, a length of 30km and at the end of the channel it is connected to a tidal flat (intertidal surface). The tidal flats are 1 meter deep, have a width of 500 meters and are 1000 meters long.

For the NM-F model simulation, a number of assumptions had to be made, because **?** did not provide all required data for the simulation. The geometry of the tidal flats was provided, but the geometry of the channel was not. Also, no value for the linear bottom friction coefficient λ was provided, neither for the channel nor for the tidal flat. The NM-F model uses quadratic bottom friction, denoted by quadratic bottom friction coefficient C_d. Via the energy criterion first introduced by **?**, a corresponding linear bottom friction coefficient λ can be obtained. The missing values were selected in such a way that a relatively good agreement was obtained between the NM-F model and the Defina Model. The used values are found in Table **??**

Another piece of missing information was how the boundary condition at the open boundary was prescribed. **?** mentions "a tidal wave with amplitude 1.0m", but whether sea level is prescribed or an incoming tidal wave is unclear (for a discussion on the difference between the two, see Section 2.1.3). The NM-F model uses an incoming wave at the open boundary, with an amplitude chosen such that the resulting sea level amplitude at the open boundary is approximately 1.0m. It turns out that an incoming wave with an amplitude of 0.6m is sufficient to obtain the desired sea level amplitude.

A comparison between the NM-F model and **?** is limited to the data that is provided in **?**. The most useful data for comparison in **?** is the along-channel velocity profile at 500m from the entrance of the tidal flat,

Parameter	Represents	Value
L_{ch}	Channel Length	30km
W_{ch}	Channel Width	300m
H_{ch}	Channel Depth	10m
$C_{d,ch}$	Quadratic bottom friction coefficient in channel	0.0025
$C_{d,tf}$	Quadratic bottom friction coefficient on tidal flat	0.06

Table 4.13: Values for parameters in the NM-F model for the simulation velocities on tidal flat.

plotted against time (Figure 2c in **?**). The velocity at the tidal flat, 500m from the entrance, has also been generated with the NM-F model. The results from the NM-F model are superposed on the original Figure 2c in **?** are shown in Figure **??**.

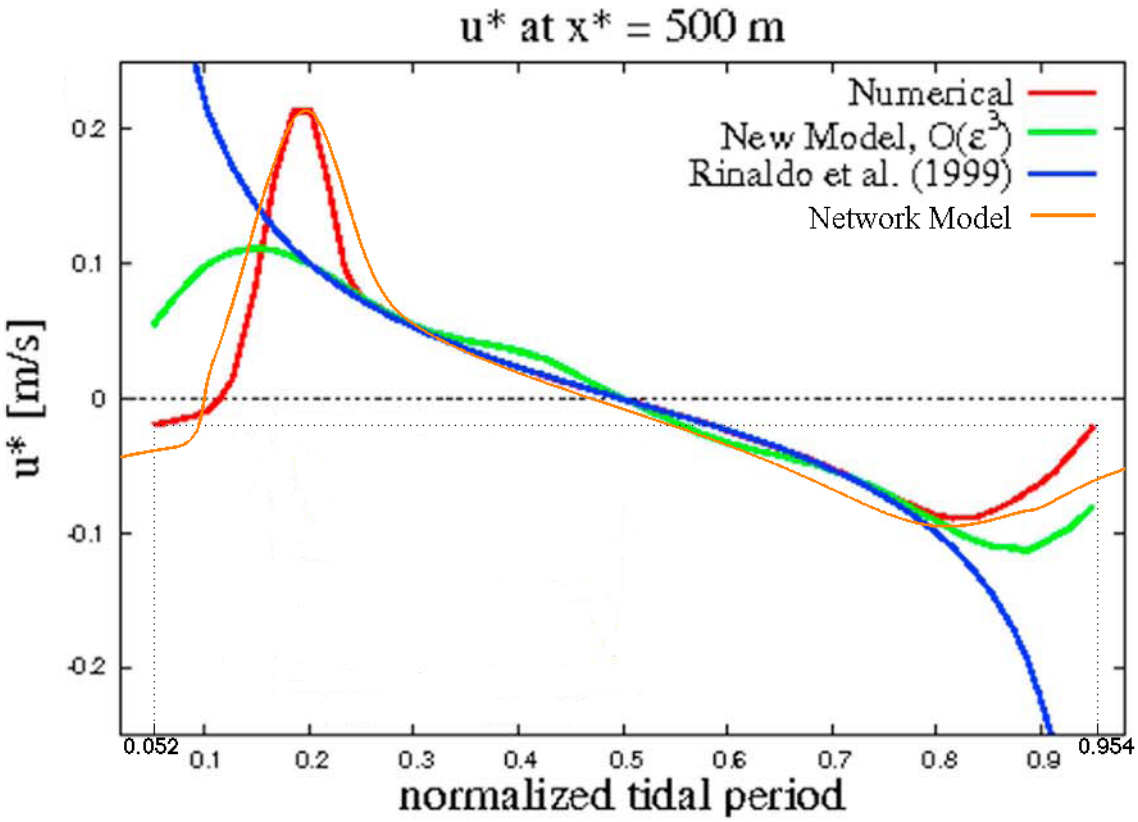

Figure 4.27: Comparing the results from the NM-F model to the original results by **?**. The results from the Defina model are shown in red (in figure: 'Numerical'), the results from the NM-F model (in figure: 'Network Model') are shown in orange. The dotted lines indicate the frequency of the Defina model.

The red line shows the velocity at 500m from the entrance of the tidal flat simulated by the Defina model and the orange line shows the velocity simulated by the NM-F model. The yellow and blue line are not considered in this comparison, because they are analytical approximations of the Defina model.

The velocity simulated by the Defina model completes one tidal cycle in 0.902 times the tidal frequency. This is not expected and a number of explanations are possible. The system may not have been in equilibrium when the results were extracted. The system may produce a different cycle each tidal period (e.g. variable wind forcing). Or the axes do not have the correct scale, while the data are correct. In all three cases qualitative comparison is still possible.

During the flooding phase, both the NM-F model and the Defina model show a sharp velocity peek of approximately 0.2ms^{-1}. The velocity peak is sharper (narrower) in the Defina model. This can be partially explained by the shorter tidal period of the Defina model, but still there is a discrepancy remaining in the sharpness of the peak that cannot be fully reproduced by the NM-F model under a wide variety of parameter values.

After the flood velocity peak, velocities gradually and almost linearly decrease to negative values in both models up to a maximum ebb current, in both models occurring around 0.8 times the tidal period. The maximum ebb currents are lightly larger in the NM-F model than in the Defina model. After the maximum ebb velocity has been reached, the increase in velocities in the Defina model is stronger than in the NM-F model. This phenomenon can also be partially explained by the shorter tidal period in the Defina model.

In conclusion, the NM-F model is capable of reproducing the from results the Defina model to a large extent, both qualitatively and quantitatively. Differences are observed in the sharpness of the flood velocity peak and the sharpness of the ebb velocity peak (both are smoother in the NM-F model). Magnitudes of the peaks and along the entire curve are reasonably agreeable.

4.2.3 NM-F model in H-geometry

The NM-F model is expected to produce more realistic results than the NM-P model, because it allows for a time delay in mass transport on the tidal flat, calculates sea level based on physics rather than a parametrisation and solves the hydrodynamic equations locally. When the NM-F model would be able to simulate cross-tidal flat mass transport, the values for cross-tidal flat mass transport would be more realistic as well. The NM-F model can be used to simulate cross-tidal flat mass transport when run in an H-geometry. If the simulation is successful, cross-tidal flat is quantified and the effect of cross-tidal flat on the channel hydrodynamics is investigated. This information can be used to assess two of the research questions of this thesis: How large is the cross-tidal flat mass transport and what is the effect of cross-tidal flat mass transport on channel hydrodynamics? To see if cross-tidal flat mass transport is reliably and realistically simulated by the NM-F model, a control run with the NM-F model executed, in which no cross-tidal flat mass transport is expected.

Simulation without cross-tidal flat mass transport

A first simulation is carried out in the same geometry as in the control run for the NM-P model (see Table **??** for parameters), with channel length 40km, channel depth 10m and channel width 200m. All other parameters in the simulation are also the same as in the control run, except for the phase difference, which is set to $\phi = 0°$. In this simulation, no cross-tidal flat mass transport is expected, because the geometry of the channels and the forcing at the open boundary are identical.

The NM-F model is initiated with all dynamic values set to zero, so $\eta = 0$ and $u = 0$ at each location in channel and tidal flat. The sea level on the tidal flat is plotted at 12 moments in time in Figure **??**. After approximately 50 minutes after the tidal wave enters the channels, the tidal wave has progressed to the location of the tidal flat and the tidal flat starts to flood. The tidal wave comes in from both sides simultaneously, because the forcing at the open boundaries of the channels is identical. The flooding is initially limited to the boundaries of the tidal flats and slowly fills the entire tidal flat. Around t=150 minutes, both waves have reached the centre of the tidal flat. It takes a tidal wave approximately 100 minutes to travel 1000m in this simulation. After the entire tidal flat has been flooded, the sea level rises more uniformly, until a maximum sea level is reached around t=267 minutes. Sea level drops faster at the edges of the tidal flat than in the interior, because at the edges the sea level is strongly affected by and directly connected to the sea level in the channels. Eventually sea level drops to almost zero at the edges, while the sea level in the interior has higher values. Just before a new tidal wave comes in (at t=733 minutes), the sea level over the tidal flat is almost uniform again.

The NM-F model is capable of simulating the hydrodynamics of the tidal flat. The resulting sea level, shown in Figure **??**, does not show any behaviour that cannot be explained by physical arguments. The progression of the wave over the tidal flat is slow, with the front of the wave moving at approximately 17cms^{-1}.

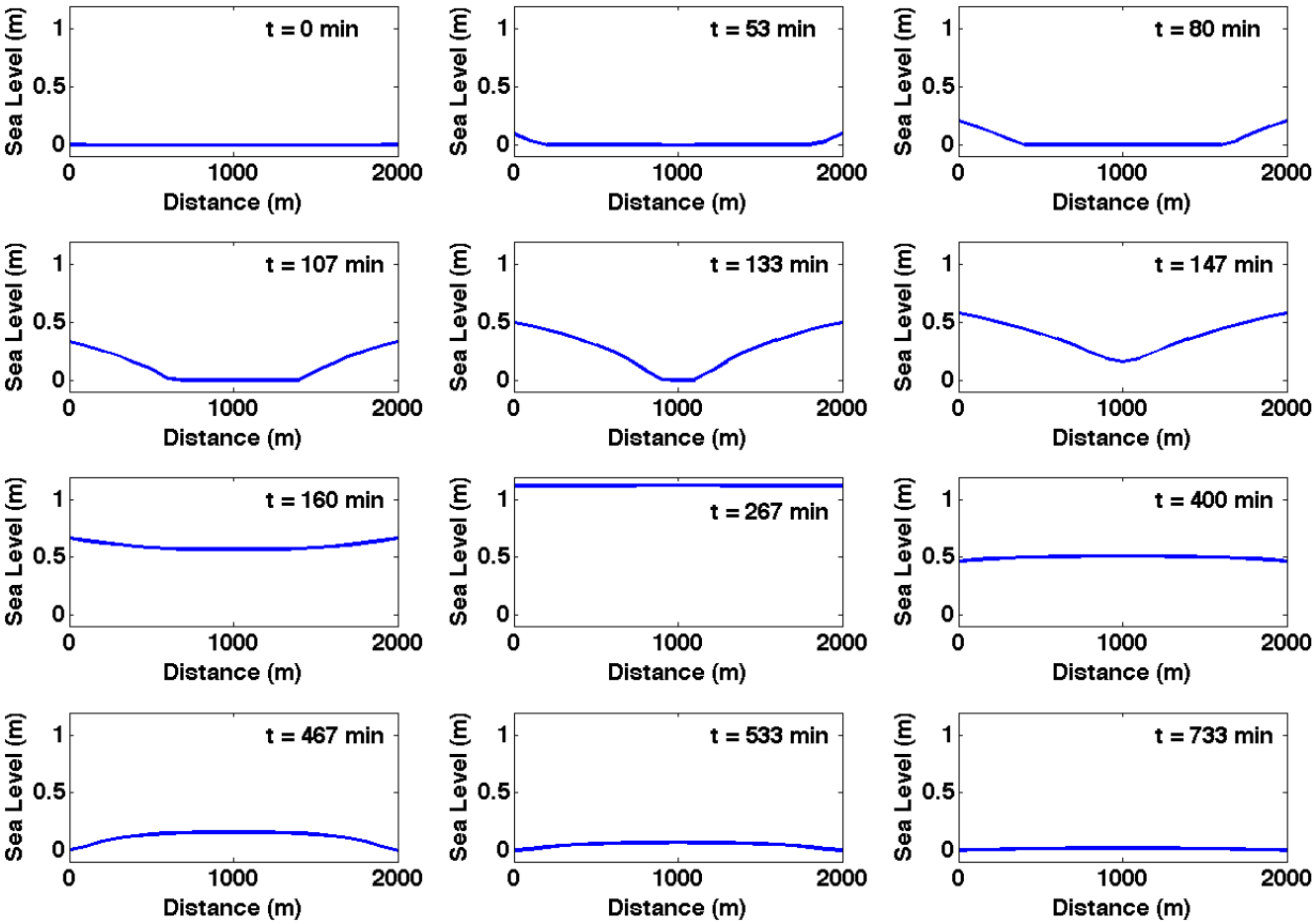

Figure 4.28: The sea level on the tidal flat at 12 different moments in time during one tidal cycle, simulated with the NM-F model.

Mass Conservation

The hydrodynamic equations in the NM-F model are formulated in such a way that mass should be conserved, both in the channels and on the tidal flat. Only during wave breaking mass is not necessarily conserved, but mass loss occurring during wave breaking is assumed to be very small. Mass conservation is most easily checked in a run in which there is no cross-tidal flat mass transport. This is achieved by prescribing the same forcing to a symmetrical system, as has been done in the previous section 'Simulation without cross-tidal flat mass transport'. Because the system is symmetrical no mass transport is expected at the centre of the tidal flat. In that case, all mass that enters channel 1 at the open boundary is expected to leave channel 1 via the open boundary during a tidal cycle, assuming the system is in equilibrium. The same is true for channel 2. The mass that enters the tidal flat on either side is expected to leave the tidal flat via the same side, because there is no cross-tidal flat mass transport.

Here, the same simulation that is used to produce Figure **??** is used to check for mass conservation. The run data are the same as in Table **??**, except the phase $\phi = 0°$ in this run. At the boundary between the tidal flat and channel 1 the cumulative mass transport is plotted in Figure **??**. When mass flows onto the tidal flat from channel 1, this is defined as positive mass transport. The cumulative mass transport is the sum of all mass that has passed the tidal flat boundary since the first time step. When there is mass conservation, it is expected that the cumulative mass transport returns to the same value after exactly 1 tidal cycle. In Figure **??** it is visible that this is not the case. During a tidal cycle mass is first transported from the channel to the tidal flat. After high water, mass is transported back from the tidal flat to the channel, but the cumulative mass does not return to the same value it had one cycle earlier. It implies that mass is lost on the tidal flat.

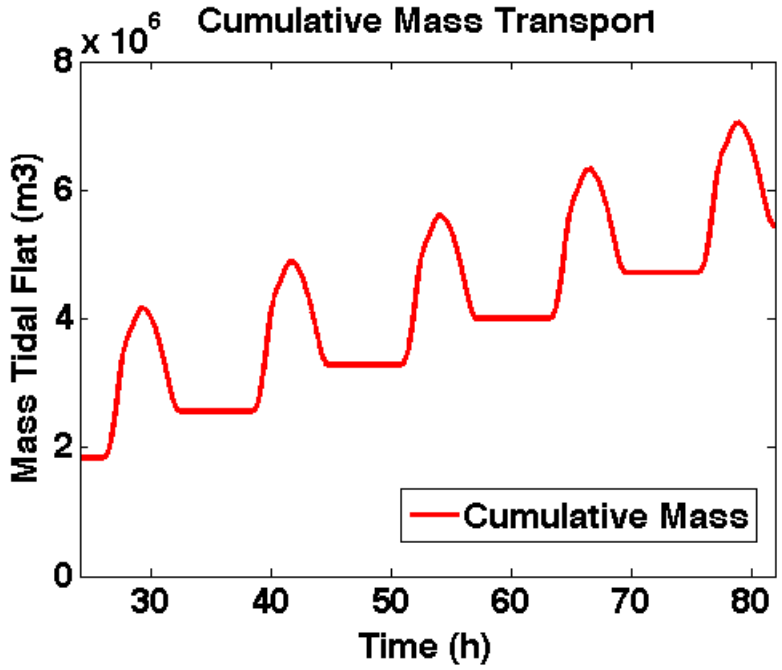

Figure 4.29: The cumulative mass transport at the boundary between channel 1 and the tidal flat during 5 tidal cycles.

In Figure **??** the cumulative mass transport is compared to the integrated mass on the tidal flat. The integrated mass is the amount of mass that is present at the tidal flat at a certain moment in time. It is calculated by integrating the sea level over the tidal flat. The tidal flat has length L_{tf}, and in the simulated run there is no mass transport at the centre of the tidal flat, at $\frac{L_{tf}}{2}$. All mass that is transported via the boundary between channel 1 and the tidal flat is somewhere between $x = 0$ and $x = L_{tf}/2$, where x is the spatial coordinate. The integrated mass on the tidal flat should be equal to the cumulative mass transport at the boundary at all times. This does not appear to be the case. The integrated mass returns to a value close to zero during each cycle, indicating that

almost all mass has left the tidal flat. The cumulative mass follows the curve of the integrated mass quite well, up until a certain point where the cumulative mass flatlines and the mass continues to leave the tidal flat. Mass flow from the tidal flat to the channel is blocked by a (spurious) boundary condition at the boundary between the channel and the tidal flat, causing the deficit between the cumulative mass and the integrated mass.

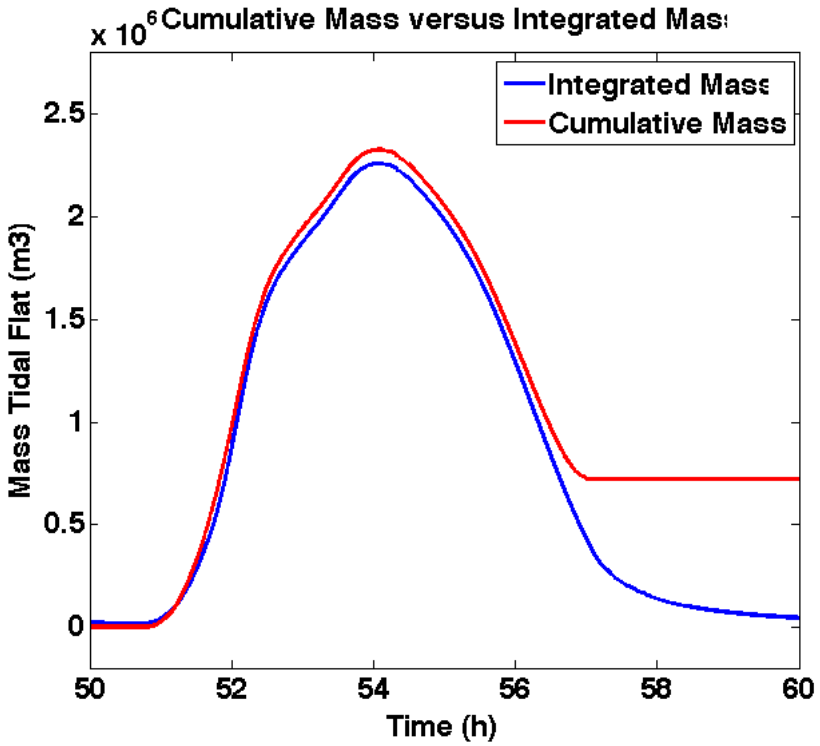

Figure 4.30: The cumulative mass transport at the boundary between channel 1 and the tidal flat is plotted in the same figure as in the integrated mass on the tidal flat during one tidal cycle.

Up until the point where the spurious boundary conditions is applied, the curves show a good agreement, with small differences between the integrated mass and the cumulative mass. During the flooding of the tidal flat, breaking waves occur. During wave breaking, mass is not necessarily conserved. The fact that the two curves show a good agreement gives confidence that the flooding phase of the tidal cycle is accurately simulated by the NM-F model.

Mass conservation has also been checked for the channels and for the nodal points in the NM-F model. They do appear to be mass conserving. Small deviation from mass conservation occur due to numerical approximation, but this is inevitable in numerical modelling.

Chapter 5

Discussion

5.1 NM-P Model

5.1.1 Harmonic Analysis

The effect of cross-tidal flat mass transport on the hydrodynamics of the channel is investigated by applying a harmonic analysis to the sea level and velocity in the channels. A harmonic analysis should only be applied when the frequencies present in the hydrodynamics are most dominantly harmonic. If that is not the case, a harmonic analysis may produce an incorrect fit and the results are spurious. A Fourier analysis is used to find the dominant harmonic frequencies in the system. If these frequencies are dominantly harmonic, a harmonic analysis is justified. In Figure **??**, a Fourier analysis of sea level and along-channel velocity is plotted for the control run of the NM-P model (parameters can be found in Table **??**).

The Fourier analysis in Figure **??** is performed in the channel at the location of the tidal flat. Here, the frequencies present in the sea level and velocity signals have a larger amplitude than at the open boundary or at any other location in the interior of the channel. All frequency peaks visible in Figure **??** coincide with a harmonic tidal frequency. No peak is observed at any frequency other than that a harmonic frequency. The conclusion is that performing harmonic analyses on the channel hydrodynamics is justified.

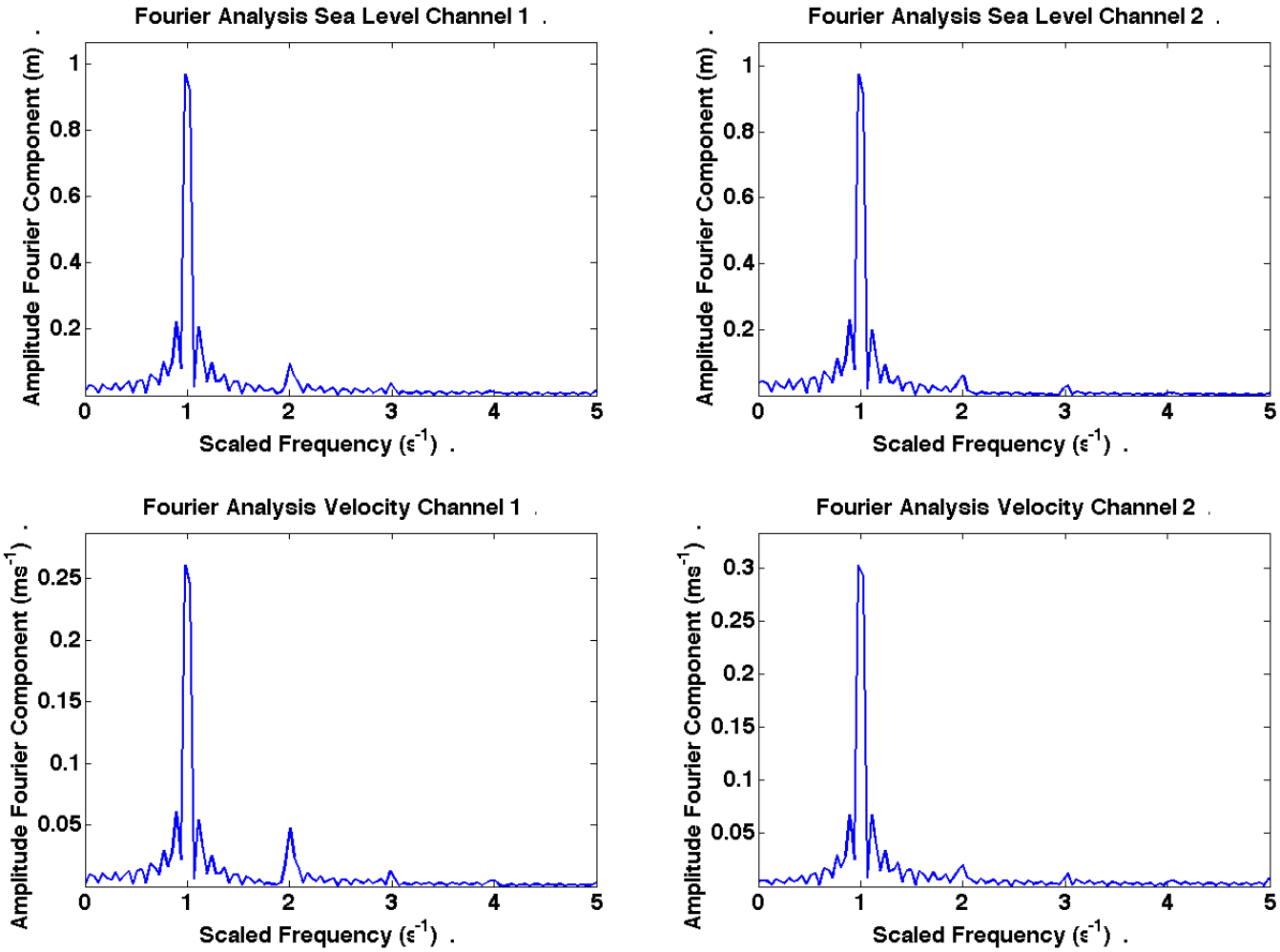

Figure 5.1: A Fourier analysis of the control run is performed at the location of the tidal flat. On the x-axis the scaled frequency is plotted, where a frequency of 1 corresponds to the M_2 tidal frequency. Results are shown for channel 1 and channel 2, for both along-channel velocity and sea level.

5.1.2 Instant mass transport

In the NM-P model it is assumed that, when mass is transported over the tidal flat from channel A to channel B, mass enters channel B at the same time the mass leaves channel A; There is no time delay between leaving one channel and entering the other. In reality mass is not transported instantly, because it needs to travel over the tidal flat to reach the other channel. Water flows slower in shallower water. When tidal flats are flooded, their initial water depth is very close to 0m, suggesting very low velocities.

The results from the NM-F run provide a good estimate for the duration of tidal flat traversing on dry tidal flats. In Figure **??**, the sea level is plotted during several stages of the tidal flat flooding. A tidal wave takes approximately 100 minutes to travel 1 kilometre on a dry tidal flat. Extrapolating this result to a tidal flat of 2km, as used in all simulations of the NM-P model results in a transport time of approximately 3 hours. This should be considered an upper boundary for the duration of cross-tidal flat mass transport. When water levels are even slightly less shallow, mass transport is much faster already, but this does not take away the fact that tidal flats are drained during each tidal cycle, during which the tidal flat becomes dry again.

An estimate for the lower boundary is made based on order of magnitude estimates. The velocity on the tidal flat is calculated via equations **??**. Assuming steady state, there is a balance between pressure gradient and bottom friction. An order of magnitude estimate for the duration of cross-tidal flat transport is found, based on scaling. When sea level between channel 1 and channel 2 differ by 1m, $\frac{\partial \eta}{\partial x} = \mathcal{O}(0.5 * 10^{-3}\text{m})$. The sea level is approximated via equation **??**, $\eta = \mathcal{O}(0.5\text{m})$. The gravitation acceleration and bottom friction are given by g=10ms^{-2} and $C_d = 10^{-2}$, respectively. These values result in a velocity amplitude of $|u|$=0.5ms^{-1} over the tidal flat. With this velocity, traversing a 2000m tidal flat would take 4000 sec, a little over 1 hour.

The duration of traversing the tidal flat, τ, scales with $\tau = L_{tf}^{\frac{3}{2}}$, where L_{tf} is the length of the tidal flat. Under the same conditions, traversing a 500m long tidal flat would take 500s, a little over 8 minutes. The value of $\tau = 500$s is based on a tidal flat that has already been flooded and on the presence of a strong pressure gradient. Simulations with the NM-F model indicate that the front of a tidal wave flooding a tidal flat moves with 0.17ms^{-2}. At this speed, it would take the front of a tidal wave approximately 50 minutes to cross a tidal flat of 500m.

The time it takes for mass to move from one side of the tidal flat to the other side varies strongly. For a tidal flat of 2000m a transport time between 1 hour and 3 hours is estimated. Compared to a tidal period of 12 hours, the transport time is not small and mass transport should not be treated as instantaneous. For a tidal flat of 500m transport time is estimated to be between 8 minutes and 50 minutes. This may still be a significant part of the tidal period. For tidal flats that are a lot smaller than 500m, the assumption of instant mass transport may be accurate. For tidal flats with length 500m and longer, the assumption that the cross-tidal flat transport is instantaneous is a very rough assumption. A more realistic calculation of the hydrodynamics of the tidal flat is required to solve this problem. In the NM-F model the tidal flat hydrodynamics are solved with the 1D shallow water equations and the time delay in cross-tidal flat mass transport is simulated more accurately. Unfortunately, the NM-F model is not mass conservation. If it were, it would be an improvement of the NM-P model and cross-tidal flat mass transport would be calculated more accurately.

5.1.3 Nodal Momentum Transfer

At the nodal points in the discretised NM-P model the tidal flat is connected to the channels. It is assumed that the tidal flat is perpendicular to both channels and that along-channel momentum is not transformed into across-channel momentum. Over the tidal flat all along-channel momentum is lost during friction. All across-channel momentum that flows into the channels at the nodal point is also lost when the mass flows from the tidal flat into the channel. These assumptions are justified by assuming that the tidal flats are perpendicular to the channels and that along-channel momentum and across-channel momentum do not interact.

A simulation is done to find the effect of cross-tidal flat momentum transfer on the cross-tidal flat mass transport (see Section 4.1.3 Varying Tidal Flat Parameterisation). In one simulation, all along-channel momentum was transported from channel 1 to channel 2 and vice versa. In the other simulation, all along-channel

momentum is dissipated on the tidal flat and stationary water is dumped into the channels. Due to this change in parameterisation of along-channel momentum transfer, the net mass transport is changed by 1%, with other quantities even less affected. The effect of taking across-channel velocity into account is not looked into, but it is expected to have a similar order of magnitude and can reasonably be neglected.

5.2 NM-F model

5.2.1 Mass Loss

A simulation with the NM-F model in an H-geometry shows that the model does not conserve mass. The mass loss occurs on the tidal flat. As a result, no accurate estimate of cross-tidal flat mass transport is found with the NM-F model. The research questions 'How large is the cross-tidal flat mass transport' and 'What is the effect of cross-tidal flat mass transport on the channel hydrodynamics' can not be answered based on the results of the NM-F model.

The mass loss only occurs during a small part of the tidal cycle. During the rest of the tidal cycle the system behaves as expected. Results obtained in this period may still be valid under some conditions.

During a tidal cycle, approximately 4% of the mass that enters the system via the tidal flat is lost on the tidal flat in the simulation of the H-geometry. Most of this lost mass would have flown out of the system at a later time anyway. When the water level start rising again at the open boundary, the system will be very similar to a system in which there is no mass loss on the tidal flat. The tidal flat will have lost almost all its mass during low water. When water levels are rising, the tidal flat will be flooded. This process is modelled accurately up to the point where mass loss occurs. Under this assumption, Figure **??** is correct up to the 9th images, at t=400 minutes.

The comparison between the NM-F model and Delft3D and the Defina model shows small differences between the results, both qualitatively and quantitatively. This is true for the entire tidal cycle, and thus also for the flooding phase of the tidal flat. The gives confidence that the flooding phase is modelled correctly in the NM-F model.

5.2.2 Prescribing Sea Level at Open Boundary

The NM-F model can be forced with one of two boundary conditions at the open boundary: Prescribing sea level and prescribing an incoming wave. The comparisons between the NM-F model and Delft3D and between the NM-F model and the Defina model show the best agreement when an incoming wave is prescribed at the open boundary. When sea level is prescribed at the open boundary, the resulting sea level and velocity in the channels contain higher harmonics, predominantly the M_4 and M_6 harmonics. These harmonics were of a much smaller amplitude when an incoming wave was prescribed at the open boundary.

A possible explanation is that the sea level at the open boundary is constructed based on the outgoing characteristic. If the outgoing characteristic carries a signal that contains higher harmonics, they are transferred to the incoming characteristic, thus keeping the higher harmonics in the system. When an incoming wave is prescribed, the outgoing characteristic does not transfer the higher harmonics and they are allowed to leave the system.

In Appendix D, the comparison between the NM-F and the Defina model is shown, in which the NM-F is forced with a fixed sea level at the open boundary. It is concluded that the theory behind the mechanism of transferring higher harmonics from the outgoing to the incoming characteristic at the open boundary is supported by the results from the NM-F model.

Chapter 6

Conclusions

Two numerical models, the NM-P model and the NM-F model, have been developed to simulate the hydrodynamics in tidally dominated coastal systems containing tidal flats. The NM-P model has been used to simulate cross-tidal flat mass transport: Mass transport from a channel over a tidal flat into another channel. **?** incorporated cross-tidal flat mass transport in a tidal network model, but so far no research had been conducted to quantify the cross-tidal flat mass transport and its effect on the hydrodynamics in the channels. The NM-F model has been used to obtain a spatial distribution of sea level and velocity over the tidal flat. A number of simulations have been executed with the NM-P model and the NM-F model to answer the research questions of this research:

- How large is the cross-tidal flat mass transport?
- How does the magnitude of the cross-tidal flat mass transport depend on the system parameters?
- What is the effect of cross-tidal flat mass transport on the harmonics of the hydrodynamic variables?
- What is the spatial distribution of sea level and velocity over a tidal flat during a tidal cycle?

The results obtained with the NM-P model have shown that cross-tidal flat mass transport can be large. Under certain conditions the amount of mass transported from channel 1 to channel 2 during a tidal cycle is found to be only 4 times as small as the total amount of mass transported into channel 1 during a tidal cycle. This should be considered an upper limit. The amount of mass that is permanently transported from one channel into the other channel (the net mass transport) is much smaller, at most 3% of total mass transported into a channel during a tidal cycle. The net mass transport is always directed from the lagging to the leading channel.

The cross-tidal flat mass transport is strongly dependent on system parameters and system settings. A phase lag between the incoming waves at the open boundary causes cross-tidal flat mass transport. The larger the phase lag, the more mass is transported over the tidal flat, both from channel 1 to channel 2 and vice versa, with a maximum transport found at 180° phase difference. The maximum net cross-tidal flat mass transport is found at $\pm 60^\circ$ phase difference. Changing the boundary condition at the open boundary from an incoming wave to prescribing sea level decreases the total mass transported, but increases the net mass transport by 20%.

The location of the tidal flat is an important geometrical variable. The closer the tidal flat is to the open boundary, the more mass is transported over the tidal flat and the larger the net cross-tidal flat mass transport is. When the height of the tidal flat is increased, when the width of the tidal flat is decreased and when the bottom friction on the tidal flat is increased, less mass is transported over the tidal flat and a smaller the net cross-tidal flat mass transport is observed.

The channel depth has a strong influence on wave progression in the channel, which in turn affects the cross-tidal flat mass transport. When the depth difference between two channels, connected by a tidal flat, becomes larger, the cross-tidal flat mass transport will be larger. Also the net cross-tidal flat mass transport increases. Decreasing the channel width in one or both channels decreases the cross-tidal flat mass transport, as well as the net cross-tidal flat mass transport.
A simulation in which the tidal flat hydrodynamics were parameterised using the original parametrisation by **?**

has yielded unphysical results. The effect of cross-tidal flat momentum transport on the magnitude of cross-tidal flat mass transport and on channel hydrodynamics is negligibly small.

In the channels the hydrodynamics are strongly affected by cross-tidal flat mass transport. In both sea level and velocity an increase in the M_4 tidal constituent is simulated. The increase in M_4 is stronger when cross-tidal flat mass transport is larger. The phase of the M_4 tidal constituent shows a standing M_4 wave landward of the tidal flat and a M_4 wave progressing from the tidal flat to the open boundary seaward of the tidal flat. The M_2 tidal constituents in both sea level and velocity is weakly affected landward of the tidal flat. Seaward of the tidal flat the amplitude of the M_2 sea level constituent of the lagging (leading) channel increases (decreases) linearly to the open boundary. The amplitude of the M_2 velocity component in the lagging (leading) channel has a negative (positive) amplitude jump at the location of the tidal flat, after which the M_2 sea level amplitude remains constant seaward of the tidal flat. The M_0 and M_6 tidal constituents are, in general, only weakly affected by cross-tidal flat mass transport.

The NM-F model has been used to find the spatial distribution of sea level and velocity during a tidal cycle. Mass was not conserved during part of the tidal cycle. As a result, only the simulation of the flooding phase is considered to be accurately simulated. During the flooding phase, the front of a dry tidal wave flowing over the tidal flat progresses at a velocity of 0.17ms^{-1}. A tidal wave requires up to 3 hours to traverse a tidal flat of 2000m. The NM-P model assumes instant mass transport from one channel to the other channel. Based on the results by the NM-F model, this is a very rough assumption.

An attempt was made to simulate cross-tidal flat mass transport in the NM-F model. Due to mass loss during part of a tidal cycle, quantification of cross-tidal flat mass transport is inaccurate.

In conclusion, cross-tidal flat mass transport is, under a variety of circumstances, an important mass flux that affects the hydrodynamics in the adjacent channels. For a more accurate simulation of cross-tidal flat mass transport and its effect on the channel hydrodynamics a more advanced description of the tidal flat hydrodynamics is suggested, as was attempted in the NM-F model.

Acknowledgements

A great number of people contributed to a successful completion of this thesis. Two persons in particular have helped me tremendously in the past year: Niels Alebregtse as my day-to-day supervisor and professor Huib de Swart as my primary supervisor. Whenever I was stuck on my research, on whichever aspect of the research, Niels was always available for advice and only three doors away. Huib set out the research goals and steered the research in the right direction whenever I was lost. I am thankful to both of them for their input in this thesis.

I received valuable input for this thesis from Wim Ridderinkhof and Tomas van Oyen, for which I would like to thank them.

The atmosphere at the university, in particular at the study association A-Eskwadraat and in the IMAU student room was great. The students in the IMAU student room have also provided feedback on my work and I share great memories working together with you in the student room. Whenever I needed to clear my mind, the members of study association A-Eskwadraat were able to provide the necessary distraction.

Bibliography

N. C. Alebregtse. Non-linear Tides in Wadden Systems: Modelling the effect of mass and momentum transfer between channels and flats. Master Thesis, 2011.

John D. Anderson. *Computational Fluid Dynamics*. McGraw-Hill, Inc., 1995

D. G. Aubrey and P. E. Speer. A study of non-linear tidal propagation in shallow inlet/estuarine systems. Part I: Observations. Estuarine, Coastal and Shelf Science, 21:185-205, 1985.

J. D. Boon and R. J. Byrne. On basin hypsometry and the morphodynamic response of coastal inlet systems. Marine Geology, 40:27-48, 1981.

M. G. Bos. *Discharge measurements structures, third revised edition*. ILRI publication, 1989

Bouma, T. J., M. B. De Vries, E. Low, L. Kusters, P. M. J. Herman, I. C. Tánczos, S. Temmerman, A. Hesselink, P. Meire and S. van Regenmortel. Flow hydrodynamics on a mudflat and in salt marsh vegetation: identifying general relationships for habitat characterisations. *Hydrobiologia (2005) 540*, 259-274, doi 10.1007/s10750-004-7149-0

J. M. Brown and A. G. Davies. Flood/ebb tidal asymmetry in a shallow sandy estuary and the impact on net sand transport. Geomorphology, 114:431-439, 2010.

Carniello, L., A. D'Alpaos, and A. Defina, 2011, Modeling wind waves and tidal flows in shallow micro-tidal basins., *Estuarine Coastal Shelf Sci.,92*, 263-276, doi:10.1016/j.ecss.2011.01.001.

Davis, R. A. jr and Duncan M. Fitzgerald. *Beaches and Coasts*. Blackwell Science Ltd., 2004

A. Defant. Physical oceanography. New York: Pergamon Press, 1961.

Defina, A.,2000, Two-dimensional shallow flow equations for partially dry areas,. *Water Resour. Res., 36(11)*, 3251-3264.

J. J. Dronkers. *Tidal computations in rivers and coastal waters*. North-Holland Publ. Co., 1964

P. Hamilton. Modelling salinity and circulation for the Columbia river estuary. *Progress in Oceanography*,25:113-156,1990

A. E. Hill and A. J. Souza. Tidal dynamics in channels: 2. Complex channel networks. Journal of Geophysical Research, 111, November 30 2006. doi: 10.1029/2006JC003670.

Le Hir, P., W. Roberts, O. Cozaillet, M. Christie, P. Bassoullet, C. Bacher. Characterization of intertidal flat hydrodynamics. *Continental Shelf Research 20 (2000)*, 1433-1459.

Lesser, G.R., Roelvink, J.A., van Kester, J.A.T.M., Stelling, G.S., 2004. Development and validation of a three dimensional morphological model. *Journal of Coastal Engineering, 51*, 883-915.

R. Leveque, Numerical Methods for conservation laws, Birkhauser, 1992

H. A. Lorentz. Het in rekening brengen van den weerstand bij schommelende vloeistofbewegingens. De Ingenieur, 37:695, 1922.

Miller, D.C., Geider, R.J., and Macintyre, H.L. 1996. Microphytobenthos: The ecological role of the 'secret garden' of unvegetated, shallow-water marine habitats. II. Role in sediment stability and shallow-water food webs. Estuaries 19: 202-212.

B. B. Paker. The relative importance of the various nonlinear mechanisms in a wide range of tidal interactions (review). In B. B. Parker, editor, *Itdal Hydrodynamics*, 237-268. John Wiley & Sons, New York, 1991.

Reijnders, P.J.H., 1976. The harbour seal (Phoca Vitulina) population in the Dutch Wadden Sea: Size and compositions. Netherlands Journal of Sea Research 10 (2): 223-235.

P. E. Speer and D. G. Aubrey. A study of non-linear tidal propagation in shallow inlet/estuarine systems. Part II: Theory. Estuarine, Coastal and Shelf Science, 21:207-224, 1985.

J. van de Kreeke and K. Robaczewska. Tide-induced residual transport of coarse sediment; application to the Ems estuary. *Netherlands Journal of Sea Research*, 31:209-220, 1993.

Van Oyen, T., S. Lanzoni, A. D'Alpaos, S. Temmerman, P. Troch, L. Carniello, 2012, A simplified model for frictionally dominated tidal flows. *Geophysical Research Letters, 39*, L12403, doi:10.1029/2012/GL051949.

C. B. Vreugdenhil. *Computational Hydraulics*. Springer-Verlag, 1989

G. B. Whitham. *Linear and Nonlinear Waves*. John Wiley & Sons, Inc., 1974

Appendices

Appendix A

Nodal Dynamics

At an internal node conservation of mass and continuity of dynamic pressure are applied, via

$$\frac{1}{2}{u_1}^2 + g\eta_1 = \frac{1}{2}{u_2}^2 + g\eta_2 = \frac{1}{2}{u_3}^2 + g\eta_3,$$
$$\sum_{i=1}^{ch_{in}} W_i(H_i + \eta_i)u_i = \sum_{j=1}^{ch_{out}} W_j(H_j + \eta_j)u_j.$$

Using $u = \frac{1}{2}(r^+ + r^-)$ and $\eta = \frac{1}{16g}(r^+ - r^-)^2 - H$ they can be transformed into

$$\begin{aligned}&\frac{1}{8}({r_1}^+ + {r_1}^-)^2 + \frac{1}{16}({r_1}^+ - {r_1}^-)^2 - gH_1 = \\ &\quad\frac{1}{8}({r_2}^+ + {r_2}^-)^2 + \frac{1}{16}({r_2}^+ - {r_2}^-)^2 - gH_2 = \\ &\quad\frac{1}{8}({r_3}^+ + {r_3}^-)^2 + \frac{1}{16}({r_3}^+ - {r_3}^-)^2 - gH_3,\end{aligned} \tag{A.1}$$

and

$$\sum_{i=1}^{ch_{in}} \frac{W_i}{32g}({r_i}^+ + {r_i}^-)({r_i}^+ - {r_i}^-)^2 = \sum_{j=1}^{ch_{out}} \frac{W_j}{32g}({r_j}^+ + {r_j}^-)({r_j}^+ - {r_j}^-)^2. \tag{A.2}$$

A.1 One incoming, two outgoing

In the case that one tidal channel or tidal flat is defined as incoming channel at the nodal point and two tidal channels or tidal flat are defined as outgoing, equation **??** becomes

$$\begin{aligned}&\frac{W_1}{32g}({r_1}^+ + {r_1}^-)({r_1}^+ - {r_1}^-)^2 = \\ &\quad\frac{W_2}{32g}({r_2}^+ + {r_2}^-)({r_2}^+ - {r_2}^-)^2 + \frac{W_3}{32g}({r_3}^+ + {r_3}^-)({r_3}^+ - {r_3}^-)^2.\end{aligned} \tag{A.3}$$

Following the argumentation in section 3.2.5, r_1^+, r_2^- and r_3^- are known at the nodal point and the system is solved for the three remaining unknowns r_1^-, r_2^+ and r_3^+. The goal is to obtain one equation for one unknown and solve for that unknown. Here, the equations are solved for r_2^+. The unknowns r_1^- and r_3^+ are expressed in terms of r_2^+ via equation **??**.

$$\begin{aligned}&\frac{1}{8}({r_1}^+)^2 + \frac{1}{8}({r_1}^-)^2 + \frac{1}{4}{r_1}^+{r_1}^- + \frac{1}{16}({r_1}^+)^2 + \frac{1}{16}({r_1}^-)^2 - \frac{1}{8}{r_1}^+{r_1}^- - gH_1 = \\ &\qquad\frac{1}{8}({r_2}^+)^2 + \frac{1}{8}({r_2}^-)^2 + \frac{1}{4}{r_2}^+{r_2}^- + \frac{1}{16}({r_2}^+)^2 + \frac{1}{16}({r_2}^-)^2 - \frac{1}{8}{r_2}^+{r_2}^- - gH_2,\end{aligned}$$

$$
\begin{aligned}
&\frac{3}{16}({r_1}^+)^2+\frac{3}{16}({r_1}^-)^2+\frac{1}{8}{r_1}^+{r_1}^- - gH_1 = \\
&\qquad \frac{3}{16}({r_2}^+)^2+\frac{3}{16}({r_2}^-)^2+\frac{1}{8}{r_2}^+{r_2}^- - gH_2, \\
&\frac{3}{16}({r_1}^-)^2+\frac{1}{8}{r_1}^+{r_1}^-+\frac{3}{16}({r_1}^+)^2-\frac{3}{16}({r_2}^+)^2-\frac{3}{16}({r_2}^-)^2-\frac{1}{8}{r_2}^+{r_2}^-+g(H_2-H_1)=0, \\
&({r_1}^-)^2+\frac{2}{3}{r_1}^+{r_1}^-+({r_1}^+)^2-({r_2}^+)^2-({r_2}^-)^2-\frac{2}{3}{r_2}^+{r_2}^-+\frac{16}{3}g(H_2-H_1)=0.
\end{aligned}
$$

With the abc-formula, the roots of ${r_1}^-$ are obtained,

$${r_1}^- = -\frac{1}{3}{r_1}^+ \pm \sqrt{-\frac{8}{9}({r_1}^+)^2+({r_2}^+)^2+({r_2}^-)^2+\frac{2}{3}{r_2}^+{r_2}^- - \frac{16}{3}g(H_2-H_1)}.$$

The Riemann invariants $r^\pm$ are given by $r^\pm = u \pm \sqrt{g(H+\eta)}$. Thus, since the result of the square root is always positive, $r^+ \geq r^-$. To fulfill this condition, the solution containing the plus-sign is omitted, leaving an equation with a unique solution for ${r_1}^-$:

$${r_1}^- = -\frac{1}{3}{r_1}^+ - \sqrt{-\frac{8}{9}({r_1}^+)^2+({r_2}^+)^2+({r_2}^-)^2+\frac{2}{3}{r_2}^+{r_2}^- - \frac{16}{3}g(H_2-H_1)}. \tag{A.4}$$

Likewise, a solution is found to express ${r_3}^+$ in terms of ${r_2}^+$.

$${r_3}^+ = -\frac{1}{3}{r_3}^- + \sqrt{-\frac{8}{9}({r_3}^-)^2+({r_2}^+)^2+({r_2}^-)^2+\frac{2}{3}{r_2}^+{r_2}^- - \frac{16}{3}g(H_2-H_3)}. \tag{A.5}$$

One equation for r_2^+ is obtained by substituting equations **??**-**??** into equation **??**, resulting in

$$
\begin{aligned}
f({r_2}^+) = {} & w_1\Big(\frac{2}{3}{r_1}^+ - \sqrt{-\frac{8}{9}({r_1}^+)^2+({r_2}^+)^2+({r_2}^-)^2+\frac{2}{3}{r_2}^+{r_2}^- - \frac{16}{3}g(h_2-h_1)}\Big)* \\
& \Big(\frac{4}{3}{r_1}^+ + \sqrt{-\frac{8}{9}({r_1}^+)^2+({r_2}^+)^2+({r_2}^-)^2+\frac{2}{3}{r_2}^+{r_2}^- - \frac{16}{3}g(h_2-h_1)}\Big)^2 + \\
& - w_2({r_2}^+ + {r_2}^-)({r_2}^+ - {r_2}^-)^2 + \\
& - w_3\Big(\frac{2}{3}{r_3}^- + \sqrt{-\frac{8}{9}({r_3}^-)^2+({r_2}^+)^2+({r_2}^-)^2+\frac{2}{3}{r_2}^+{r_2}^- - \frac{16}{3}g(h_2-h_3)}\Big)* \\
& \Big(-\frac{4}{3}{r_3}^- + \sqrt{-\frac{8}{9}({r_3}^-)^2+({r_2}^+)^2+({r_2}^-)^2+\frac{2}{3}{r_2}^+{r_2}^- - \frac{16}{3}g(h_2-h_3)}\Big)^2 \\
& = 0.
\end{aligned}
\tag{A.6}
$$

The derivative of this equation (required for the Newton-Raphson method, see section A.3) is given by

$$
\begin{aligned}
\frac{\partial f}{\partial {r_2}^+} = {} & \frac{1}{3}({r_2}^- + 3{r_2}^+)\Big(\\
& 4W_1{r_1}^+ + W_1\sqrt{48g(H_1-H_2)+9({r_2}^+)^2-8({r_1}^+)^2+6{r_2}^-{r_2}^++9({r_2}^-)^2} + \\
& - 3W_2{r_2}^- + 3W_2{r_2}^+ + \\
& - 4W_3{r_3}^- + W_3\sqrt{48g(H_3-H_2)+9({r_2}^+)^2-8({r_3}^-)^2+6{r_2}^-{r_2}^++9({r_2}^-)^2} \\
& \Big).
\end{aligned}
\tag{A.7}
$$

A.2 Two incoming, one outgoing

For two incoming channels or tidal flats and one outgoing tidal channel or tidal flat, equation **??** translates to

$$
\begin{aligned}
&\frac{w_1}{32g}({r_1}^+ + {r_1}^-)({r_1}^+ - {r_1}^-)^2 + \frac{w_2}{32g}({r_2}^+ + {r_2}^-)({r_2}^+ - {r_2}^-)^2 = \\
&\qquad \frac{w_3}{32g}({r_3}^+ + {r_3}^-)({r_3}^+ - {r_3}^-)^2.
\end{aligned}
\tag{A.8}
$$

The unknowns of the system are r_1^-, r_2^- and r_3^+. The system is solved for r_2^- and r_1^- and r_3^+ are expressed as functions of r_2^-. Continuity of dynamic pressure results in equations **??**-**??**. Substituting them into equation **??** results in

$$\begin{aligned} f(r_2{}^-) = {} & w_1\Big(\frac{2}{3}r_1{}^+ - \sqrt{-\frac{8}{9}(r_1{}^+)^2 + (r_2{}^+)^2 + (r_2{}^-)^2 + \frac{2}{3}r_2{}^+r_2{}^- - \frac{16}{3}g(h_2-h_1)}\Big)* \\ & \Big(\frac{4}{3}r_1{}^+ + \sqrt{-\frac{8}{9}(r_1{}^+)^2 + (r_2{}^+)^2 + (r_2{}^-)^2 + \frac{2}{3}r_2{}^+r_2{}^- - \frac{16}{3}g(h_2-h_1)}\Big)^2 + \\ & + w_2(r_2{}^+ + r_2{}^-)(r_2{}^+ - r_2{}^-)^2 + \\ & - w_3\Big(\frac{2}{3}r_3{}^- + \sqrt{-\frac{8}{9}(r_3{}^-)^2 + (r_2{}^+)^2 + (r_2{}^-)^2 + \frac{2}{3}r_2{}^+r_2{}^- - \frac{16}{3}g(h_2-h_3)}\Big)* \\ & \Big(-\frac{4}{3}r_3{}^- + \sqrt{-\frac{8}{9}(r_3{}^-)^2 + (r_2{}^+)^2 + (r_2{}^-)^2 + \frac{2}{3}r_2{}^+r_2{}^- - \frac{16}{3}g(h_2-h_3)}\Big)^2 \\ & = 0. \end{aligned} \tag{A.9}$$

A.3 Solving Matching Numerically

The resulting equation for one unknown, say r_2^+, is a polynomial of degree three. It has multiple analytical solutions, of which only one is physically correct. To circumvent this problem, an approximation of r_2^+ is made based on continuity of sea level rather than continuity of dynamic pressure. The approximation yields an analytically unique value for r_2^+. The physically correct value of r_2^+ will be 'close' to the approximated value. A numerical method (Newton-Raphson) will be used to obtain a solution r_2^+ based on continuity of dynamic pressure.

To determine which of the solutions for $f(r_2^+)$ is physically correct, an approximate value for r_2^+ is constructed based on continuity of sea level ($\eta_i = \eta_j \quad \forall\, i,j$) rather than continuity of dynamic pressure. An approximate solution for r_2^+, r_2^{+*}, is obtained via this method.

When it is assumed that $\eta << h$, an equation can be found that is more easily solvable for $r_2{}^-$. The Riemann variables are given by $r^\pm = u \pm 2\sqrt{g(h+\eta)}$. For small values of ϵ, $(1+\epsilon)^n \approx 1 + n\epsilon$.

$$\begin{aligned} r^\pm &= u \pm 2\sqrt{g(h+\eta)}, \\ &= u \pm 2\sqrt{gh}(1+\frac{\eta}{h})^{\frac{1}{2}}, \\ &\approx u \pm 2\sqrt{gh}(1+\frac{1}{2}\frac{\eta}{h}), \\ &\approx u \pm 2\sqrt{gh} \pm \sqrt{\frac{g}{h}}\eta. \end{aligned} \tag{A.10}$$

From this, an expression is found for sea level η and velocity u.

$$u = \frac{1}{2}(r^+ + r^-), \tag{A.11}$$

$$\eta = \frac{r^+ - r^-}{2\sqrt{\frac{g}{h}}} - 2h. \tag{A.12}$$

Continuity of dynamic pressure contains a u^2-term, which causes nonlinearities. Since the goal is to find an approximate solution for the system, the boundary condition continuity of sea level is applied instead of continuity of dynamic pressure. With this new boundary conditions, the criteria at the nodal point are

$$\eta_1 = \eta_2 = \eta_3, \tag{A.13}$$

$$w_1u_1(h_1+\eta_1) = w_2u_2(h_2+\eta_2) + w_3u_3(h_3+\eta_3). \tag{A.14}$$

The aim is to find one equation for ${r_2}^+$ in terms of known variables ${r_1}^+$, ${r_2}^-$ and ${r_3}^-$. Eliminate ${r_1}^-$ and ${r_3}^+$ through equation **??**.

$$\begin{aligned}
\eta_1 &= \eta_2, \\
\frac{1}{2}\sqrt{\frac{h_1}{g}}({r_1}^+ - {r_1}^-) - 2h_1 &= \frac{1}{2}\sqrt{\frac{h_2}{g}}({r_2}^+ - {r_2}^-) - 2h_2, \\
\sqrt{\frac{h_1}{g}}({r_1}^+ - {r_1}^-) &= \sqrt{\frac{h_2}{g}}({r_2}^+ - {r_2}^-) - 4(h_2 - h_1), \\
{r_1}^+ - {r_1}^- &= \sqrt{\frac{h_2}{h_1}}({r_2}^+ - {r_2}^-) - 4\sqrt{\frac{g}{h_1}}(h_2 - h_1), \\
{r_1}^- &= {r_1}^+ - \sqrt{\frac{h_2}{h_1}}({r_2}^+ - {r_2}^-) + 4\sqrt{\frac{g}{h_1}}(h_2 - h_1).
\end{aligned} \tag{A.15}$$

Likewise, via $\eta_2 = \eta_3$, an equation can be constructed for ${r_3}^+$,

$${r_3}^+ = {r_3}^- + \sqrt{\frac{h_2}{h_3}}({r_2}^+ - {r_2}^-) - 4\sqrt{\frac{g}{h_3}}(h_2 - h_3). \tag{A.16}$$

Equation **??** can now be written with just one unknown variable, ${r_2}^+$,

$$\begin{aligned}
&\frac{1}{2}h_1 W_1(2{r_1}^+ - \sqrt{\frac{h_2}{h_1}}({r_2}^+ - {r_2}^-) + 4\sqrt{\frac{g}{h_1}}(h_2 - h_1)) = \\
&\qquad \frac{1}{2}h_2 W_2({r_2}^+ + {r_2}^-) + \frac{1}{2}h_3 W_3(2{r_3}^- + \sqrt{\frac{h_2}{h_3}}({r_2}^+ - {r_2}^-) - 4\sqrt{\frac{g}{h_3}}(h_2 - h_3)).
\end{aligned} \tag{A.17}$$

Equation **??** can be rewritten into an equation of the shape ${r_2}^+ = ...$

$$\begin{aligned}
&\Big(W_1\sqrt{h_1 h_2} + W_2 h_2 + W_3\sqrt{h_2 h_3}\Big){r_2}^+ = \\
&\qquad 2W_1 h_1 {r_1}^+ + \Big(-W_2 h_2 + W_1\sqrt{h_1 h_2} + W_3\sqrt{h_2 h_3}\Big){r_2}^- \\
&\qquad -2W_3 h_3 {r_3}^- + 4\sqrt{g}\Big(W_1\sqrt{h_1}(h_2 - h_1) + w_3\sqrt{h_3}(h_2 - h_3)\Big),
\end{aligned} \tag{A.18}$$

or,

$$\begin{aligned}
{r_2}^+ = &\frac{1}{W_1\sqrt{h_1 h_2} + W_2 h_2 + W_3\sqrt{h_2 h_3}}\Big(2W_1 h_1 {r_1}^+ + \\
&\Big(-W_2 h_2 + W_1\sqrt{h_1 h_2} + W_3\sqrt{h_2 h_3}\Big){r_2}^- - 2W_3 h_3 {r_3}^- + \\
&4\sqrt{g}\Big(W_1\sqrt{h_1}(h_2 - h_1) + W_3\sqrt{h_3}(h_2 - h_3)\Big)\Big).
\end{aligned} \tag{A.19}$$

Equation **??** provides a linear approximation of the solution of ${r_2}^+$.

It is expected that r_2^{+*} is 'close' to the physically correct solution r_2^+ Via an iterative method, Newton-Raphson (NR), physically correct solution is calculated. NR solves for the zero's of a system. The method works as follows:

$$(r_2^+)_{n+1} = (r_2^+)_n - \frac{f((r_2^+)_n)}{f'((r_2^+)_n)}, \tag{A.20}$$

with $f'(r_2^+) = \frac{\partial f}{\partial r_2^+}$ and $(r_2^+)_0$ as initial guess for r_2^+. As initial guess r_2^{+*} is used. The NR method only works if the initial guess is good enough.

The derivative $f'(r_2^+)$ is obtained analytically by differentiating function $f(r_2^+)$ with respect to r_2^+. For the situation with one incoming and two outgoing channel, the derivation is given in Appendix A.1.

With the physically correct value for r_2^+ known, the other unknown values of the nodal point are now easily obtained via continuity of dynamic pressure (equation **??**). The method is now applied for r_2^+, but can also be applied to any of the other unknowns.

Appendix B

Continuity of Dynamic Pressure

The cross-sectionally averaged momentum balance (equation **??**) is valid at every location in the channels. When the NM-F model is considered, it is also valid at the tidal flat. By shifting all terms to the left hand side, equation **??** becomes

$$\frac{\partial u}{\partial t} + u\frac{\partial u}{\partial x} + g\frac{\partial \eta}{\partial x} + C_d\frac{|u|u}{H+\eta} = 0,$$

or, alternatively,

$$\frac{\partial u}{\partial t} + \frac{\partial}{\partial x}\Big(\frac{1}{2}u^2 + g\eta\Big) + C_d\frac{|u|u}{H+\eta} = 0. \tag{B.1}$$

Equation **??** is valid at any location in the channel, so a surface integral any area in the system should result in zero as well,

$$\iint \left(\frac{\partial u}{\partial t} + \frac{\partial}{\partial x}\Big(\frac{1}{2}u^2 + g\eta\Big) + C_d\frac{|u|u}{H+\eta}\right)\mathrm{d}A = 0, \tag{B.2}$$

where A is the area of the domain under consideration. Via Green's theorem it is rewritten into

$$\iint \left(\frac{\partial u}{\partial t} + C_d\frac{|u|u}{H+\eta}\right)\mathrm{d}A + \oint \Big(\frac{1}{2}u^2 + g\eta\Big)\cdot \mathrm{d}\vec{l} = 0, \tag{B.3}$$

where $\vec{l}$ is the boundary of area A. Equation **??** is valid for any area A, also for infinitesimally small area's. The surface integral then reduces to zero, such that,

$$\oint \Big(\frac{1}{2}u^2 + g\eta\Big)\cdot \mathrm{d}\vec{l} = 0. \tag{B.4}$$

When an infinitesimally small area is chosen around a nodal point, the line integral will be taken over more than one channel, each with a different velocity u and sea level η. Equation **??** only has a solution when $(\frac{1}{2}u^2 + g\eta)$ is constant over the nodal point. Dynamic pressure is thus constant at nodal points.

Formally, this theory should be derived for a 2D horizontal momentum balance, in which across-channel velocity is also considered. In this thesis, the velocity only has an along-channel component. Incorporation of across-channel velocity in this derivation would have led to the same result.

Appendix C

Discretization Shallow Water Equations NM-P model

C.1 Non-dimensionalizing equations

Starting from equation **??** and equation **??**, non-dimensionalizing is applied to all variables in the system. A dimensional variable, such a velocity u^*, is split in a typical dimensional magnitude scale U and a dimensionless variable $\tilde{u}$, such that $u^* = U\tilde{u}$. In this subsection, superscript * indicates a dimensional variable and a tilde indicates a dimensionless variable. The characteristic scales, with which the variables are scaled, can be found in Table **??**, including derived scaling parameters.

The scaling of time t^* is based on tidal frequency ω, because this is the dominant time period under consideration. The characteristic scale of x^* is L_T, $\frac{1}{2\pi}$ times the tidal wavelength. The velocity scale for u_{tf} is derived from the Broad-crested weir formula (see equation **??**). The Froude number is defined as the ratio of characteristic velocity to the phase speed of a shallow water wave. Scaling is applied to equation **??** and equation **??**. Using $c = L_T\omega$, this results in

$$\frac{\partial\tilde{u}}{\partial\tilde{t}} = -\frac{\partial\tilde{\eta}}{\partial\tilde{x}} - \mathrm{Fr}\tilde{u}\frac{\partial\tilde{u}}{\partial\tilde{x}} - \lambda\frac{\tilde{|u|}\tilde{u}}{1+\mathrm{Fr}\tilde{\eta}}, \tag{C.1}$$

$$\frac{\partial\tilde{\eta}}{\partial\tilde{t}} = -\frac{\partial\tilde{u}}{\partial\tilde{x}} - \mathrm{Fr}\frac{\partial(\tilde{\eta}\tilde{u})}{\partial\tilde{x}}. \tag{C.2}$$

The above equations are valid for tidal channels. When tidal channel are connected to tidal flats, the boundary conditions need to be incorporated and an extra term appears in both the momentum balance and the continuity equation, producing the scaled version of equation **??** and equation **??**.

$$\frac{\partial\tilde{u}}{\partial\tilde{t}} = -\frac{\partial\tilde{\eta}}{\partial\tilde{x}} - \mathrm{Fr}\tilde{u}\frac{\partial\tilde{u}}{\partial\tilde{x}} - \lambda\frac{\tilde{|u|}\tilde{u}}{1+\mathrm{Fr}\tilde{\eta}} + M_m\frac{\tilde{\eta}_{tf}\tilde{u}_{tf}}{1+\mathrm{Fr}\tilde{\eta}}, \tag{C.3}$$

$$\frac{\partial\tilde{\eta}}{\partial\tilde{t}} = -\frac{\partial\tilde{u}}{\partial\tilde{x}} - \mathrm{Fr}\frac{\partial(\tilde{\eta}\tilde{u})}{\partial\tilde{x}} - M_c\tilde{\eta}_{tf}\tilde{u}_{tf}. \tag{C.4}$$

C.2 Discretization

The system of equations described by equations **??**-**??** is nonlinear. In general, nonlinear systems cannot be solved analytically. An approximate solution can be found when discretization is applied. The equations are solved for a fixed number of time steps at a finite number of grid points in the along channel direction of a channel. At each grid point x_i a numerical value for sea level η_i and velocity u_i is obtained each time step, where subscript i indicates the ith grid point. Each time step, the new values for η_i and u_i are calculated numerically via a Runge-Kutta(4) time integration scheme (see section 3.1).

	Variable	Scaling
Sea level deviation in channel(m)	η^*	N
Sea level on tidal flat(m)	η^*_{tf}	N
Time (s)	t^*	ω^{-1}
Undisturbed water depth (m)	h^*	H
Channel width (m)	w^*	W
Spatial coordinate (m)	x^*	L_T
Velocity in channel(ms^{-1})	u^*	$U = \frac{gN}{c}$
Velocity on tidal flat (ms^{-1})	${u_{tf}}^*$	$V = f\sqrt{gN}$
Phase speed of wave (ms^{-1})	c^*	$\sqrt{gH}$
Froude number	Fr	$\frac{U}{c} = \frac{N}{H}$
Friction coefficient channel	λ	$\frac{C_d U}{H\omega}$
Friction coefficient tidal flat	λ'	$\frac{C_{d,tf} V}{N\omega}$
Momentum coefficient tidal flat transport	M_m	$\frac{NV}{\omega HW}$
Continuity coefficient tidal flat transport	M_c	$\frac{V}{\omega W}$

Table C.1: Characteristic scales of variables in the system and parameters derived from scaling. N is the amplitude of the incoming tidal wave, ω is the frequency of the incoming tidal wave, H is the (constant) depth of a channel, W is the width of a channel, L_t is $\frac{1}{2\pi}$ times the tidal wavelength, g is the gravitational acceleration, f is the barrier friction coefficient (Section 2.1.2) and C_d and $C_{d,tf}$ are bottom friction coefficients.

C.2.1 Spatial Discretization

A channel is divided in nx equidistant points in the along-channel direction, distance Δx apart. At each grid point, the new values for η_i and u_i are calculated through differential equations **??** and **??** by discretizing the right hand side of the equations. For the discretization of derivatives, the central differencing method is applied,

$$\frac{\partial f}{\partial x}\Big|_i = \frac{f_{i+1} - f_{i-1}}{2\Delta x} + \mathcal{O}(\Delta x^2), \tag{C.5}$$

which is order $\mathcal{O}(\Delta x)$ accurate. At the extreme points of the domain ($i = 1$,$i = nx$), central differencing cannot be applied. To solve this problem and still maintain $\mathcal{O}(\Delta x)$ accuracy, a Taylor expension is made of $\frac{\partial f}{\partial x}|_i$:

$$\frac{\partial f}{\partial x}\Big|_i = \frac{\partial f}{\partial x}\Big|_{i+\frac{1}{2}} - \frac{1}{2}\Delta x \frac{\partial^2 f}{\partial x^2}\Big|_{i+\frac{1}{2}} + \mathcal{O}(\Delta x^2) \qquad \text{at } i = 1, \tag{C.6}$$

$$\frac{\partial f}{\partial x}\Big|_i = \frac{\partial f}{\partial x}\Big|_{i-\frac{1}{2}} + \frac{1}{2}\Delta x \frac{\partial^2 f}{\partial x^2}\Big|_{i-\frac{1}{2}} + \mathcal{O}(\Delta x^2) \qquad \text{at } i = nx. \tag{C.7}$$

The second derivative is given by central differencing as

$$\frac{\partial^2 f}{\partial x^2}\Big|_i = \frac{f_{i+\frac{1}{2}} - 2f_i + f_{i-\frac{1}{2}}}{2\Delta x^2} + \mathcal{O}(\Delta x^2),$$

which can be substituted back into equations **??** (for $i = 1$) and **??** (for $i = nx$). This results in

$$\frac{\partial f}{\partial x}\Big|_1 = \frac{-3f_1 + 4f_2 - 1f_3}{\Delta x}, \tag{C.8}$$

$$\frac{\partial f}{\partial x}\Big|_{nx} = \frac{3f_{nx} - 4f_{nx-1} + 1f_{nx-2}}{\Delta x}. \tag{C.9}$$

With these equations, derivates at the extreme points of the domain can be calculated.

For internal points in the domain ($1 < i < nx$), the right hand size of equations **??** and **??** are spatially discretised as

$$\left.\frac{\partial u}{\partial t}\right|_i = -\frac{\eta_{i+1}-\eta_{i-1}}{2\Delta x} - \frac{1}{2}\mathrm{Fr}\frac{(u_{i+1})^2-(u_{i-1})^2}{2\Delta x} - \lambda\frac{|u_i|u_i}{1+\mathrm{Fr}\eta_i}, \tag{C.10}$$

$$\left.\frac{\partial \eta}{\partial t}\right|_i = -\frac{u_{i+1}-u_{i-1}}{2\Delta x} - \mathrm{Fr}\frac{u_{i+1}\eta_{i+1}-u_{i-1}\eta_{i-1}}{2\Delta x}. \tag{C.11}$$

The tildes are omitted, so variables u and η are dimensionless variables. The left hand size requires temporal discretization, which is presented in the next section. Notice that momentum advection in equation **??** is the discretised form of $\frac{1}{2}\frac{\partial u^2}{\partial x}$.

At internal nodes where tidal channel and tidal flat are connected, the boundary conditions are numerically taken into account via

$$\left.\frac{\partial u}{\partial t}\right|_i = -\frac{\eta_{i+1}-\eta_{i-1}}{2\Delta x} - \frac{1}{2}\mathrm{Fr}\frac{(u_{i+1})^2-(u_{i-1})^2}{2\Delta x} - \lambda\frac{|u_i|u_i}{1+\mathrm{Fr}\eta_i} + M_m\frac{\eta_{tf}|_i u_{tf}|_i}{1+\mathrm{Fr}\eta_i}\frac{W_{tf}}{\Delta x}, \tag{C.12}$$

$$\left.\frac{\partial \eta}{\partial t}\right|_i = -\frac{u_{i+1}-u_{i-1}}{2\Delta x} - \mathrm{Fr}\frac{u_{i+1}\eta_{i+1}-u_{i-1}\eta_{i-1}}{2\Delta x} - M_c\eta_{tf}|_i u_{tf}|_i\frac{W_{tf}}{\Delta x}. \tag{C.13}$$

C.2.2 Temporal Discretization

As temporal discretisation the RK(4) scheme was used described in Section 3.1.

C.2.3 Courant Criterium

When numerical values for Δx and Δt are chosen, the Courant criterium is taken into account (see e.g. **?**). The criterium states that instabilities may occur when the ratio of Δx over Δt becomes larger than the typical phase speed of a wave in the system, so $\frac{\Delta x}{\Delta t} \leq c = \sqrt{gH}$.

C.2.4 Discretization of Advection Terms

Advection of Momentum

Advection of momentum can be expressed as $u\frac{\partial u}{\partial x}$ (non-conservational form) or $\frac{1}{2}\frac{\partial u^2}{\partial x}$ (conservational form). Analytically, the expressions are equivalent. In discretised form, however, they are not. Parametrization $u\frac{\partial u}{\partial x}$ translates to $u_i\frac{u_{i+1}-u_{i-1}}{2\Delta x}$, which is unequal to $\frac{1}{2}\frac{(u_{i+1})^2-(u_{i-1})^2}{2\Delta x}$. To select one of these parameterizations, a simulation of the Burgers equation has been carried out. The Burgers equation includes advection of momentum, and has an analytical solution. The quality of the two parameterizations is tested to the analytical solution. The experiment is shown in section C.3

The conclusion is that the discretization of $\frac{1}{2}\frac{\partial u^2}{\partial x}$ produces better results than discretization of $u\frac{\partial u}{\partial x}$. The conservational form of momentum advection produces better results than the non-conservational form. Textbooks suggest that, for a hyperbolic system of equations, conservational form is always preferred. For the discussion, see Appendix C.3.

Advection of Sea Level

Advection of sea level can also be expressed in two analytically equivalent terms, $\frac{\partial(u\eta)}{\partial x}$ and $u\frac{\partial \eta}{\partial x} + \eta\frac{\partial u}{\partial x}$. Discretised, they translate to $\frac{u_{i+1}\eta_{i+1} - u_{i-1}\eta_{i-1}}{2\Delta x}$ and $u_i\frac{\eta_{i+1}\eta_{i-1}}{2\Delta x} + \eta_i\frac{u_{i+1}-u_{i-1}}{2\Delta x}$, respectively, and these expression are not the same. Because the system is hyperbolic, conservational form is preferred (section C.3), and advection of sea level should be parameterised as $\frac{\partial(u\eta)}{\partial x}$, with corresponding discretization.

C.3 Burgers Experiment

The Burgers equation is a non-linear differential equation with an exact solution. The equation is given by

$$\frac{\partial u}{\partial t} + u\frac{\partial u}{\partial x} = \nu\frac{\partial^2 u}{\partial x^2}, \tag{C.14}$$

and can be alternatively written as

$$\frac{\partial u}{\partial t} + \frac{1}{2}\frac{\partial u^2}{\partial x} = \nu\frac{\partial^2 u}{\partial x^2}. \tag{C.15}$$

In these equations, $u = u(x,t)$ and ν represents a viscosity coefficient. Initial conditions are provided as $u(x,0) = f(x)$.

Cole-Hopf transformation
Via the so-called Cole-Hopf transformation (see e.g. **?**), an exact solution is obtained for the Burgers equation. Function $u(x,t)$ is written in terms of another function $\phi(x,t)$, as

$$u = -2\nu\frac{\frac{\partial\phi}{\partial x}}{\phi}.$$

When this is plugged into equation **??**, it will read

$$-2\nu\frac{\partial}{\partial t}\Big(\frac{\frac{\partial\phi}{\partial x}}{\phi}\Big) + 4\nu^2\frac{\frac{\partial\phi}{\partial x}}{\phi}\frac{\partial}{\partial x}\Big(\frac{\frac{\partial\phi}{\partial x}}{\phi}\Big) = -2\nu^2\frac{\partial^2}{\partial x^2}\Big(\frac{\frac{\partial\phi}{\partial x}}{\phi}\Big).$$

After a number of simplification, it reduces to the heat equation,

$$\frac{\partial\phi}{\partial t} = \nu\frac{\partial^2\phi}{\partial x^2}, \tag{C.16}$$

of which the analytical solution is known. When $\phi(x,t)$ solves the heat equation, $u(x,t)$ solves Burgers equation. The initial condition for $u(x,t)$ is $f(x)$, which translates to

$$f(x) = -2\nu\frac{\frac{\partial\phi(x,0)}{\partial x}}{\phi(x,0)}$$

in terms of $\phi(x,0)$. Inversely, $\phi(x,0)$ is expressed in terms of $f(x)$ as

$$\phi(x,0) = \psi(x) = C\exp[-F(x)],$$

with $F(x) = \frac{1}{2\nu}\int_0^x f(x')\mathrm{d}x'$ and C an arbitrary constant, for simplicity taken as $C = 1$ from here on.

At each time t a solution for function $\phi(x,t)$ is obtained that solves the heat equation (equation **??**). Function $u(x,t)$, solving the Burgers equation at any time t is now found by translating $\phi(x,t)$ back in terms of $u(x,t)$,

$$u(x,t) = -2\nu\frac{\partial}{\partial x}\ln\Big(\frac{1}{\sqrt{4\pi\nu t}}\int_{-\infty}^{\infty}\psi(x')\exp\big(\frac{-(x-x')^2}{4\nu t}\big)\mathrm{d}x'\Big)$$

Experiment
A simulation of the Burgers equation with an initial Gaussian distribution and a small diffusivity coefficient ν is made using two different discretizations of the Burgers equation. The two discretization are quantitatively compared to the analytical solution of the same problem, obtained via the Cole-Hopf transformation. An equidistant spatial grid is used with nx grid point, each a distance Δx apart.

The two discretizations are the discretised versions of equations **??**-**??**. At internal nodes ($1 < i < nx$), they are given by

$$u(t+\Delta t)_i = u(t)_i + \Big(- u_i \frac{u_{i+1} - u_{i-1}}{2\Delta x} + \nu \frac{u_{i+1} - 2u_i + u_{i-1}}{\Delta x^2} \Big) \Delta t, \tag{C.17}$$

$$u(t+\Delta t)_i = u(t)_i + \Big(\frac{1}{2} \frac{u_{i+1}^2 - u_{i-1}^2}{2\Delta x} + \nu \frac{u_{i+1} - 2u_i + u_{i-1}}{\Delta x^2} \Big) \Delta t. \tag{C.18}$$

The initial Gaussian distribution used is

$$u(x,0) = f(x) = \frac{1}{\sqrt{2\pi}\sigma} \exp\big(- \frac{(x-\mu)^2}{2\sigma^2} \big),$$

with $\mu = 50$m and $\sigma = 5$m. Furthermore, viscosity coefficient ν has value $\nu = 0.01\text{m}^2\text{s}^{-1}$, spatial step $\Delta x = 1$m and time step $\Delta t = 1$s. The discretization of equation **??** is named $\mathcal{D}_1$ and the discretization of equation **??** is named $\mathcal{D}_2$. In the domain $x \epsilon [0 \quad 100]$, the quality of both $\mathcal{D}_1$ and $\mathcal{D}_2$ is evaluated at each grid point by comparing the value at that grid point to the value of the exact, analytical solution at the same grid point. Two measures for error are established, one in a cumulative absolute sense and another in a cumulative squared sense:

$$\xi_{abs}(t) = \sum_{i=1}^{nx} |u_i(t) - u_i^{exact}(t)|, \qquad \xi_{sq}(t) = \sum_{i=1}^{nx} (u_i(t) - u_i^{exact}(t))^2.$$

The experiment is run for 300 seconds (300 time steps). The spatial distribution of u at time $t = 300$ are shown in Figure **??**a, along with the original distribution at $t = 0$. In Figure **??**b the variables ξ_{abs} and ξ_{sq} are plotted against time for both discretizations $\mathcal{D}_1$ and $\mathcal{D}_2$.

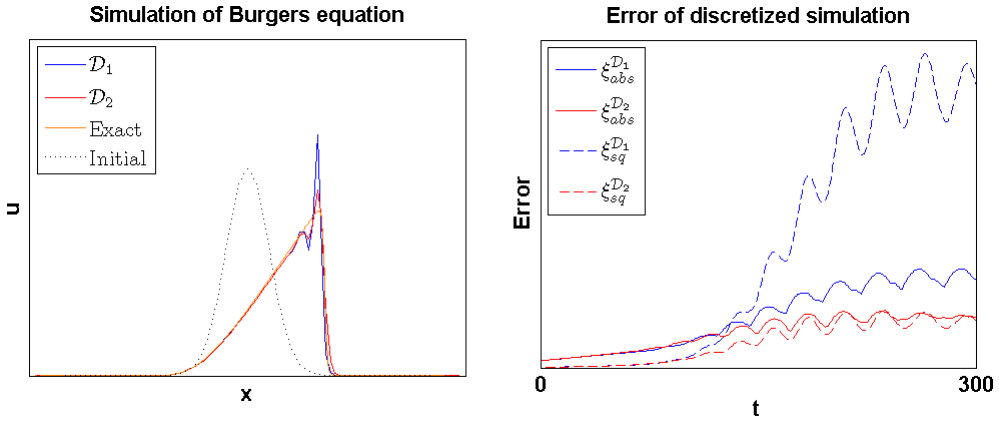

Figure C.1: In the left figure (Figure a), the initial distribution (black dotted line) is calculated after 300 seconds, using two discretizations ($\mathcal{D}_1$ and $\mathcal{D}_2$) and an exact solution. In the right figure (Figure b), the error (both absolute and squared) of both discretizations is plotted. The squared error is multiplied by 200 to be of the same order of magnitude as the absolute error.

In Figure **??**a, it is obvious that both discretizations do not show skill at simulation the front of the wave. The grid spacing appears to be too coarse to capture the front of the wave. Discretization $\mathcal{D}_1$ shows a distribution that is closer to the exact solution than $\mathcal{D}_2$. This is confirmed when the errors the distribution are considered (Figure

??b).

The absolute error, ξ_{abs} gradually increases for both discretizations. After approximately 120 seconds, the absolute errors start to diverge and show oscillatory behavior. From 120 seconds on, the absolute error of discretization $\mathcal{D}_1$, $\xi_{abs}^{\mathcal{D}_1}$ is smaller (by about one third) than the error of discretization $\mathcal{D}_2$, $\xi_{abs}^{\mathcal{D}_2}$.

The same conclusion is drawn when the squared error is consider. Until 100 seconds, no difference between the discretizations is observed. After 100 seconds, the errors start to diverge and oscillate. The squared error of discretization $\mathcal{D}_1$, $\xi_{sq}^{\mathcal{D}_1}$ becomes a lot larger than the error of $\mathcal{D}_2$, $\xi_{abs}^{\mathcal{D}_2}$. In both error measures, discretization $\mathcal{D}_2$ provides more accurate solutions than $\mathcal{D}_1$.

On top of the result of this simulation, several text books (e.g. **?** and **?**) advice to use the conservational form of the Burgers equation (discretization $\mathcal{D}_2$). More generally, they advice to use the conservational form for any hyperbolic system if possible.

Based on this knowledge, equations that can be written in conservational form, will be modelled as equation in conservative form.

Appendix D

?: Prescribing Sea Level at Open Boundary

The NM-F model is applied to the domain presented in **?** (see Figure **??**). At the open boundary, both sea level and an incoming wave can be prescribed. When sea level is prescribed at the open boundary, both the velocity and the sea level in the domain contain higher frequency oscillations than the prescribed M_2 tidal frequency. The magnitude of the higher frequency oscillations depends on geometry and appears to increase with increasing tidal channel length. Two model runs (run 3 and run 16) with the NM-F model are shown, for two different geometries (parameters can be found in Table **??**). In run 16, the parameters are the same as in the run shown in Figure **??**.

For both runs the velocity is plotted 500m from the entrance of the tidal flat. The results are plotted over the original figure taken from **?**. For run 3, the results are shown in Figure **??**

In run 3 large wiggles are visible, in run 16 the wiggles have a smaller amplitude, but are still visible. The same wiggles are present in the tidal channel, although not as clear as on the tidal flat. A Fourier analysis of the velocity at the end of the channel (at 5km from the open boundary in run 3, at 30km from the open boundary in run 16) shows the presence of higher frequencies (Figures **??**-**??**).

In Figure **??** (run 3) the along-channel velocity (right) shows several exited frequencies, of which the most dominant has the M_2 tidal frequency. The higher frequencies appear to have a frequency equal to a multiple of the original tidal frequency and are called harmonics. The sea level (left) does not show any obvious exited frequencies. In Figure **??** (run 16) there are fewer exited frequencies. The strongest velocity peak is still the initial M_2 tidal signal, but is has declined in amplitude because it is close to the end of the channel. The M_4 and M_6 harmonics are strongly exited, up to 40% of the amplitude of the M_2 tidal signal. The M_8 and M_14 harmonics are weakly exited. A harmonic analysis of the tidal channel shows that the exited frequencies are present throughout the entire channel (Figures **??**-**??**). In the original NM-F model run, in which an incoming wave was prescribed at the open boundary (Figure **??**), the harmonics are much less present in the tidal channel (Figure **??**).

So why are harmonics much stronger exited when sea level is prescribed at the open boundary? A possible

Parameter	Represents	Value Run 3	Value Run 16
L_{ch}	Channel Length	5km	30km
W_{ch}	Channel Width	50m	300m
H_{ch}	Channel Depth	10m	10m
$C_{d,ch}$	Quadratic bottom friction coefficient in channel	0.0025	0.0025
$C_{d,tf}$	Quadratic bottom friction coefficient on tidal flat	0.03	0.06

Table D.1: Values for parameters in the NM-F model for the simulation of the Van Oyen Domain.

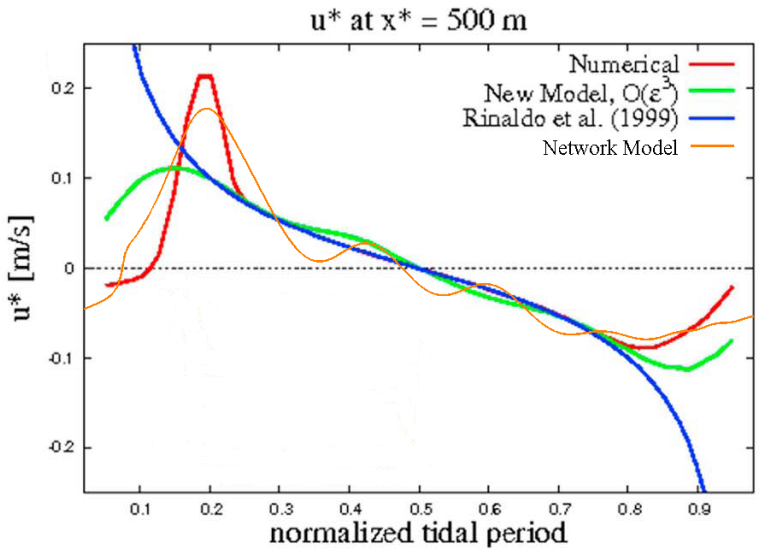

Figure D.1: Along-channel velocity at 500m from the entrance of the flat during one tidal cycle. The orange line shows the velocity in the NM-F model with the parameters of run 3

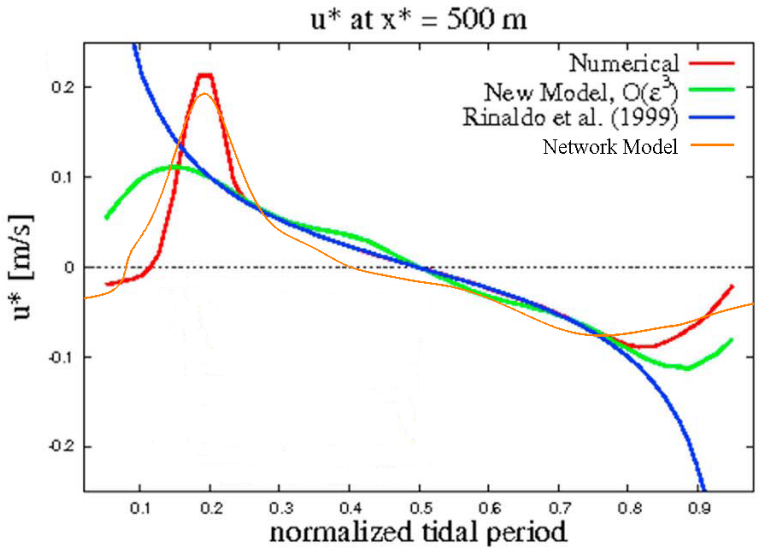

Figure D.2: Along-channel velocity at 500m from the entrance of the flat during one tidal cycle. The orange line shows the velocity in the NM-F model with the parameters of run 16

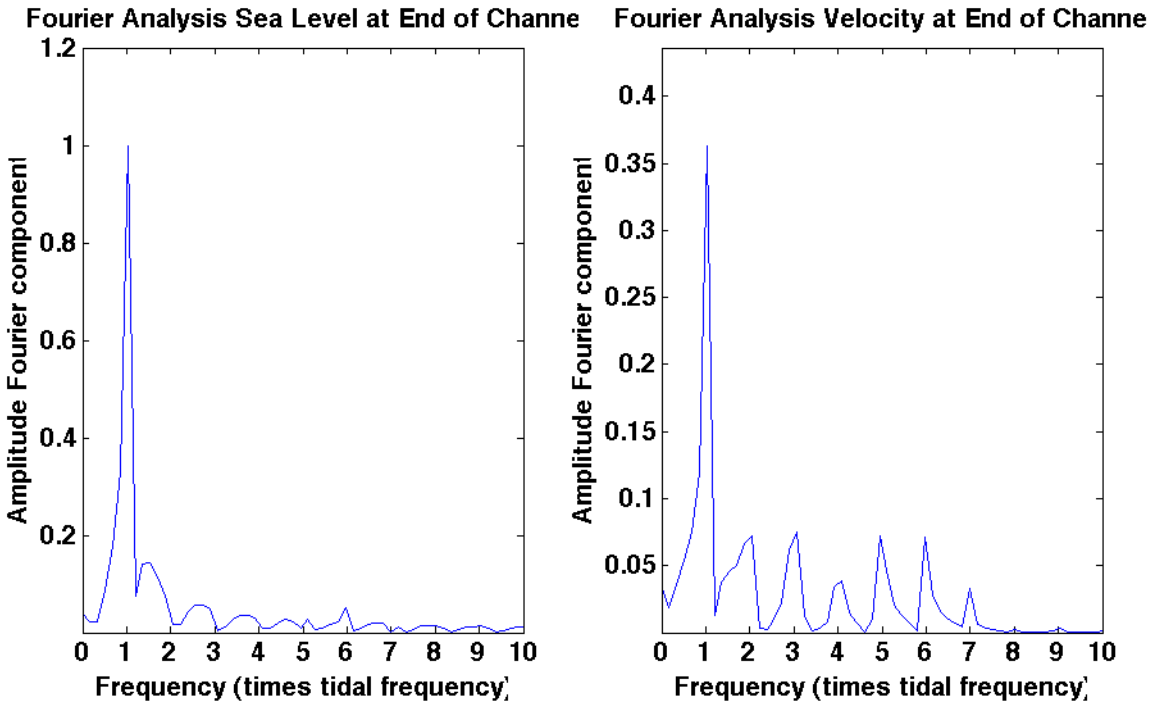

Figure D.3: Fourier Analysis of Velocity and Sea Level at the end of the tidal channel for run 3.

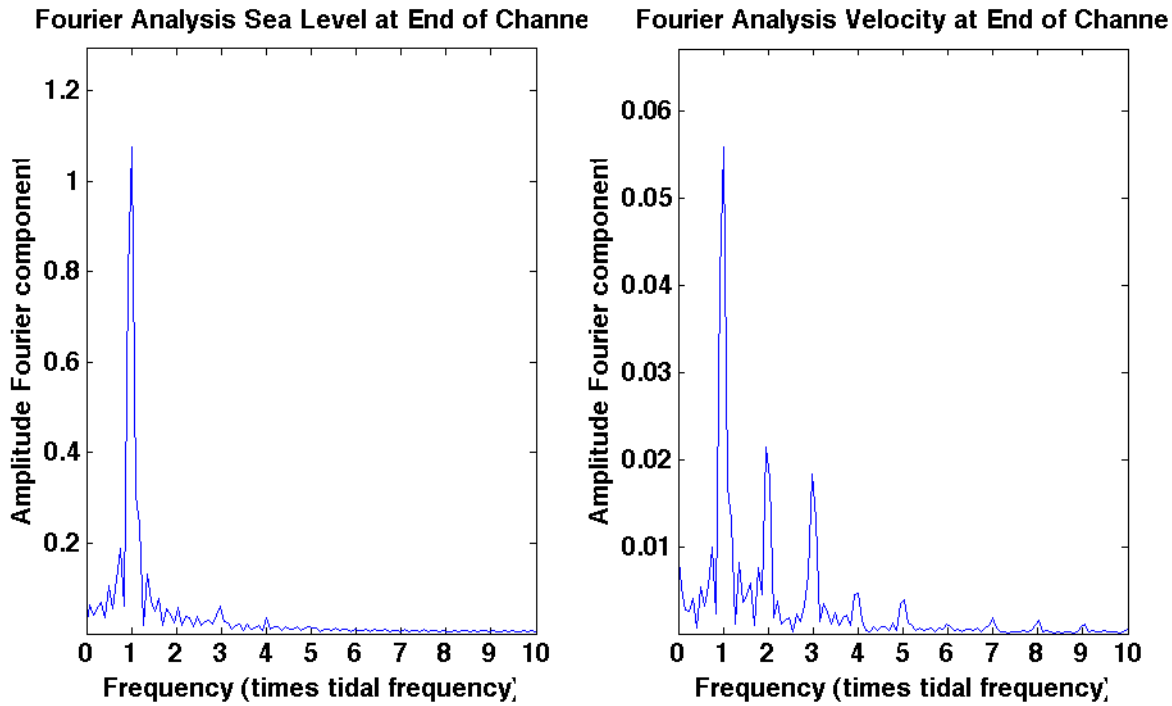

Figure D.4: Fourier Analysis of Velocity and Sea Level at the end of the tidal channel for run 16.

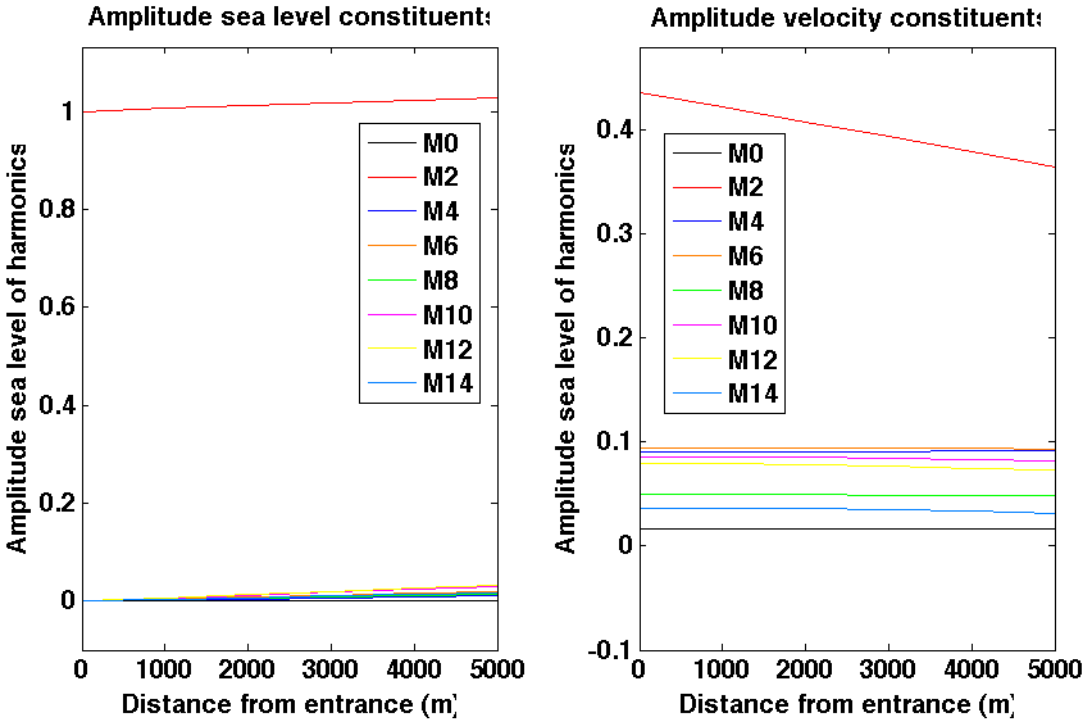

Figure D.5: Harmonic Analysis of Velocity and Sea Level in the tidal channel for run 3.

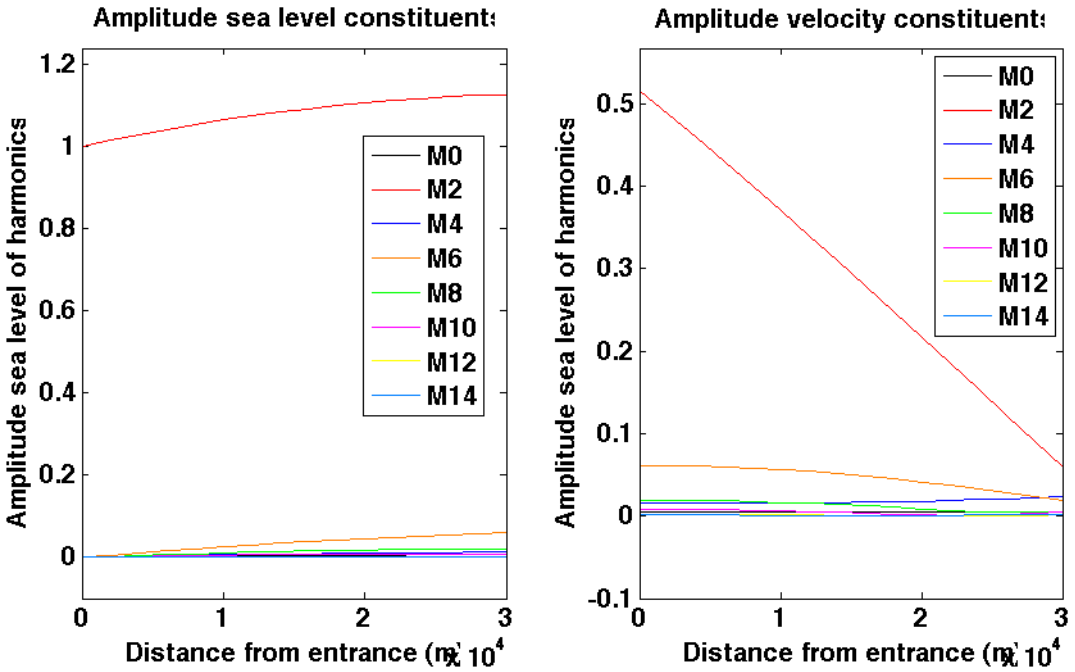

Figure D.6: Harmonic Analysis of Velocity and Sea Level in the tidal channel for run 16.

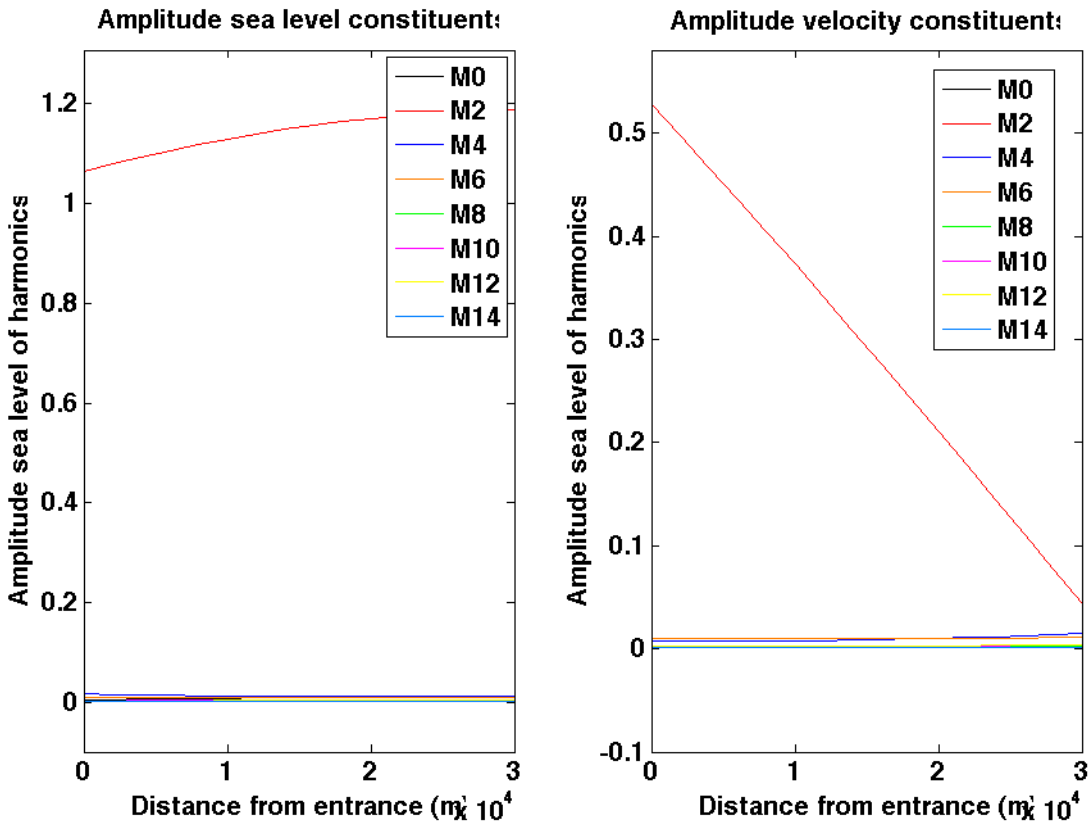

Figure D.7: Harmonic Analysis of Velocity and Sea Level in the tidal channel for original NM-F model run

explanation is that the higher harmonics that are generated on the tidal flat and in the channel are allowed to leave the system on the outgoing characterstic r^- when an incoming wave is prescribed at the open boundary. When sea level is prescribed at the open boundary, the incoming characterstic is constructed based on the outgoing characterstic, and when the outgoing characterstic carries a signal with higher harmonics, these higher harmonics are transferred to the incoming signal, thus 'feeding' the system a harmonic signal.

To test this hypothesis, two criteria should be true:

- A system in which an incoming wave is prescribed at the open boundary should have a signal with stronger harmonics on the outgoing r^- characterstic than the incoming r^+ characterstic at the open boundary.
- A system in which sea level is prescribed at the open boundary should show the same harmonics at the outgoing and incoming characterstic at the open boundary.

To test the first criterion, the harmonics are plotted for the original run from Figure **??**. The harmonics of r^+ and r^- are shown for the entire channel in Figure **??**.
At the open boundary the negative r^- characterstics carries a number of harmonics with an amplitude of one or

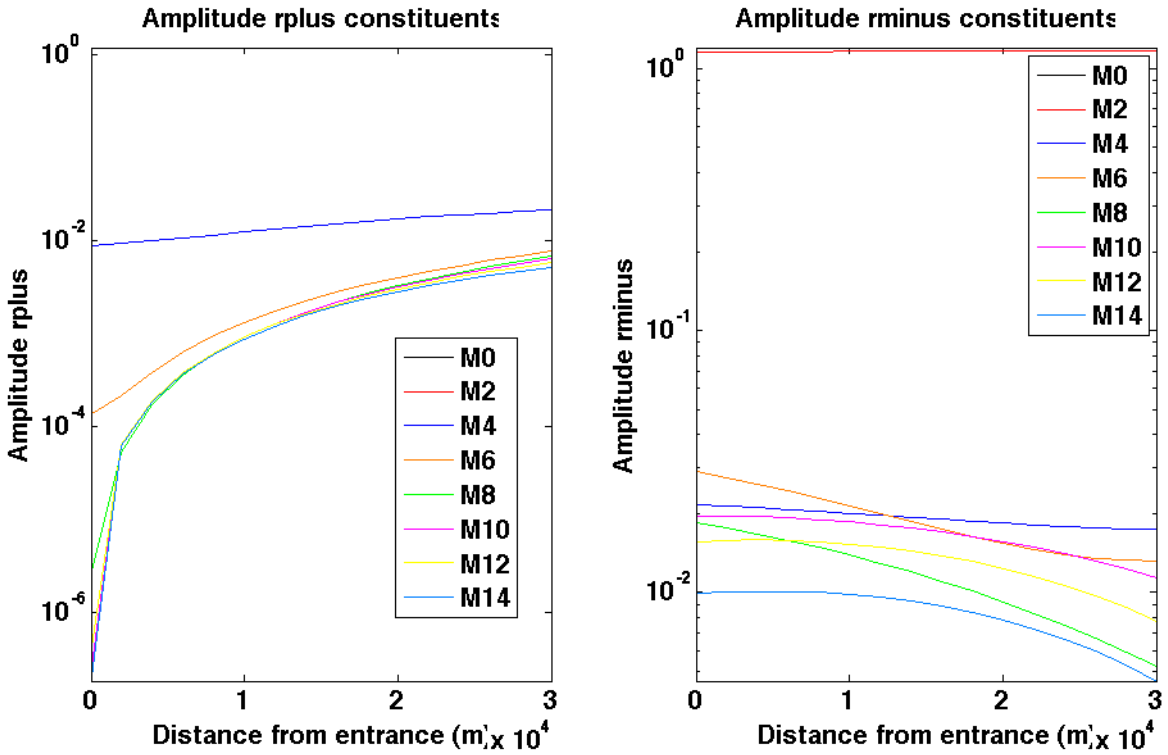

Figure D.8: Harmonic Analysis of Velocity and Sea Level in the tidal channel for original NM-F model run

two centimeters. The positive r^+ characterstic shows only a very small M_4 component at the open boundary, most likely caused by friction (which, in the NM-F model, is applied directly after a new value for r^+ is added to the domain). In case an incoming wave is prescribed at the open boundary, a pure M_2-signal is to be expected in theory, so not finding any strong harmonics is line with that theory. Thus, the first criterion is confirmed.

To test the second criterion, the harmonics are plotted for run 16. They are shown in Figure **??**.

In Figure **??** it is shown that all harmonics, except for M_4, have the same amplitude at the open boundary on the positive r^+ characterstic and the negative r^- characterstic. The difference in M_4 can be explained by the fact that quadratic friction is applied after a new positive characterstic is prescribed at the open boundary, producing overtides, predominantly M_4.

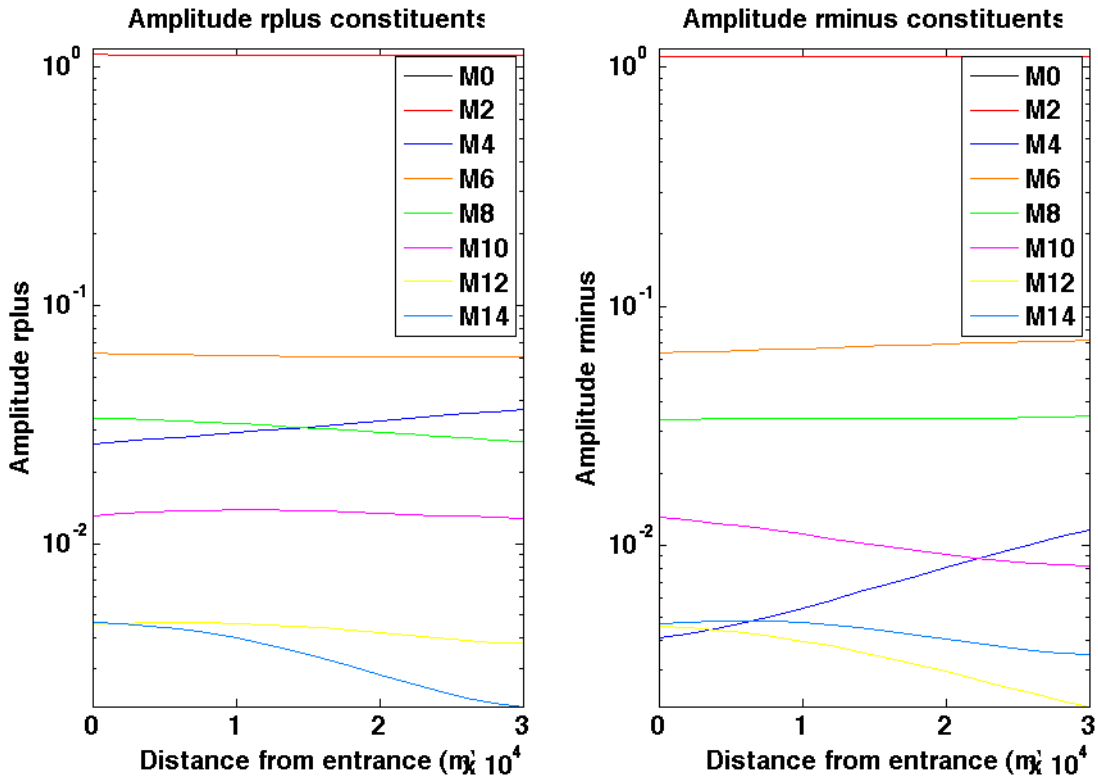

Figure D.9: Harmonic Analysis of Velocity and Sea Level in the tidal channel for run 16

With both criteria confirmed, our hypothesis is also confirmed. The wiggles (higher harmonics) in Figures **??-??** are caused by the transfer of harmonics from the negative to the positive characterstic at the open boundary.

Appendix E

Hamilton Parameterisation

? defines the sea level on the tidal flat as

$$\eta_{tf} = \frac{\max(\eta_1, 0) + \max(\eta_2, 0)}{2}. \tag{E.1}$$

This corresponds to a linear interpolation of η_1 and η_2 over the tidal flat and taking its value at $x = \frac{L_{tf}}{2}$, at half the length of the tidal flat. When the sea level in a channel adjacent to the tidal flat drops below $H_{tf} = 0$, the sea level on the tidal flat is set to zero instead.

To calculate velocities over the tidal flats, **?** identified three cases, depending on sea levels η_1 and η_2:
Case 1. $\eta_1 < 0$, $\eta_2 < 0$,
Case 2. $\eta_1 > 0$, $\eta_2 < 0$ and $\eta_1 < 0$, $\eta_2 > 0$,
Case 3, $\eta_1 > 0$, $\eta_2 > 0$.

Case 1
In Case 1, the sea levels in either channels are below the height of the tidal flat. In that case there is no water on the tidal flat and no transport is established, so

$$\eta_{tf} = 0, \tag{E.2a}$$

$$u_{tf} = 0. \tag{E.2b}$$

Case 2
The sea level is above the tidal flat in one channel and below the tidal flat in the other channel. Water will be transported from the higher channel, over the tidal flat, into the lower channel. To describe this situation, **?** uses a theory originally developed for weirs.

A weir is a barrier placed in a channel to alter the flow characteristics, for example the discharge of water. Although one can argue whether a tidal flat can be considered a weir, theory used to describe weirs can be applied to a tidal flat as well. When a tidal flat is considered to be a weir, it is best characterised by a so called broad-crested weir. A typical broad-crested weir is shown in Figure **??**. Via equation **??** the sea level over the tidal flat is given by

$$\eta_{tf} = \begin{cases} \frac{\eta_1}{2}, & \eta_1 > 0 \text{ and } \eta_2 < 0, \\ \frac{\eta_2}{2}, & \eta_1 < 0 \text{ and } \eta_2 > 0. \end{cases} \tag{E.3}$$

The velocity over the tidal flat is then determined by the so called broad-crested weir formula, given by

$$u_{tf} = \begin{cases} f\sqrt{g\eta_{tf}}, & \eta_1 > 0 \text{ and } \eta_2 < 0, \\ -f\sqrt{g\eta_{tf}}, & \eta_1 < 0 \text{ and } \eta_2 > 0, \end{cases} \tag{E.4}$$

where f is a barrier friction coefficient and g is the gravitational acceleration. Hamilton does not provide a value or formula to determine f. In literature (e.g. **?**) a value of $f = (\frac{2}{3})^{\frac{3}{2}}$ is given for idealised situations; Idealised in

Figure E.1: A broad-crested weir on the Grand River in Grand Rapids, MI. Photo credit: Alex Mead.

the sense that centripetal forces are absent, no viscous or turbulent effects are considered and a uniform velocity distribution is assumed. Because these effects cannot be ignored, a first and second correction term (C_1 and C_2) are provided in **?**. The correction terms are constants in the idealised formula,

$$u_{tf} = \pm C_1 C_2 (\frac{2}{3})^{\frac{3}{2}} \sqrt{g \eta_{tf}},$$

with

$$C_1 = 0.93 + 0.10 \frac{\eta_{tf}}{L_{tf}}.$$

Given the length of tidal flats (usually $L_{tf} \geq 10m$) and the fact that sea level on tidal flat is, in general, of order $\mathcal{O}(1\text{m})$, C_1 can be approximated by $C_1 = 0.93$. The second correction term, C_2 is also provided in **?**, correcting for the presence of velocities in the approach to a weir. In the NM-P model, these velocities are zero and $C_2 = 1$, which provides a constant numerical value for f: $f \simeq 0.51$.

The variables u_{tf} and η_{tf} are, in this approach, diagnostically determined, based on the sea level of the channels adjacent to the tidal flat. Instantaneous equilibrium is assumed when either η_1 or η_2 changes.

Case 3
In this case, the water level on either side of the tidal flat is above the tidal flat. **?** applies a momentum balance to calculate the change in u_{tf} every time step. Equation **??** is still applied to calculate sea level. The governing equations are

$$\eta_{tf} = \frac{\eta_1 + \eta_2}{2}, \tag{E.5}$$

$$\frac{\partial u_{tf}}{\partial t} = -g \frac{\eta_2 - \eta_1}{L_{tf}} - C_{d,tf} \frac{u_{tf} |u_{tf}|}{\eta_{tf}}, \tag{E.6}$$

with $C_{d,tf}$ a bottom friction coefficient, g the gravitational acceleration and L_{tf} the length of the tidal flat. In equation **??** the first term on the r.h.s. is a pressure gradient and the second term on the r.h.s. is bottom friction. Bottom friction is, in general, stronger over a tidal flat than in a channel, so $C_{d,tf}$ has a higher value than C_d used in the channel.

During a tidal cycle, the system generally goes from Case 1, via Case 2 to Case 3. When Case 3 is reached, velocity on the tidal flat u_{tf} already has a nonzero value. After a maximum water level is reached, water starts to retreat, going back from Case 3, via Case 2 to Case 1. When going from Case 3 to Case 2, velocity u_{tf} is no longer a prognostic variable, but a diagnostic variable. A jump in u_{tf} can be expected here.

Mass and Momentum Transfer

When the water level in at least one of the channels connected to the tidal flat exceeds the tidal flat level, a mass transport is established from one channel into the other channel (Case 2 and Case 3). Values for the variables η_{tf} and u_{tf} are known and the mass transport $q[\mathrm{m}^3\mathrm{s}^{-1}]$ can be calculated via $q = \eta_{tf} u_{tf} W_{tf}$, where W_{tf} is the width of the tidal flat. In the parameterisation by **?** model, mass transfer is instantaneous; When mass flows out of one channel, it immediately enters the other.

? does not explicitly treat momentum transfer over the tidal flat. The broad crested weir formula (equation **??**) is derived for situations where momentum loss over the weir can be neglected, so it is implicitly assumed that all momentum leaving one channel enters the other channel.